The Pennsylvania State University
The Graduate School
College of Engineering

LITHIUM ION BATTERY MODELING, ESTIMATION, AND AGING FOR HYBRID ELECTRIC VEHICLE APPLICATIONS

A Dissertation in
Department of Mechanical and Nuclear Engineering
by
Tanvir R. Tanim

Submitted in Partial Fulfillment
of the Requirements
for the Degree of

Doctor of Philosophy

December 2015

The dissertation of Tanvir R. Tanim was reviewed and approved* by the following:

Christopher D. Rahn
Professor of Mechanical Engineering
Dissertation Co-Adviser, Co-Chair of Committee

Chao-Yang Wang
William E. Diefender Chair of Mechanical Engineering
Dissertation Co-Adviser, Co-Chair of Committee

Hosam Fathy
Associate Professor of Mechanical Egineering

Srinivas Tadigadapa
Professor of Electrical Engineering

Karen A. Thole
Professor of Mechanical Engineering
Head, Department of Mechanical Engineering

*Signatures are on file in the Graduate School.

Abstract

Reducing greenhouse gas emissions and improving the fuel efficiency of automobiles, trucks, and buses can be achieved by partial and full electrification of the vehicle sector. Lithium ion battery technology is the leading candidate for vehicle electrification. Despite many advantages of lithium ion battery technology, over-conservative pack design due to a lack of advanced battery management hinders its widespread deployment in the transportation sector. This dissertation introduces a model-based approach for safe and efficient advanced lithium ion battery management.

Low order, explicit models of lithium ion cells are critical for real-time battery management system (BMS) applications. Li-ion cell response varies significantly with temperature and cell temperature measurements are often available. This study presents a 7^{th} order, single particle model with electrolyte diffusion and temperature dependent parameters (ESPM-T model). The impedance transfer function coefficients are explicit in terms of the model parameters, simplifying the implementation of temperature dependence yet providing an accurate model. The 7^{th} order, linear, electrolyte enhanced, single particle model (ESPM) is used as the basis for a Luenberger SOC observer for a lithium ion cell. Isothermal and non-isothermal observer performances are compared with a commercially-available finite volume code and the benefits of temperature measurement are shown for a

wide range of temperature and pulse C-rates.

The ESPM is then extended to a nonlinear, electrolyte-enhanced, single particle model (NESPM), which includes nonlinearities associated with open circuit voltage and Butler-Volmer (B-V) kinetics. The model is validated with experimental full charge, discharge, and HEV cycles from 4.5 Ah high power and 20 Ah high energy graphite (gr)/$LiFePO_4$ (LFP) cells. The NESPM is capable of operating up to $3C$ constant charge-discharge cycles and up to 25C and 10 sec charge-discharge pulses within 35-65% state of charge (SOC) with less than 2% error for the 4.5 Ah high power cell. For the 20 Ah high energy cell, the NESPM model is capable of operating up to $2C$ constant charge-discharge cycles and up to 10C and 10 sec charge-discharge pulses within 30-90% SOC window with 3.7% maximum error.

An aging model due to solid electrolyte interphase layer growth is added to the NESPM model. The NESPM aging model is then simplified to obtain explicit formulas for capacity fade and impedance rise that depend on the battery parameters and current input history. These simple aging models can be implemented in online model based battery SOH estimation. The formulas show that aging increases with SOC, operating temperature, time, and root mean square (RMS) current. The formula predicts that HEV current profiles with the (i) same average SOC, (ii) small SOC swing, (iii) same operating temperature, (iv) same cycle length, and (v) same RMS current, will have the same cell capacity fade.

The single cell ESPM-T model is extended to a pack model with three cells in parallel to develop thermal management strategies to extend battery life within a desired performance window. Instead of defining battery End of Life (EOL) as an arbitrary percent of capacity loss, it is defined as the cycle number when

the battery voltage first hits the maximum or minimum voltage limits for a given drive cycle. In practice, this is when the battery management system must reduce the input current, and the desired performance can no longer be achieved. Three thermal management strategies are simulated to show that elevated temperature operation can significantly extend battery life/reduce battery size while maintaining the desired performance. The effect of cell mismatch in pack performance and life is also analyzed and thermal management strategies to mitigate the mismatch effect are proposed.

Table of Contents

List of Figures

List of Tables

List of Symbols

a_s	active surface area per electrode unit volume, cm^2/cm^3
A	electrode plate area, cm^2
c	concentration of Li in a phase, mol/cm^3
$c_{e,0}$	average concentration of Li in electrolyte phase, mol/cm^3
D	diffusion coefficient of Li, cm^2/s
E_{act}	activation energy, J/mol
F	Faraday's constant, 96,487 C/mol
I	applied current, A
i_0	exchange current density of electrode reaction, A/cm^2
j	exchange current density of electrode reaction, A/cm^3
j^{Li}	reaction current resulting in production or consumption of Li, A/cm^3
L	cell width, cm
Q	capacity, Ah
r	radial coordinate within active material particle, cm
R	universal gas constant, 8.3143 J/mol K
R_c	contact resistance, Ωcm^2
R_{ct}	charge transfer resistance, Ωcm^2

R_f	film resistance on an electrode surface, Ωcm^2
R_s	radius of active material particles, cm
s	Laplace transform variable
T	absolute temperature, K
t	time, s
U	open circuit, or equilibrium potential of an electrode reaction, V
V	voltage, V
t_+^0	transference number of Li^+ with respect to solvent velocity
x	negative electrode solid phase stoichiometry and cell width spatial coordinate, cm
y	positive electrode solid phase stoichiometry and state variable model output

Greek symbol

α_a, α_c	anodic and cathodic transfer coefficients for an electrode reaction
δ	thickness, cm
ε	volume fraction or porosity of a phase
η	overpotential of an electrode reaction, V
κ	Li^+ conductivity of electrolyte, S/cm
κ_D	Li^+ diffusional conductivity of electrolyte, A/cm
σ	e^- conductivity of electrode solid matrix, S/cm
ϕ	phase potential, V
Ψ	generic physiochemical property
ω	frequency, rad/s

Matrix/Vector

A,B,C,D	state variable model matrices
l	observer (state estimator) gain matrix
u	state variable model input vector
x	state vector
y	state variable model output vector

Subscript

e	electrolyte phase
max	maximum value
n	negative electrode
p	positive electrode
ref	reference value
rms	root mean square
s	separator
s, e	solid electrolyte interface
sei	solid electrolyte interface layer
0%	zero state of charge reference state
100%	100% state of charge reference state

Superscript

eff	effective
Li	lithium species
$+$	ion

Acknowledgments

I would like to gratefully and sincerely thank Dr. Christopher Rahn for his guidance, understanding, patience, and most importantly, his hands-on advising approach during my graduate studies at Penn State. His mentorship was paramount in providing a well-rounded experience consistent with my long-term career goals. He encouraged me to not only grow as researcher but also as an instructor and an independent thinker. I appreciate the opportunity to work independently to nurture my own individuality and self-sufficiency. For everything you have done for me, Dr. Rahn, I thank you. It was fun working with you.

I am grateful to Dr. Chao-Yang Wang for the motivation, constant encouragement, and confidence in me during my graduate studies at Penn State. I would also like to thank my committee members, Dr. Hosam Fathy, and Dr. Srinivas Tadigadapa for their input, valuable discussions, and accessibility. I would like to thank Dr. Yancheng Zhang, Dr. Guangsheng Zhang, and Mayank Garg for their assistance with my experiments.

I am extremely grateful to my parents Md Roushan Ali and Farzana Parveen for their unconditional love and support. Their continuous encouragement and prayers kept me going on during challenging times of my graduate study. I thank my wife Rakiba Wazi for her support, quiet patience, and unwavering love. Her tolerance of my occasional vulgar moods is a proof of her unyielding devotion and love.

Finally, I thank all my labmates and friends for all their help and support during my graduate studies.

I dedicate this work to my wonderful parents.

"Life is the unfolding and development of a being under circumstances tending to press it down." -Swami Vivekananda

Chapter 1
Introduction

1.1 Research Contributions and Motivation

1.1.1 Research Contributions

This dissertation presents contributions in the area of lithium ion battery electrochemical and aging modeling, state of charge (SOC) and state of health (SOH) estimation, thermal management strategies to extend battery life, with focus on their application in advanced battery management systems of hybrid and electric vehicles. The highlights of this dissertation are as follows:

- Development of a low order, electrolyte enhanced single particle battery models with electrolyte diffusion dynamics and temperature dependent parameters that can be easily implemented on advanced battery management systems.

- Development of a control oriented solid electrolyte interphase layer growth model to identify the main battery aging parameters for HEV applications.

- Development of a pack model with three cells in parallel to develop thermal management strategies to extend battery life within a desired performance window for HEV applications.

1.1.2 Research Motivation

Reducing greenhouse gas emissions and improving the fuel efficiency of automobiles, trucks, and buses can be achieved by partial and full electrification of the vehicle sector [1]. The U.S. Corporate Average Fuel Economy (CAFE) standard will double the conventional internal combustion engine's fuel efficiency to 54.5 miles per gallon [2] by 2025, saving consumers $1.7 trillion in fuel costs and reducing oil consumption by 12 billion barrels. Most of the vehicles in the U. S. are expected to be hybrid electric vehicles (HEVs) and plug in hybrid electric vehicles (PHEVs) by 2034 and 2045, respectively [3, 4], to meet the CAFE standard.

Li-ion batteries are the leading candidates for HEVs and PHEVs, as they offer 40 - 50% weight reduction and 30 - 40% volume reduction along with superior coulometric and energy efficiency compared to their closest rivals, Ni-MH batteries [5]. Lithium-ion batteries also have a longer cycle life, low self-discharge rate and no memory effect compared to Ni-MH batteries. Despite this better performance, the Li-ion battery technology did not gain widespread popularity till now. There are several reasons behind this. One of the main reasons is the over conservative pack design to prevent premature battery life due to lack of advanced battery management in response to different operating and usage conditions, which significantly increases the vehicle cost. The end of life (EOL) goal of an EV and PHEV is set to 10 years and for HEV it is 15 years [6]. So it is also imperative to accurately predict the battery degradation (capacity fade and impedance rise) over its entire life time. Important battery control and management decisions depend on the accurate prediction of capacity fade and impedance rise. New thermal management strategies to increase battery life without sacrificing performance is also needed to satisfy the stringent EOL goal.

The battery system consists of a battery pack and the battery management system (BMS). The BMS ensures safe and efficient power utilization, estimate state of charge (SOC) and state of health (SOH), and balance cell strings [5]. Accurate cell electrochemical and aging models that capture the fast cell dynamics in different operating conditions of vehicle applications are critical for high performance and advanced BMS design. BMS are often based on equivalent circuit models [7–13] that are relatively easy to implement but lack the important underlying physio-chemical processes of the cell and require empirical parametrization for precise estimation.

This method is chemistry and operating condition dependent, expensive, and time consuming. Physics-based reduced order electrochemical and aging models on the other hand include important battery dynamics, are explicitly dependent on the physical cell parameters, and accurately predict battery response and age [14, 15]. Physical model-based advanced battery management would enable system engineers to design accurate SOC and SOH estimators, identify the main controlling aging parameters, and optimally design and operate battery packs to enhance life within a desired performance window.

1.2 Background

1.2.1 Li-ion Cell Modeling and SOC Estimation

One of the major tasks of a BMS is to estimate SOC, the percentage of maximum available charge at the current time. SOC can not be measured directly, so the measured voltage and current are used to estimate the SOC. Coulomb counting through current integration is a SOC estimation method but it requires accurate knowledge of the initial state of the cell. As with all open loop estimators, the estimated SOC may drift away due to sensor error and model mismatch. Model-based SOC estimation using feedback, is more reliable but requires an accurate cell model that captures the cell dynamics under varied operating conditions over the life of the pack. Equivalent circuit models are often used to estimate SOC [16–19] but they lack underlying physio-chemical processes of the cell and require extensive empirical parametrization. Plett [7–9] first introduces the use of Kalman filtering for equivalent circuit models of Li-ion cells. Lee *et al.* [20] report a reduced order extended Kalman filter based on equivalent circuit model. Hu [21] designs a Luenberger observer based on an equivalent circuit model.

Full order, physics based, electrochemical models are often not the best candidates for state estimator design because they consists of non-linear, coupled, partial differential equations (PDEs), that must be simplified and discretized to be used for real-time estimation on-board a vehicle. Reduced order models have been developed by many researchers that simplify the full order electrochemical models. These reduced order models capture the dominant cell dynamics at a specific SOC and temperature and sufficiently low C-rate. Smith *et al.* [15, 22]

develop a 7^{th} order isothermal model in state variable form using residue grouping that predicts internal cell potentials, concentration gradients, and estimate SOC from current and voltage measurements. The model does not provide explicit relationships between the cell internal parameters and the coefficients of impedance transfer function. Lee *et al.* [23] extend this work by obtaining an analytic transfer function for solid phase potential, electrolyte phase potential, and concentration distribution. Klein *et al.* [24] reduce the full electrochemical model by assuming constant electrolyte concentration and approximating solid phase diffusion using volume averaging. Incorporating a temperature corrective term in the energy equation enables accurate SOC estimation at moderate C-rates (current/battery capacity) [25].

Single particle model (SPM) based observers have also been reported in literature [26–28]. The SPM is a simplified, physics based, fundamental model where the current density is assumed to be uniform in each electrodes and all of the active material particles are in parallel . The associated diffusion equations are solved assuming average electrochemical reaction rate. The electrolyte dynamics modeled by a diffusion resistance, assuming instantaneous Li-ion transfer across the cell leads to significant error at high C-rates [29]. Rahimian *et al.* [30] derived an isothermal SPM by polynomial approximation of electrolyte dynamics in terms of 13 differential algebraic equations which are solved by COMSOL Inc. Marcicki *et al.* [31] recently proposed a SPM that includes a time-varying resistance and first order truncated liquid diffusion dynamics.

The performance and dynamic response of a Li-ion cell is strongly dependent on temperature and C-rate. The accuracy with which one can estimate SOC is directly related to the accuracy of the underlying model [5]. SOC estimators drive the voltage and SOC estimate error to zero if the model is accurate. Model mismatch introduces phantom currents that contribute the inaccurate SOC estimate. A BMS capable of achieving excellent model based SOC estimation at room temperature, for example, may fail to estimate SOC accurately during cold or hot start when large model mismatch occurs due to not incorporating the actual thermal conditions. The temperature dependent cell physio-chemical processes must reflect through the cell model and the model is the backbone of accurate SOC estimation. A simplified, real-time, and physics based model that can be used in BMS to predict cell response and estimate SOC in a wider range of cell operating conditions is in critical need.

1.2.2 Model Based Li-ion Cell Aging Prediction

Model based accurate battery life prediction is one of the demanding tasks of an advanced BMS for pack warranty and accurately accomplish different control, estimation, and management tasks in order to optimize battery usage and minimize degradation. HEV current profiles are dynamic, consisting of repeated charge and discharge pulses. The challenge is to choose the best cells for a specific application and optimal pack size to maximize fuel economy at minimum cost, taking into consideration the fact that batteries age and their performance degrades. It is very important to understand usage associated with a specific application influences cell degradation. Accurate modeling and prediction of the battery SOH is crucially important for the BMS to efficiently and economically control, estimate, and manage the pack to prevent unexpected performance deterioration and premature EOL.

Lithium Iron Phosphate (LFP) cathode-based Li-ion batteries possess high temperature abuse tolerance, low cost, and an environmentally benign nature [32,33]. LFP cathodes are extremely stable due to their olivine crystalline structure. Continuous small scale side reactions at the solid electrolyte interphase (SEI) layer of the negative carbonaceous graphite (gr) anode, however, is considered to be the main cause of aging [34–36].

The intercalation/deintercalation processes in LFP is thought to occur through a two phase process between a Li-poor $Li_{\epsilon}FePO_4$ phase and a Li-rich $Li_{1-\epsilon'}FePO_4$ phase [37–39]. Srinivasan and Newman [37] develop a core-shell model initially proposed by Padhi *et al.* [32] with a growing shell of $LiFePO_4$ (Li-rich phase) on a shrinking $FePO_4$ (Li-poor phase) core during discharge. This core-shell model is improved by other researchers [40–42] through tracking of multiple two-phase boundaries for repeated charge-discharge cycles but the simulation is complicated and computationally demanding. A relatively simplified phase-change diffusivity model is proposed by Thorat [43]. A phase-field model, based on the Cahn-Hilliard theory is also reported for the LFP electrode [44]. Interestingly, some recent studies also claim that the two distinct phase processes during lithiation/delithiation in a LFP cathode occur only at low currents. Large currents suppress the phase transformation [45–47] in the LFP cathode. It is also reported that LFP active material shows resistive reactant property which attributes in increasing cell impedance as charge or discharge proceeds [48,49].

Mathematical models of the cycleable lithium consumption in the negative electrode that contributes to SEI growth are reported by many researchers [50–52]. Ramadass *et al.* [53] first propose a simplified control-oriented incremental aging model of the negative electrode in conjunction with a 1D full order electrochemical model. Randall *et al.* [54] further reduce this aging model and propose an iterative approach to calculate the SEI side reaction current density to quantify cell aging. The SEI aging process is coupled with the cell electrochemistry, so model-based aging analysis requires an accurate electrochemical model. An accurate coupled electrochemical aging model would allow systems engineers to identify the main controlling battery aging parameters to develop life extending battery management algorithms and estimate SOH more accurately.

1.2.3 Life-Extending Thermal Management for Heterogeneous Lithium ion Battery Packs in Hybrid Electric Vehicles

HEVs are the most predominant forms of vehicle electrification in the current market. HEV packs are relatively small and low cost but provide a significant increase in fuel efficiency. HEVs operate in a relatively small (40-80%) SOC window but at very high charge/discharge rates (*e.g.* 20C). Thus, an HEV pack contributes more power than energy and its End of Life (EOL) occurs when the requisite power can no longer be provided. Two factors influence the EOL of HEV packs: Heterogeneity and temperature.

Battery packs have many cells in series and parallel to provide the desired voltage and power. Although every effort is made to select cells that are identical, even new packs are heterogeneous due to manufacturing and material variations between cells. Placing cells in parallel multiplies the pack capacity and available current and placing cells in series multiplies the voltage. Cells in a pack, however, age differently due to initial heterogeneity and temperature and current non-uniformity across the pack. Additionally, packs are typically divided into smaller modules that may not be replaced at the same time. Thus, every pack has some degree of heterogeneity with cells of different age, capacity, and/or impedance placed in parallel. The older cells have less capacity and/or higher impedance than newer cells. Cells in parallel have the same voltage, so weaker cells source/sink less current than stronger cells. This increases the RMS current passing through the stronger cells and degrades

them at a faster rate. Mismatched cells in parallel may also push the pack to a voltage limit more quickly, limiting the discharge/charge power. Thus, there are two possible problems associated with mismatched cells in parallel: Power loss and over-aging.

Questions of aging, over-aging, and life hinge on the definition of EOL. According to the U.S.-Advanced Battery Consortium (USABC), battery EOL is reached when the capacity or peak power of a cell, module, or pack at 80% DOD reduces to 80% of its rated capacity or peak power [55]. HEV Li-ion batteries are optimized for high power and operate on charge sustaining control strategies within a narrow SOC window [22, 56]. Thus, the 80% DOD is not an appropriate EOL definition. Pack charge/discharge power typically occurs when the voltage reaches user-defined maximum/minimum limits. An HEV battery pack at EOL cannot provide the desired power and/or performance when the pack voltage hits the maximum/minimum voltage limits due to increased internal impedance and/or capacity fade.

Lithium ion battery performance and life are strongly dependent on temperature. Increased temperature reduces reaction overpotential, reducing internal impedance and the associated voltage swings under high current. Thus, if one increases the temperature of a cell at EOL, then the voltage will no longer exceed the prescribed limits and the cell's life will be extended. Elevated temperature also increases the aging kinetics, however, so a balance must be struck to achieve maximum life. Determining an optimal operating temperature that maximizes EOL involves tradeoffs between capacity fade and impedance reduction at elevated temperature. The systems oriented and temperature dependent Li-ion battery performance and aging models developed in this thesis are essential tools for the optimal design of life-extending thermal management strategies. The dynamics of mismatched cells in parallel would also determine if and how thermal control can be used to maximize power and minimize degradation.

1.3 Overview of the Dissertation

Chapter 2 presents the development of a 7^{th} order, electrolyte enhanced single particle model (ESPM) with electrolyte diffusion and temperature dependent parameters (ESPM-T). The impedance transfer function coefficients are explicit in terms of the model parameters, simplifying the implementation of temperature dependence. The fundamental governing charge and Li ion conservation and Butler-Volmer equations are linearized at an operating state of charge set point and solved using analytical techniques to produce the impedance transfer function from input current to output voltage. The ESPM-T model is compared with a commercially available finite volume based model and results show accurate matching of pulse responses over a wide range of temperature and C-rates for a gr/NCM cell.

Chapter 3 uses the 7^{th} order ESPM as the basis for a Luenberger SOC observer for a lithium ion cell. Isothermal and non-isothermal simulations compare the SOC from a commercially-available finite volume code and the SOC estimate for a wide range of temperature and pulse C-rates. Arrhenius relationships between the ESPM model parameters and the sensed temperature significantly improve SOC estimation.

Chapter 4 derives a nonlinear, electrolyte-enhanced, single particle model (NE-SPM). The model is validated with experimental full charge, discharge, and HEV cycles from a 4.5 Ah high power and 20 Ah high energy graphite gr/LFP cells. Inclusion of electrolyte dynamics, nonlinear kinetics, and nonlinear OCPs in the conventional SPM significantly improve the models operating range.

Chapter 5 includes aging due to solid electrolyte interphase layer growth with the previously developed NESPM model. The NESPM aging model is then simplified to obtain explicit formulas for capacity fade and impedance rise that depend on the battery parameters and current input history. The formulas show that aging increases with SOC, operating temperature, time, and root mean square (RMS) current. Single cell experimental aging tests are performed to support the model conclusions.

Chapter 6 extends the single cell models to a pack model with three cells in parallel to develop thermal management strategies to extend battery life without sacrificing performance for HEV applications. Instead of defining battery EOL as an arbitrary percent of capacity loss, the maximum cycle number is used as

EOL when the battery voltage hits 3.6V/2V (maximum/minimum) voltage limits. This is the practical limit of operation without reduced performance. Effect of cell mismatch on pack performance and life has also been analyzed.

Chapter 7 presents the conclusions and future work.

Chapter 2
A Temperature Dependent, Single Particle, Lithium Ion Cell Model Including Electrolyte Diffusion

2.1 Introduction

Low order, explicit models of lithium ion cells are critical for real-time battery management system (BMS) applications. This chapter presents a 7^{th} order, electrolyte enhanced single particle model (ESPM) with electrolyte diffusion and temperature dependent parameters (ESPM-T). The impedance transfer function coefficients are explicit in terms of the model parameters, simplifying the implementation of temperature dependence. The ESPM-T model is compared with a commercially available finite volume based model and results show accurate matching of pulse responses over a wide range of temperature (T) and C-rates (I). The voltage response to 30 sec pulse charge-discharge current inputs is within 5% of the commercial code for $25^oC < T < 50^oC$ at $I \leq 12.5C$ and $-10^oC < T < 50^oC$ at $I \leq 1C$ for a graphite/NCM lithium ion cell.

2.2 Mathematical Modeling

Figure 2.1 shows the three domains of the 1D Li-ion cell model: Porous anode with spherical graphite particles, porous separator, and porous cathode with spherical active material particles (e.g. lithium nickel manganese cobalt oxide (NCM), lithium cobalt oxide (LCO), lithium manganese oxide (LMO), or lithium iron phosphate (LFP)). The electrolyte is typically 1.2M $LiPF_6$ in propylene carbonate (PC)/ ethylene carbonate (EC)/ dimethyl carbonate (DMC) and saturates all three domains. A micro porous polymer or gel polymer separator isolates the direct electron path between the positive and negative electrodes, but allows Li-ions to diffuse through. Aluminum (Al) and copper (Cu) foil current collectors are attached at the ends of positive and negative electrodes, respectively.

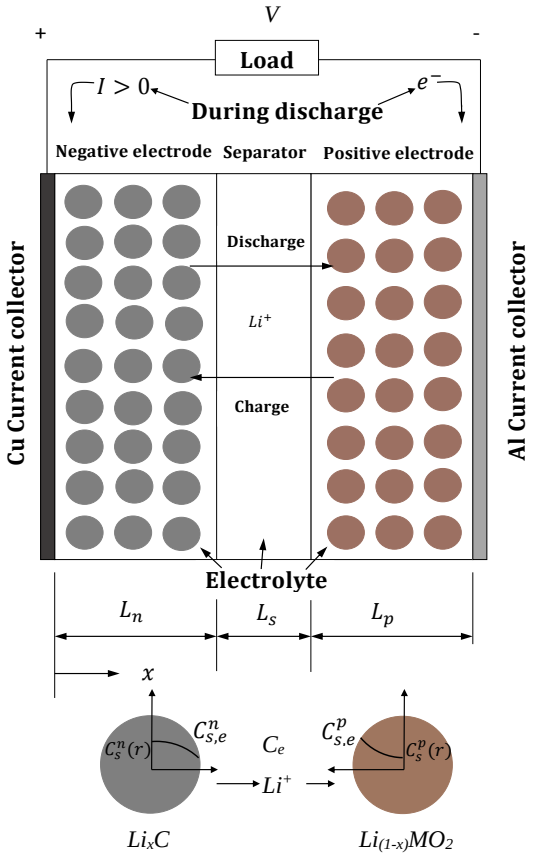

Figure 2.1. Schematic diagram of a coupled, 1D, single-particle, Li-ion cell model.

During discharge, Li-ions de-intercalate from the negative electrode

$$Li_xC \overset{\text{discharge}}{\rightleftharpoons} C + xLi^+ + xe^-, \tag{2.1}$$

and intercalate into the positive electrode for LMO active material particles

$$Li_{(1-x)}MO_2 + xLi^+ + xe^- \overset{\text{discharge}}{\rightleftharpoons} LiMO_2, \tag{2.2}$$

where M stands for a metal. The opposite reactions occur during charge.

2.2.1 Governing Equations

The electrochemical model of a Li-ion cell can be described by four governing equations: Conservation of Li-ion (Li^+) and conservation of charge (e^-) in both the solid and electrolyte phases. Conservation of Li^+ in a single, spherical, solid phase particle is described by Fick's law of diffusion:

$$\frac{\partial c_s}{\partial t} = \frac{D_s}{r^2}\frac{\partial}{\partial r}\left(r^2\frac{\partial c_s}{\partial r}\right), \tag{2.3}$$

where $c_s(x, r, t) : (0, L) \times (0, R_s) \times R^+ \rightarrow [0, c_{s,max}]$ is the concentration of Li^+ in the solid particle. The model parameters are defined in Table 2.1. The rate at which ions exit or enter the particle equals the volumetric reaction rate at the particle surface, j^{Li}, and zero at the particle center, written as the boundary conditions,

$$\left(\frac{\partial c_s}{\partial r}\right)_{r=0} = 0, \tag{2.4}$$

$$\left(D_s\frac{\partial c_s}{\partial r}\right)_{r=R_s} = -\frac{j^{Li}}{a_s F}, \tag{2.5}$$

where $j^{Li} > 0$ for ion discharge and the interfacial surface area, $a_s = \frac{3\varepsilon_s}{R_s}$. Eqs. (2.3) - (2.5) are applied on a continuum basis across both electrodes. The solid phase potential depends on the particle surface concentration, $c_{s,e}(x, t) = c_s(x, R_s, t)$. Diffusion in Cartesian coordinates governs the conservation of Li^+ in the electrolyte phase

$$\varepsilon_e\frac{\partial c_e}{\partial t} = D_e^{eff}\frac{\partial^2 c_e}{\partial x^2} + \frac{1 - t_+^0}{F}j^{Li}, \tag{2.6}$$

where $c_e(x,t) : (0,L) \times R^+ \rightarrow [0, c_{e,max}]$ is electrolyte concentration and ε_e and D_e are different in each domain (anode, separator and cathode). The Bruggeman relation $D_e^{eff} = D_e \varepsilon_e^{1.5}$ accounts for the tortuous path of Li^+ transport through the porous electrodes and separator. Ensuring zero flux at the current collectors and continuity of concentration and flux through the adjoining domains within the cell, produces the boundary conditions

$$\left(\frac{\partial c_e^n}{\partial x}\right)_{x=0} = 0, \tag{2.7}$$

$$\left(D_n^{eff}\frac{\partial c_e^n}{\partial x}\right)_{x=L_n} = \left(D_s^{eff}\frac{\partial c_e^s}{\partial x}\right)_{x=L_n}, \tag{2.8}$$

$$c_e^n(L_n,t) = c_e^s(L_n,t), \tag{2.9}$$

$$\left(D_s^{eff}\frac{\partial c_e^s}{\partial x}\right)_{x=L_n+L_s} = \left(D_p^{eff}\frac{\partial c_e^p}{\partial x}\right)_{x=L_n+L_s}, \tag{2.10}$$

$$c_e^n(L_n+L_s,t) = c_e^p(L_n+L_s,t), \tag{2.11}$$

$$\left(\frac{\partial c_e^p}{\partial x}\right)_{x=L_n+L_s+L_p} = 0, \tag{2.12}$$

where

$$c_e(x,t) = \begin{cases} c_e^n(x,t) & \text{for } x \in (0,L_n), \\ c_e^s(x,t) & \text{for } x \in (L_n, L_n+L_s), \\ c_e^p(x,t) & \text{for } x \in (L_n+L_s, L). \end{cases}$$

Conservation of charge in the solid phase of each electrode is

$$\sigma^{eff}\frac{\partial^2 \phi_s}{\partial x^2} = j^{Li}, \tag{2.13}$$

where solid phase potential

$$\phi_s(x,t) = \begin{cases} \phi_s^n(x,t) & \text{for } x \,\epsilon\, (0,L_n), \\ \phi_s^p(x,t) & \text{for } x \,\epsilon\, (L_n+L_s, L). \end{cases}$$

The fields at the current collectors are proportional to the applied current and

zero at the separator

$$-\sigma_n^{eff}\left(\frac{\partial\phi_s^n}{\partial x}\right)_{x=0}=\sigma_p^{eff}\left(\frac{\partial\phi_s^p}{\partial x}\right)_{x=L}=\frac{I}{A}, \tag{2.14}$$

$$\left(\frac{\partial\phi_s^n}{\partial x}\right)_{x=L_n}=\left(\frac{\partial\phi_s^p}{\partial x}\right)_{x=L_n+L_s}=0, \tag{2.15}$$

where $I>0$ indicates discharge. The effective conductivity of the solid phase σ^{eff} can be calculated from $\sigma^{eff}=\sigma\varepsilon_s$, where σ is the reference conductivity of the active material. The linearized electrolyte phase charge conservation equation [57–59]

$$\kappa^{eff}\frac{\partial^2\phi_e}{\partial x^2}+\frac{\kappa_d^{eff}}{c_{e,0}}\frac{\partial^2 c_e}{\partial x^2}+j^{Li}=0 \tag{2.16}$$

has boundary conditions

$$\left(\frac{\partial\phi_e^n}{\partial x}\right)_{x=0}=0, \tag{2.17}$$

$$\left[\left(\kappa_n^{eff}\frac{\partial\phi_e^n}{\partial x}\right)+\left(\kappa_{d,n}^{eff}\frac{\partial c_e^n}{\partial x}\right)\right]_{x=L_n}=\left[\left(\kappa_s^{eff}\frac{\partial\phi_e^s}{\partial x}\right)+\left(\kappa_{d,s}^{eff}\frac{\partial c_e^s}{\partial x}\right)\right]_{x=L_n}, \tag{2.18}$$

$$\phi_e^n(L_n,t)=\phi_e^s(L_n,t), \tag{2.19}$$

$$\left[\left(\kappa_s^{eff}\frac{\partial\phi_e^s}{\partial x}\right)+\left(\kappa_{d,s}^{eff}\frac{\partial c_e^s}{\partial x}\right)\right]_{x=L_n+L_s}=\left[\left(\kappa_p^{eff}\frac{\partial\phi_e^p}{\partial x}\right)+\left(\kappa_{d,p}^{eff}\frac{\partial c_e^p}{\partial x}\right)\right]_{x=L_n+L_s}, \tag{2.20}$$

$$\phi_e^s(L_n+L_s,t)=\phi_e^p(L_n+L_s,t), \tag{2.21}$$

$$\left(\frac{\partial\phi_e^p}{\partial x}\right)_{x=L_n+L_s+L_p}=0, \tag{2.22}$$

where

$$\phi_e(x,t)=\begin{cases}\phi_e^n(x,t) & \text{for } x\in(0,L_n),\\ \phi_e^s(x,t) & \text{for } x\in(L_n,L_n+L_s),\\ \phi_e^p(x,t) & \text{for } x\in(L_n+L_s,L).\end{cases}$$

The Bruggeman relation $\kappa^{eff}=\kappa\varepsilon_e^{1.5}$ calculates the effective ionic conductivity of individual domain. The effective diffusional conductivity

$$\kappa_d^{eff}=\frac{2RT\kappa^{eff}}{F}\left(t_+^0-1\right)\left(1+\frac{d\ln f_\pm}{d\ln c_e}\right), \tag{2.23}$$

according to concentrated solution theory. Butler-Volmer (B-V) kinetics

$$j^{Li} = a_s i_0 \left[\exp\left(\frac{\alpha_a F \eta}{RT}\right) - \exp\left(-\frac{\alpha_c F \eta}{RT}\right) \right], \tag{2.24}$$

couples the four conservation Eqs. (2.3), (2.6), (2.13), and (2.16) describing the four field variables $c_{s,e}, c_e, \phi_s$ and ϕ_e. Overpotential

$$\eta = \phi_s - \phi_e - U(c_{s,e}), \tag{2.25}$$

drives the electrochemical reaction rate. The exchange current density in Eq. (2.24) depends on the solid particle surface, electrolyte concentrations, and temperature

$$i_0(x,t) = k(T) c_e^{\alpha_a} \left(c_{s,max} - c_{s,e}\right)^{\alpha_a} c_{s,e}^{\alpha_c}. \tag{2.26}$$

Finally, the cell voltage is

$$V(t) = \phi_s^p(L,t) - \phi_s^n(0,t) - \frac{R_c}{A} I(t), \tag{2.27}$$

where R_c is the contact resistance. Finite difference discretization of the governing Eqs. (2.3) - (2.22) can produce hundreds of state equations, requiring expensive computation for onboard estimation and control. To reduce the model order for real-time computation, we use efficient discretization techniques and retain only the most significant dynamics of the full order model.

2.2.2 Low Order Electrolyte Enhanced Single Particle Model (ESPM) Formulation

In a conventional isothermal SPM, current density is assumed to be uniformly distributed across each electrode. Thus, all the active material particles are in parallel and each electrode can be replaced by a single spherical particle with radius R_s but Li-ion storage capacity is equal to the electrode storage capacity. The electrolyte dynamics are neglected, resulting in under predicted voltage swings and transients. The assumptions of the ESPM are: (i) infinite solid phase conductivity in the individual electrodes resulting no ohmic loss, (ii) uniform current distribution in the individual electrodes, (iii) linearized conservation equations in the electrolyte domain, and (iv) all properties are evaluated at the equilibrium point (at 50% SOC). Assumptions (i), (ii), and (iv) are also used in SPM models.

Conservation of Li in the single electrode particle for the SPM is solved by taking the Laplace transform of the particle diffusion Eq. (2.3) and applying boundary conditions (2.4) - (2.5). The solid state diffusion impedance transfer function at the particle surface of a spherical particle is

$$\frac{\widetilde{C}_{s,e}(s)}{J^{Li}(s)} = \frac{1}{a_s F}\left(\frac{R_s}{D_s}\right)\left[\frac{\tanh(\beta)}{\tanh(\beta)-\beta}\right], \tag{2.28}$$

where $\beta = R_s\sqrt{\frac{s}{D_s}}$ and the tilde indicates a small perturbation from the equilibrium condition [60] $c_{s,e}(t) = \bar{c}_{s,e} + \widetilde{c}_{s,e}(t)$. Note that at equilibrium, $\bar{\eta}$, $\bar{j}$, and $\bar{c_e}$ are zero so, tildes are unnecessary. Capital letters indicate a variable has been Laplace transformed. Conservation of charge in the electrode (2.13) is simplified by integrating in each electrode domain and applying the boundary conditions (2.14) - (2.15). The final transfer functions are

$$\frac{J_n^{Li}(s)}{I(s)} = \frac{1}{AL_n}, \tag{2.29}$$

$$\frac{J_p^{Li}(s)}{I(s)} = -\frac{1}{AL_p}, \tag{2.30}$$

where the assumed uniform current distributions are defined as $J_p^{Li}(s) = \frac{1}{L_p}\int_{L_n+L_s}^{L} J^{Li}(x,s)\mathrm{d}x$ and $J_n^{Li}(s) = \frac{1}{L_n}\int_{0}^{L_n} J^{Li}(x,s)\mathrm{d}x$, in the positive and negative electrodes, respectively.

Using Eqs. (2.28) - (2.30), the solid phase surface concentrations are

$$\frac{\widetilde{C}^p_{s,e}(s)}{I(s)} = -\frac{1}{a^p_s F A L_p}\left(\frac{R^p_s}{D^p_s}\right)\left[\frac{\tanh(\beta^p)}{\tanh(\beta^p)-\beta^p}\right], \tag{2.31}$$

$$\frac{\widetilde{C}^n_{s,e}(s)}{I(s)} = \frac{1}{a^n_s F A L_n}\left(\frac{R^n_s}{D^n_s}\right)\left[\frac{\tanh(\beta^n)}{\tanh(\beta^n)-\beta^n}\right], \tag{2.32}$$

in the positive and negative electrodes, respectively. These transcendental transfer functions are infinitely differentiable and can be discretized using a Padé approximation [61, 62]. Prasad *et al.* [29] experimentally validated a 3^{rd} order Padé approximation with a 10 Hz bandwidth, sufficiently high for current EV applications. The 3^{rd} order Padé approximations of (2.31) and (2.32) are

$$\frac{\widetilde{C}^p_{s,e}(s)}{I(s)} = \frac{21\left[\frac{1}{a^p_s F A R^p_s L_p}s^2 + \frac{60D^p_s}{a^p_s F A\left[R^p_s\right]^3 L_p}s + \frac{495\left[D^p_s\right]^2}{a^p_s F A\left[R^p_s\right]^5 L_p}\right]}{s^3 + \frac{189D^p_s}{\left[R^p_s\right]^2}s^2 + \frac{3465\left[D^p_s\right]^2}{\left[R^p_s\right]^4}s}, \tag{2.33}$$

$$\frac{\widetilde{C}^n_{s,e}(s)}{I(s)} = -\frac{21\left[\frac{1}{a^n_s F A R^n_s L_n}s^2 + \frac{60D^n_s}{a^n_s F A[R^n_s]^3 L_n}s + \frac{495[D^n_s]^2}{a^n_s F A[R^n_s]^5 L_n}\right]}{s^3 + \frac{189D^n_s}{[R^n_s]^2}s^2 + \frac{3465[D^n_s]^2}{[R^n_s]^4}s}. \tag{2.34}$$

The linearized B-V Eq.(2.24) is

$$\frac{\eta(s)}{J^{Li}(s)} = \frac{R_{ct}}{a_s}, \tag{2.35}$$

where the charge transfer resistance, $R_{ct} = \frac{RT}{i_0(\alpha_a+\alpha_c)F}$. Combining Eqs. (2.29), (2.30) and (2.35),

$$\frac{\eta_p(s)}{I(s)} = -\frac{R^p_{ct}}{a^p_s}\frac{1}{AL_p}, \tag{2.36}$$

$$\frac{\eta_n(s)}{I(s)} = \frac{R^n_{ct}}{a^n_s}\frac{1}{AL_n}. \tag{2.37}$$

Combining Eqs. (2.25) and (2.27) and linearizing around an equilibrium produces the voltage deviation

$$\widetilde{V}(t) = \eta_p(L,t) - \eta_n(0,t) + \phi_e(L,t) - \phi_e(0,t) + \frac{\partial U_p}{\partial c_{s,e}} \widetilde{c}^{\,p}_{s,e}(L,t) - \frac{\partial U_n}{\partial c_{s,e}} \widetilde{c}^{\,n}_{s,e}(0,t) - \frac{R_c}{A} I(t), \tag{2.38}$$

where the negative terminal is assigned as ground. Taking the Laplace transform of Eq. (2.38) produces the impedance transfer function

$$\frac{\widetilde{V}(s)}{I(s)} = \frac{\eta_p(L,s)}{I(s)} - \frac{\eta_n(0,s)}{I(s)} + \frac{\Delta\phi_e(L,s)}{I(s)} + \frac{\partial U_p}{\partial c_{s,e}} \frac{\widetilde{C}^{p}_{s,e}(L,s)}{I(s)} - \frac{\partial U_n}{\partial c_{s,e}} \frac{\widetilde{C}^{n}_{s,e}(0,s)}{I(s)} - \frac{R_c}{A}. \tag{2.39}$$

The open circuit potential (OCP) slopes $\frac{\partial U_p}{\partial c_{s,e}}$ and $\frac{\partial U_n}{\partial c_{s,e}}$ can be evaluated at any SOC from the empirically measured open circuit potential functions for the cathode and anode, respectively.

The open circuit potential (OCP) slopes $\frac{\partial U_p}{\partial c_{s,e}}$ and $\frac{\partial U_n}{\partial c_{s,e}}$ can be evaluated at any SOC from the empirically measured open circuit potential functions for the cathode and anode, respectively. In Eq. (2.39), the voltage associated with the electrolyte dynamics $\frac{\Delta\phi_e(L,s)}{I(s)}$ is calculated from the linearized Li-ion species conservation equation (2.16) assuming the reaction rate is equal to the average volumetric reaction rates in Eqs. (2.29) and (2.30). Integral method analysis (IMA) [5, 26, 63–65] is used to solve the Li-ion conservation Eq. (2.6) across the three domains of the cell. Substituting Eqs. (2.29) and (2.30) into Eq. (2.6) for the anode, separator and cathode,

$$\varepsilon_{e,n} s C^n_e(s) - D_n \frac{\partial^2 C^n_e(s)}{\partial x^2} - b_1 I(s) = 0 \quad \text{for } x \in (0, L_n), \tag{2.40}$$

$$\varepsilon_{e,s} s C^s_e(s) - D_s \frac{\partial^2 C^s_e(s)}{\partial x^2} = 0 \quad \text{for } x \in (L_n, L_n + L_s), \tag{2.41}$$

$$\varepsilon_{e,p} s C^p_e(s) - D_p \frac{\partial^2 C^p_e(s)}{\partial x^2} + b_2 I(s) = 0 \quad \text{for } x \in (L_n + L_s, L), \tag{2.42}$$

where $b_1 = \frac{1-t^0}{FAL_n}$, $b_2 = \frac{1-t^0}{FAL_p}$, and the superscript '$eff$' on diffusivity has been removed for simplicity. In the minimal IMA, the quadratic Li-ion concentration profiles in the individual domains are

$$C^n_e(x,s) = c_{0,n}(s) + c_{1,n}(s)x + c_{2,n}(s)x^2 \quad \text{for } x \in (0, L_n), \tag{2.43}$$

$$C_e^s(x,s) = c_{0,s}(s) + c_{1,s}(s)x + c_{2,s}(s)x^2 \quad \text{for } x \in (L_n, L_n + L_s), \tag{2.44}$$

$$C_e^p(x,s) = c_{0,p}(s) + c_{1,p}(s)x + c_{2,p}(s)x^2 \quad \text{for } x \in (L_n + L_s, L), \tag{2.45}$$

where $c_{0,n}, c_{1,n}, \ldots, c_{2,p}$ are the coefficients of the quadratic concentration distributions in x. Note that Eqs. (2.43)- (2.45) are third order in time/Laplace domain. These quadratic distributions are substituted into Eqs. (2.40) - (2.42), integrated and applied the associated boundary conditions (2.7)- (2.12). Solving the nine equations for the nine unknown coefficients in Eqs. (2.43) - (2.45) yields the transfer functions,

$$\frac{C_e^n(s)}{I(s)} = \frac{p_{2,n}(x)s^2 + p_{1,n}(x)s + p_{0,n}}{s\left(q_{3,n}s^2 + q_{2,n}s + q_{1,n}\right)}, \tag{2.46}$$

$$\frac{C_e^s(s)}{I(s)} = \frac{p_{2,s}(x)s^2 + p_{1,s}(x)s + p_{0,s}}{s\left(q_{3,n}s^2 + q_{2,n}s + q_{1,n}\right)}, \tag{2.47}$$

$$\frac{C_e^p(s)}{I(s)} = \frac{p_{2,p}(x)s^2 + p_{1,p}(x)s + p_{0,p}}{s\left(q_{3,n}s^2 + q_{2,n}s + q_{1,n}\right)}, \tag{2.48}$$

where the coefficients $p_{0,n}, p_{1,n}, \ldots, q_{3,n}$ are given in Appendix A. Now substituting Eqs. (2.29) - (2.30) into Eq. (2.16), the electrolyte charge conservation equations in the three domains of the cell are

$$\kappa_n \frac{\partial^2 \phi_e^n(s)}{\partial x^2} + \kappa_{d,n} \frac{\partial^2 C_e^n(s)}{\partial x^2} + b_3 I = 0, \tag{2.49}$$

$$\kappa_s \frac{\partial^2 \phi_e^s(s)}{\partial x^2} + \kappa_{d,s} \frac{\partial^2 C_e^s(s)}{\partial x^2} = 0, \tag{2.50}$$

$$\kappa_p \frac{\partial^2 \phi_e^p(s)}{\partial x^2} + \kappa_{d,p} \frac{\partial^2 C_e^p(s)}{\partial x^2} - b_4 I = 0, \tag{2.51}$$

where $b_3 = \frac{1}{AL_n}$, $b_4 = \frac{1}{AL_p}$, $\kappa_{d,n} = \frac{\kappa_{d,n}^{eff}}{c_{e,0}}$, $\kappa_{d,s} = \frac{\kappa_{d,s}^{eff}}{c_{e,0}}$, $\kappa_{d,p} = \frac{\kappa_{d,p}^{eff}}{c_{e,0}}$, and the conductivities are assumed constant in each domain (anode, cathode, and separator). Equations (2.49) - (2.51) and their associated boundary conditions, Eqs. (2.17) - (2.22), are singular due to the zero flux at $x = 0$ and $x = L_n + L_s + L_p$. This situation can be avoided by defining electrolyte voltage difference relative to $\phi_e(0, s)$ [5,14,22].

We define the electrolyte phase voltage differences

$$\Delta\phi_e^n(x,s) = \phi_e^n(x,s) - \phi_e^n(0,s) \quad \text{for } x \in (0, L_n),$$
$$\Delta\phi_e^s(x,s) = \phi_e^s(x,s) - \phi_e^n(0,s) \quad \text{for } x \in (L_n, L_n + L_s),$$
$$\Delta\phi_e^p(x,s) = \phi_e^p(x,s) - \phi_e^n(0,s) \quad \text{for } x \in (L_n + L_s, L).$$

At this point of the derivation the electrolyte concentration profile in each individual domain of the cell is known and expressed as Eqs. (2.46) - (2.48). Integrating Eqs. (2.49) - (2.51) with respect to x in the individual cell domains and subtracting $\phi_e^n(0,s)$ gives

$$\kappa_n \Delta\phi_e^n + \kappa_{d,n}\left[C_e^n(x,s) - C_e^n(0,s)\right] + \frac{b_3 I x^2}{2} = C_{1n}x, \tag{2.52}$$

$$\kappa_s \Delta\phi_e^s + \kappa_{d,s} C_e^s(x,s) - \frac{\kappa_s \kappa_{d,n}}{\kappa_n} C_e^n(0,s) = C_{1s}x + C_{2n}, \tag{2.53}$$

$$\kappa_p \Delta\phi_e^p + \kappa_{d,p} C_e^p(x,s) - \frac{\kappa_p \kappa_{d,n}}{\kappa_n} C_e^n(0,s) - \frac{b_4 I x^2}{2} = C_{1p}x + C_{2p}, \tag{2.54}$$

where $C_{1,n}, \ldots, C_{2,p}$ are constants of integration. Eqs. (2.52) - (2.54) are solved analytically using the associated boundary conditions (2.18) - (2.22). After further simplification, the electrolyte phase potential difference is

$$\frac{\Delta\phi_e(L,s)}{I(s)} = \frac{R_2 s^2 + R_1 s + R_0}{L_2 s^2 + L_1 s + L_0}. \tag{2.55}$$

The coefficients $R_0, \ldots, L_2$ are listed in Appendix A. Equations (2.33), (2.34), (2.36), (2.37), and (2.55) are substituted into Eq. (2.39) to produce the ESPM impedance transfer function

$$\frac{\widetilde{V}(s)}{I(s)} = K + \frac{K_1 + K_2}{s} + \frac{b_{00}s^6 + b_{01}s^5 + b_{02}s^4 + b_{03}s^3 + b_{04}s^2 + b_{05}s + b_{06}}{s^6 + a_{01}s^5 + a_{02}s^4 + a_{03}s^3 + a_{04}s^2 + a_{05}s + a_{06}}, \tag{2.56}$$

where the coefficients $a_{01}, \ldots, a_{06}, b_{00}, \ldots, b_{06}, K, K_1,$ and K_2 are explicitly given in terms of the model parameters in Appendix B.

Table 2.1. Model parameters of the 1.78 Ah high power gr/NCM Li-ion cell

Parameter	Negative electrode	Separator	Positive electrode
Thickness, L (cm)	40×10^{-4}	25×10^{-4}	36.55×10^{-4}
Particle radius, R_s (cm)	5×10^{-4}		5×10^{-4}
Active material volume fraction, ε_s	0.662		0.58
Porosity (electrolyte phase volume fraction), ε_e	0.3	0.4	0.3
Maximum solid phase concentration, $c_{s,max}$ (mol cm^{-3})	31.08×10^{-3}		51.83×10^{-3}
Stoichiometry at 0% SOC, $x_{0\%}$, $y_{0\%}$	0.001		0.955473
Stoichiometry at 100% SOC, $x_{100\%}$, $y_{100\%}$	0.790813		0.359749
Average electrolyte concentration, $c_{e,0}$ (mol cm^{-3})		1.2×10^{-3}	
Exchange current density, $i_{0,ref}$ (A cm^{-2})	2.8×10^{-3}		2.0×10^{-4}
Activation energy of i_0 (kJ mol^{-1})	92		58
Charge transfer coefficient, α_a, α_c	0.5, 0.5		0.5, 0.5
Li^+ transference number, t_0^+		0.38	
Film resistance, R_f (Ω cm^2)	0		0
Solid phase Li diffusion coefficient, $D_{s,ref}$ (cm^2 s^{-1})	1.4×10^{-10}		2.0×10^{-10}
Electrode plate area, A (cm^2)		1020.41	
Activation energy of D_s (kJ mol^{-1})	30		25
Contact resistance, R_c (Ω cm^2)		6	
$U_p(y)$, (V)	$-10.72y^4 + 23.88y^3 - 16.77y^2 + 2.595y + 4.563$ for $y \,\epsilon\, (0,1)$		
$U_n(x)$, (V)	$0.1493 + 0.8493\exp(-61.79x) + 0.3824\exp(-665.8x) - \exp(39.42x - 41.92) - 0.03131\tan^{-1}(25.59x - 4.099) - 0.009434\tan^{-1}(32.49x - 15.74)$ for $x \,\epsilon\, (0.3,1)$		

2.2.3 ESPM With Temperature Effect (ESPM-T)

The transfer function Eq. (2.56) is converted to a state space realization using observer canonical form [66] which produces seven ordinary differential equations (ODEs). For isothermal ESPM simulation at a particular temperature all the coefficients are constants and lsim in MATLAB simulates the test response. For non-isothermal case (ESPM-T) the coefficients are updated with cell temperature obtained from AutoLion-ST output and simulated using ode45.

$$\dot{\mathbf{x}}(t) = \mathbf{A}\mathbf{x}(t) + \mathbf{B}\mathbf{u}(t) \tag{2.57}$$

$$\mathbf{y}(t) = \mathbf{C}\mathbf{x}(t) + \mathbf{D}\mathbf{u}(t) \tag{2.58}$$

where $\dot{\mathbf{x}} = \frac{d\mathbf{x}}{dt}$, $\mathbf{x}\,\epsilon\,R^7$ is the state vector, $\mathbf{u}(t) = I(t)$ is the input vector, $\mathbf{y}(t) = [dV(t), dSOC(t)]^T$, is the output vector, $\mathbf{A}\,\epsilon\,R^{7\times7}$ is the state matrix, $\mathbf{B}\,\epsilon\,R^{7\times1}$ is the input matrix, $\mathbf{C}\,\epsilon\,R^{2\times7}$ is the output matrix, and $\mathbf{D}\,\epsilon\,R^{2\times1}$. The $SOC = SOC_i - \frac{1}{Q}\int_0^t I(\tau)\mathrm{d}\tau$, where Q is the nominal cell capacity.

For the gr/NCM chemistry simulated in this paper, most significant temperature dependent parameters are solid phase diffusion coefficient, exchange current density, electrolyte diffusion coefficient, electrolyte ionic conductivity, and electrolyte diffusional ionic conductivity. Arrhenius equation

$$\psi = \psi_{ref} \exp\left[\frac{E_{act,\psi}}{R}\left(\frac{1}{T_{ref}} - \frac{1}{T}\right)\right], \tag{2.59}$$

is used to calculate solid particle diffusion coefficient and exchange current density. The temperature dependent property ψ (*e.g.* $D_s^p, D_s^n,$ and i_0) depends on the reference value and the activation energy $E_{act,\psi}$. The empirical correlations for electrolyte properties are extracted from Val∅en *et al.* [67]:

$$D_e\,(T) = 10^{-\left[4.43+\frac{54}{T-\left(229+c_{e,0}\right)}+0.22c_{e,0}\right]}, \tag{2.60}$$

$$\kappa(T) = c_{e,0}[(-10.5+0.074T-6.96\times10^{-5}T^2)+c_{e,0}(0.668-.0178T-2.8\times10^{-5}T^2) + c_{e,0}^2(0.494-8.86\times10^{-4}T^2)]^2, \tag{2.61}$$

$$\kappa_{d,i} = \frac{2RT\kappa_i^{eff}}{F}\left(t_0^+ - 1\right)\left(1 + \frac{d\ln f_\pm}{d\ln c_e}\right) = -\frac{2RT\kappa_i^{eff}}{F}\left(t_0^+ - 1\right)\nu\left(T\right), \qquad (2.62)$$

where $\kappa_i^{eff} = \kappa\left(T\right)\varepsilon_i^{1.5}$ and subscript i denotes individual domain. The empirical correlation

$$\nu\left(T\right) = 0.601 - 0.24c_{e,0}^{\frac{1}{2}} + 0.982\left[1 - 0.0052(T - 293)\right]c_{e,0}^{\frac{3}{2}}. \qquad (2.63)$$

2.3 Results and Discussion

2.3.1 Comparison of SPM and ESPM With AutoLion-ST Under Isothermal Conditions

In this work, EC Power's AutoLion-ST is considered to be the truth model and used to compare the accuracy of reduced order SPM, ESPM, and ESPM-T. AutoLion-ST is a 1D, fully non-linear, finite volume based model in MATLAB/ SIMULINK. It uses robust numerical algorithms to simulate electrochemical and thermal interactions of Li-ion batteries over a wide range of operating conditions [68]. Figure 2.2(a) - (c) compare the SPM, ESPM and AutoLion-ST voltage responses at 25^oC and 50% initial SOC corresponding to the pulse current input in Fig. 2.2(e). The zoomed in Fig. 2.2(a) shows that the SPM response deviates significantly from the ESPM and AutoLion-ST voltage responses, even at lower C-rates. The ESPM voltage response, however, closely matches AutoLion-ST, including 20C-10 sec pulses (see zoomed view in Fig. 2.2(b)).

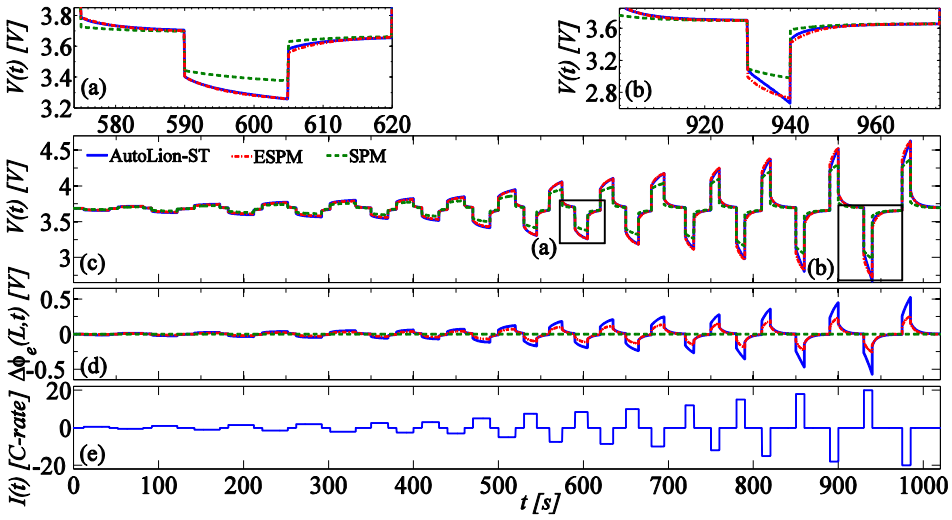

Figure 2.2. Voltage response of AutoLion-ST, ESPM and SPM at 25^oC and 50% initial SOC: (a) magnified voltage during $8.5C$ discharge pulse (left box in Fig. 2.2(c)), (b) magnified voltage during $20C$ discharge pulse (right box in Fig. 2.2(c)), (c) voltage response, (d) electrolyte potential difference, and (e) pulse current input.

Figure 2.2(d) shows the time response of the electrolyte potential $\Delta\phi_e(t) = \phi_e(L,t) - \phi_e(0,t)$ is strongly C-rate dependent. This internal variable can not be predicted by ECMs. The ESPM, however, is based on the fundamental equations of the cell and internal variables such as $\Delta\phi_e(t)$ can be predicted. The ESPM predicts electrolyte potential difference accurately at low C-rates but has almost 50% (314 mV) error at high C-rates. The quadratic concentration distributions and constant current distributions contribute into this error at higher C-rates. Although $\Delta\phi_e(t)$ is underpredicted by the ESPM it is a significant improvement over SPM which neglects electrolyte dynamics entirely.

One can tune the SPM contact resistance to account for the unmodeled electrolyte dynamics. At higher C-rates, however, the SPM voltage response overshoots the AutoLion-ST voltage response due to the neglect of electrolyte diffusion dynamics [29]. Although ESPM underpredicts $\Delta\phi_e(t)$ at higher C-rates, the ESPM's voltage accurately matches the AutoLion-ST's voltage (see Fig. 2.2(b)). Overprediction of overpotentials resulting from the linearization of the B-V kinetic equation compensates for the underpredicted $\Delta\phi_e(t)$. The maximum voltage error between the ESPM and AutoLion-ST is 3% (62 mV) for the 20C - 10 sec pulse.

2.3.2 Performance of the ESPM Away From the Linearized Point

To test the validity of the ESPM away from the linearization SOC, Fig. 2.3 simulates a hybrid current cycle operating in a larger 35 - 65% SOC window. Fig. 2.3(c) compares the voltage responses of the ESPM and AutoLion-ST for the current input shown in Fig. 2.3(e). Fig. 2.3(d) shows the corresponding SOC swing. Worst case scenarios at the highest and lowest SOCs are presented in the zoomed in Figs. 2.3(a) and 2.3(b), with 20C - 10 sec and 15C - 15 sec pulses, respectively. The voltage error increases with distance from the linearization point and increasing C-rate. The increased error is caused due the B-V linearization, OCP linearization, and constant properties assumptions (at 50% SOC) in the ESPM. Nevertheless, the maximum error between the ESPM and AutoLion-ST voltage responses remains less than 4.3% (137 mV) during the entire simulation.

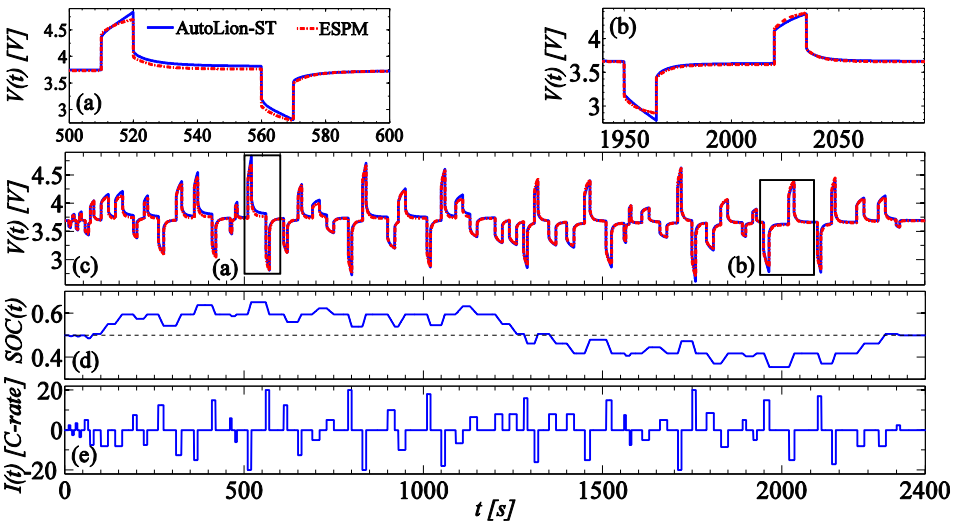

Figure 2.3. Voltage response of AutoLion-ST and ESPM at 25^oC and 50% initial SOC: (a) magnified voltage during $20C$ pulse (left box in Fig. 2.3(c)), (b) magnified voltage during $15C$ pulse (right box in Fig. 2.3(c)), (c) voltage response, (d) SOC, and (e) pulse current input.

2.3.3 Comparison of ESPM and ESPM-T With AutoLion-ST Under Non-isothermal Conditions

Figure 2.4 shows the influence of cell initial temperature on the voltage response by comparing the simulation results from ESPM, ESPM-T, and AutoLion-ST. The cell temperature, as predicted by AutoLion-ST starts at 10^oC and increases under adiabatic conditions to a temperature limit of 25^oC over the course of the simulation. The AutoLion-ST model includes a cooling system that prevents the cell temperature from exceeding 25^oC. The ESPM is isothermal at 25^oC and the ESPM-T temperature dependent physio-chemical properties are updated using the AutoLion-ST output temperature as one could use a temperature sensor on-board a vehicle. ESPM voltage response does not match the AutoLion-ST results at low temperature, even at very low C-rates. The highly nonlinear current distribution along each electrode due to sluggish reaction kinetics, reduced electrolyte diffusivity, and ionic conductivity may attribute the voltage difference at low temperatures. As the cell temperature approaches 25^oC, ESPM and ESPM-T produces identical voltage responses that closely match AutoLion-ST voltage response. The magnified Figs. 2.4(a) and 2.4(b) at 2.5C and 20C, respectively, show the relative agreement of these simulation methods. Overall, ESPM-T matches AutoLion-ST to within 3% for the entire 10^oC - 25^oC temperature range and up to 20C rates.

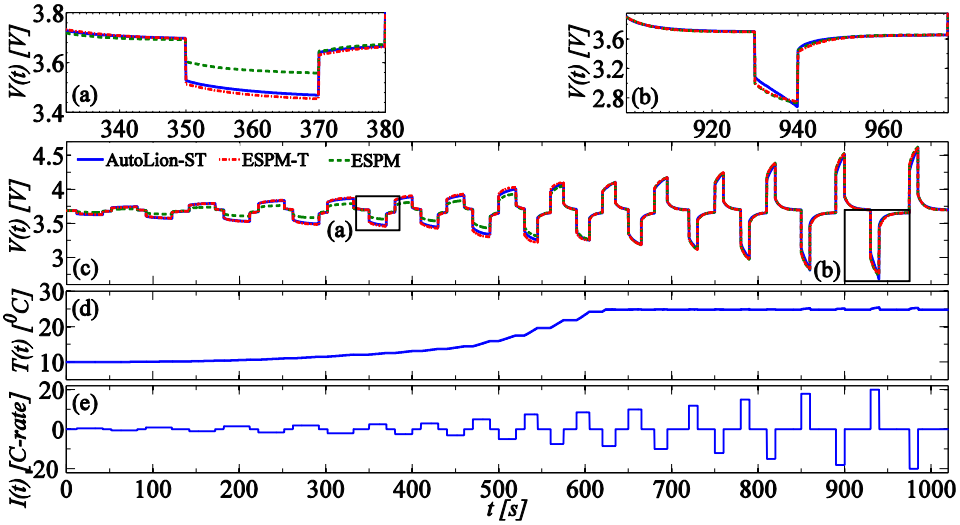

Figure 2.4. Voltage response of AutoLion-ST, ESPM-T and ESPM from 10^oC initial temperature and 50% initial SOC : (a) magnified voltage during 2.5C discharge pulse (left box in Fig. 2.4(c)), (b) magnified voltage during 20C discharge pulse (right box in Fig. 2.4(c)), (c) voltage response, (d) cell temperature, and (e) pulse current input.

2.3.4 Operating Range of ESPM-T

Figure 2.5 shows that the accuracy of the ESPM-T model depends on both current rate and temperature. In this simulation, the cell starts at 0^oC and, under adiabatic conditions, the temperature grows to 25^oC. Low temperature and low C-rate (t<200 sec) produces modest errors. Moderate C-rates at low temperatures produce large errors and high C-rates at higher temperatures produce the least errors.

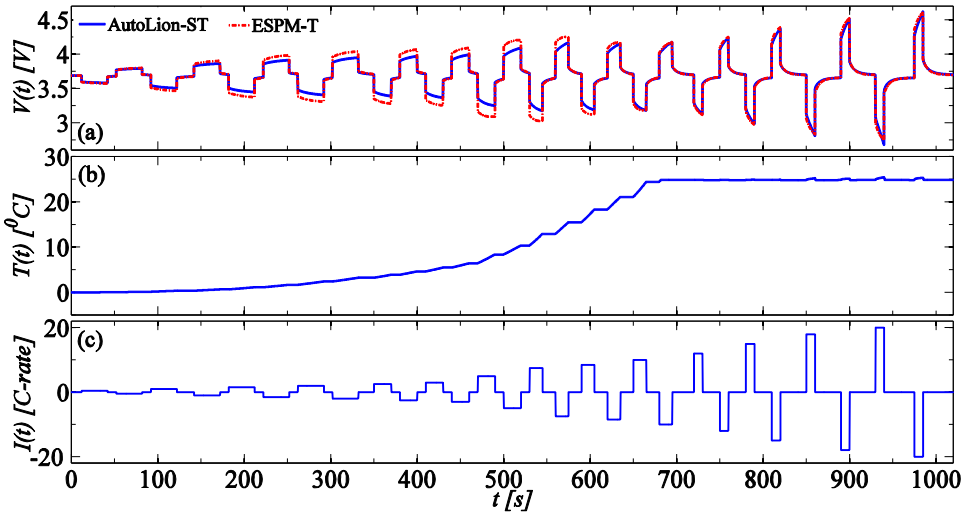

Figure 2.5. Voltage response of AutoLion-ST and ESPM-T from 0^oC and 50% initial SOC: (a) voltage response, (b) cell temperature, and (c) pulse current input.

To identify the working range of ESPM-T, we separate the C-rate and temperature effects by simulating constant hybrid pulse cycles at different temperatures. The temperature range is from -10^oC to 50^oC for 1C, 2C, 5C, 7.5C, 10C, and 12.5C constant hybrid 30 sec pulse cycles. Figure 2.6 shows an example case of adiabatic simulation of 7.5C - 30 sec pulse charge-discharge cycle. As the cell temperature increases with time, the initial voltage error between the AutoLion-ST and ESPM-T diminishes.

Figure 2.7 summarizes the maximum voltage error relative to AutoLion-ST at different C-rates versus cell temperature. Each curve is for a different C-rate pulse cycle as shown in Fig. 2.6(c). As the cell warms up due to cycling, the temperature increases and the maximum voltage error for the corresponding pulse is evaluated. The error eventually decreases with increasing temperature and decreasing C-rate, although the error increases slightly for $T > 25^oC$ due to slight asymmetry between

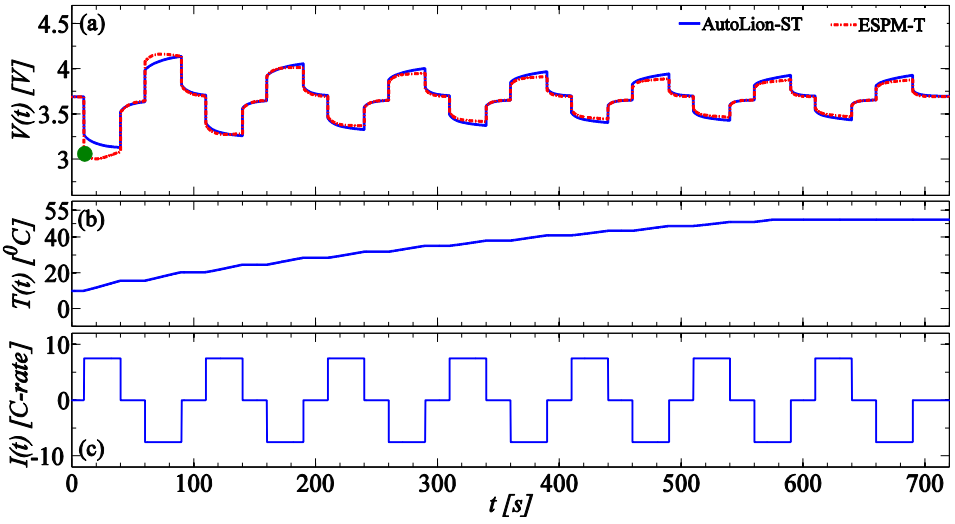

Figure 2.6. Voltage response of AutoLion-ST and ESPM-T from 10^oC and 50% initial SOC: (a) voltage response, (b) cell temperature, and (c) 7.5C hybrid pulse charge-discharge cycle.

Table 2.2. Computation time of different Li-ion cell models

Li-ion cell model	Solver	Computation time (s)
AutoLion-ST	Non-linear solver	12.5
ESPM-T	ode45	2.5
ESPM	lsim	1.05
SPM	lsim	1

charge and discharge voltage errors. To maintain errors less than 1% requires $T > 17^oC$ and $I < 5C$. If 5% errors are acceptable then 12.5C is possible for $T > 25^oC$ and 1C for $T > -10^oC$. The green solid dot in Fig. 2.7 corresponds to the green solid dot in Fig. 2.6(a).

Computation time of a 20 min simulation at 1 Hz sampling rate on an Intel^R Core^{TM} 2 Quad 2.4 GHz desktop computer of AutoLion-ST and other reduced order models are shown in Table 2.2. ESPM and ESPM-T models are respectively 11.9 and 5 times faster than AutoLion-ST in this case.

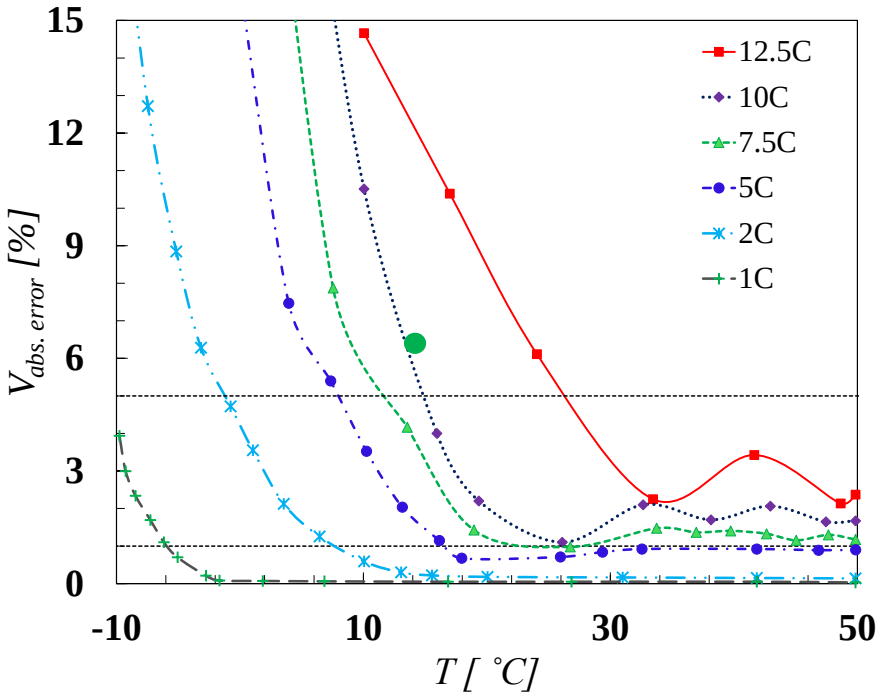

Figure 2.7. ESPM-T error relative to AutoLion-ST for different C-rate pulse cycles (see Fig. 2.6(c)) versus cell temperature. The green solid dot corresponds to the dot in Fig. 2.6(a).

2.4 Conclusions

The traditional SPM neglects electrolyte diffusion only provides satisfactory performance over narrow C-rate and temperature ranges. Using only seven states, the ESPM developed in this paper includes an IMA model of electrolyte diffusion and matches the AutoLion-ST pulse response up to 20C at room temperature with 3% (62 mV) error. The ESPM linearized at 50% SOC, has slightly higher voltage error (4.3%/137 mV) for wider SOC swing (35 - 65%). The ESPM-T model updates the ESPM parameters with temperature, maintaining the voltage response to pulse charge-discharge current inputs to within 5% of the AutoLion-ST for $25^oC < T < 50^oC$ at 12.5C and $-10^oC < T < 50^oC$ at 1C.

Chapter 3
State of Charge Estimation of a Lithium Ion Cell Based on A Temperature Dependent, Electrolyte Enhanced, Single Particle Model

3.1 Introduction

State of charge (SOC) estimation provides critical information to system engineers and end users of consumer electronics to electric vehicles. The accuracy of model-based SOC estimation depends on the accuracy of the underlying model, including temperature effects that greatly influence cell dynamics. This chapter uses a 7^{th} order, linear, electrolyte enhanced, single particle model (ESPM) as the basis for a Luenberger SOC observer for a lithium ion cell. Isothermal and non-isothermal simulations compare the SOC from a commercially-available finite volume code and the SOC estimate for a wide range of temperature ($0 \leq T \leq 50\ ^oC$) and pulse C-rates ($|I| \leq 15C$). Arrhenius relationships between the ESPM model parameters and the sensed temperature improve SOC estimation. At low temperature ($T < 10^oC$) and low C-rates, temperature measurement reduces the RMS SOC estimation error by up to ten times. At high temperature $T \geq 40^oC$ and high C-rates ($|I| \leq 15C$), temperature measurement decreases SOC estimation error by more than three

times.

3.2 Model-Based Luenberger State Estimator Design

Figure 3.1 shows a block diagram of a Luenberger observer for cell state estimation. The cell dynamics are represented in state-variable form (Eqs. (2.57) - (2.58)). $V(t)$ is the measured cell voltage from an actual battery pack. For the present study, AutoLion-ST provides the voltage, current, and temperature data in place of an actual cell.

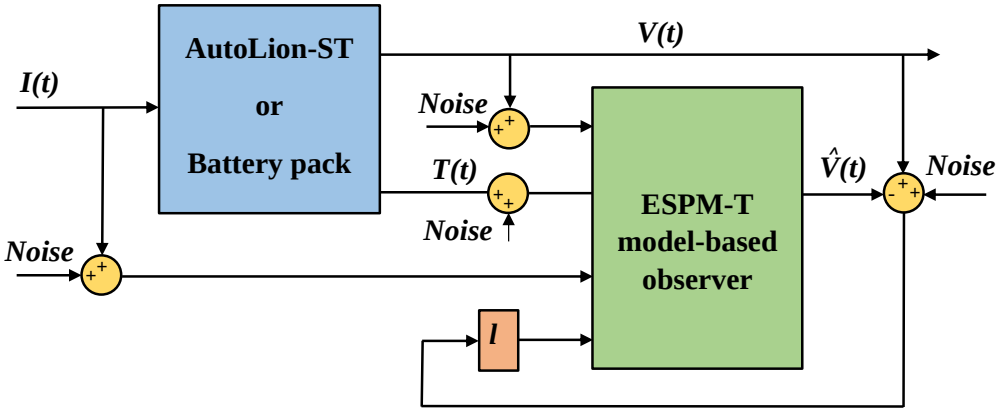

Figure 3.1. Block diagram of the Luenberger SOC estimator

The state estimator equations are

$$\dot{\hat{\mathbf{x}}}(t) = \mathbf{A}(T)\hat{\mathbf{x}}(t) + \mathbf{B}(T)\mathbf{u}(t) + \mathbf{l}(\mathbf{y} - \hat{\mathbf{y}}), \tag{3.1}$$

$$\hat{\mathbf{y}}(t) = \mathbf{C}(T)\hat{\mathbf{x}}(t) + \mathbf{D}(T)\mathbf{u}(t), \tag{3.2}$$

where $\hat{\mathbf{x}}$ is the state estimate, the observer gain matrix is $\mathbf{l}\,\epsilon\,R^{7\times1}$, and error $\mathbf{e}(t) = \mathbf{x}(t) - \hat{\mathbf{x}}(t)$. The feedback term, $\mathbf{l}(\mathbf{y} - \hat{\mathbf{y}})$ in the estimator equations compensate for model mismatch and noise. When the actual and estimated outputs differ due to different initial conditions, sensor noise, and model mismatch, then

there is a correction term and the estimator tends to reduce the error.

If the estimator and the cell have the same dynamics, initial conditions, and input, then the estimated state (and voltage) will perfectly track the actual state. The convergence is guaranteed if the model and the experimental system are identical, there is no sensor noise, and the gain matrix $\mathbf{l}$ is chosen to place the poles of $(\mathbf{A} - \mathbf{l}\mathbf{C}^T)$ in the left half of the complex plane.

3.3 Results and Discussion

HEVs require high C-rate charge-discharge pulses to assist a vehicle within a strict SOC window [56]. Considering that, a 1020 sec hybrid pulse current input with a maximum C-rate of ±20C is simulated for a high power 1.78 Ah Li-ion cell. The ESPM and ESPM-T-based observer's performance are compared with AutoLion-ST. The accurate estimation ranges of ESPM and ESPM-T-based observers are identified in terms of temperature and C-rates.

The AutoLion-ST outputs are current, voltage, and temperature. ESPM and ESPM-T-based observers use these voltage and current (and temperature for ESPM-T) measurements to estimate the SOC. The hybrid current pulse profile in Fig. 3.2(g) is charge conserving and operating around 50% SOC. Current and voltage noise of 100 mA and 10 mV, respectively, are added. The observer gain matrix, $\mathbf{l} = [l_1, l_2, l_3, l_4, l_5, l_6, l_7]^T$ is tuned manually to obtain a reasonably fast transient decay and low steady state SOC error and the same for all the simulations in this study.

3.3.1 Isothermal Simulation

Figure 3.2 compares the voltage and SOC estimates of the ESPM-based Luenberger observer with AutoLion-ST response at a representative temperature of 25^oC. The magnified views of the voltage response in Figs. 3.2(a) and 3.2(b) at low and high C-rates, respectively, show very good agreement between the observer response and the AutoLion-ST voltage response. The insertion of electrolyte dynamics in the ESPM model significantly improves the performance relative to the traditional SPM that considers the electrolyte as a static resistor, resulting in voltage overshoots at higher C-rates [29]. The zoomed in Figs. 3.2(c) and 3.2(d) of the SOC plot (Fig.

3.2(f)) show the initial transient and steady state performance, respectively. The SOC error diminishes quickly $< 2.0\%$ within 200 sec from an initial estimator SOC error of 25%. During the most aggressive part (700 sec to 950 sec) of the hybrid cycle, the maximum SOC error is $< 3.1\%$.

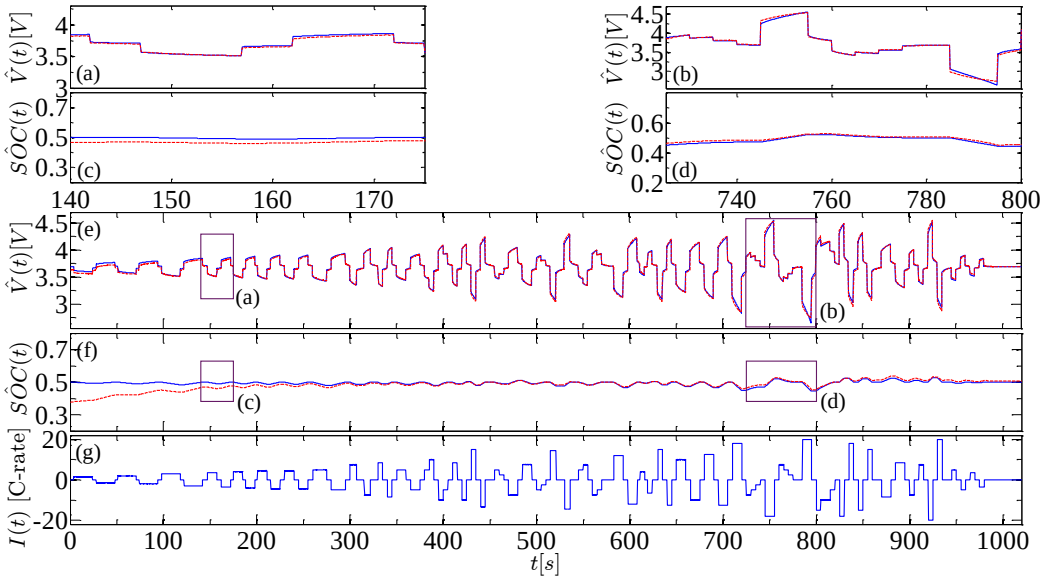

Figure 3.2. Isothermal ESPM-based observer response (red-dashed) and AutoLion-ST simulation (blue-solid) from a 25% initial SOC error at 25^oC temperature: (a) magnified voltage during 3.5C pulse (left box in Fig. 3.2(e)), (b) magnified voltage during 20C pulse (right box in Fig. 3.2(e)), (c) magnified observer SOC transients (left box in Fig. 3.2(f)), (d) magnified observer SOC at steady state (right box in Fig. 3.2(f)), (e) estimated voltage response, (f) estimated SOC, and (g) pulse current input.

3.3.2 Non-isothermal Simulation

Figure 3.3 compares the ESPM-based observer, ESPM-T-based observer, and AutoLion-ST voltage and SOC response for an adiabatic simulation of the hybrid cycle starting from 0^oC to 50^oC. An external cooling loop in AutoLion-ST regulates the cell temperature at 50^oC for t>700 sec. The temperature output of the AutoLion-ST is fed into the ESPM-T-based observer to update the state matrices. The ESPM estimator has constant state matrices corresponding to 25^oC.

The ESPM-based estimator's voltage response significantly undershoots and overshoots at low and high temperatures as shown in Figs. 3.3(a) and 3.3(b), respectively. Thus, the ESPM-based SOC estimate is poor at temperatures away from the set point of 25^oC. ESPM-T updates the temperature dependent battery parameters and is much more accurate through out the temperature range for low C-rates at the beginning of the cycle. At high C-rates and low temperature (100-350 sec), however, the ESPM-T estimated voltage overshoots the actual voltage. This is due to the unmodeled distributed current within the electrodes and sluggish reaction kinetics at low temperature and high C-rates. The ESPM-T-based estimator's initial transients decay within 200 sec. Once the battery warms up due to self heating, the ESPM-T-based observer estimates the AutoLion-ST's voltage response very well up to 50^oC and tracks the actual SOC (Figs. 3.3(c) and 3.3(d)) within a maximum error of 2.7% during that most aggressive part of the hybrid cycle. The ESPM observer, however, fails to provide accurate SOC estimate at higher temperature as shown in Figs. 3.3(b) and 3.3(d).

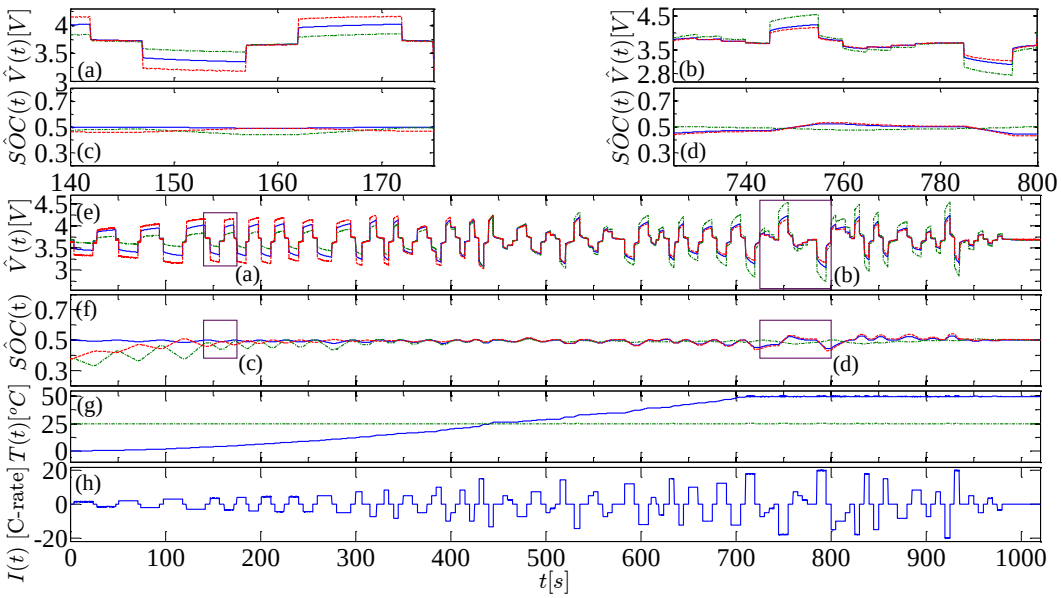

Figure 3.3. ESPM estimates (green-dot-dashed), ESPM-T estimates (red-dashed), and adiabatic AutoLion-ST simulation (blue-solid) from a 25% initial SOC error: (a) magnified voltage during 3.5C pulse (left box in Fig. 3.3(e)), (b) magnified voltage during 20C pulse (right box in Fig. 3.3(e)), (c) magnified observer SOC transients (left box in Fig. 3.3(f)), (d) magnified observer SOC at steady state (right box in Fig. 3.3(f)), (e) voltage, (f) SOC, (g)temperature, and (h) pulse current input.

3.3.3 Accurate Estimation Ranges

The previous simulations show that estimation accuracy depends on C-rate and temperature. To further study these effects, we simulate a constant hybrid pulse cycle at different temperatures with zero initial estimator error and calculate the root-mean squares (RMS) error. The RMS error gives a good measure of the steady state error of the estimator. The temperature ranges from 0^oC to 50^oC for 1C to 15C constant 20 sec pulses are considered. Fig. 3.4 shows an example 1200 sec long, 20sec-10C pulse charge-discharge cycle used to develop Figs. 3.5 and 3.6. The cell is power limited at low temperatures and high C-rates so those cases are not included.

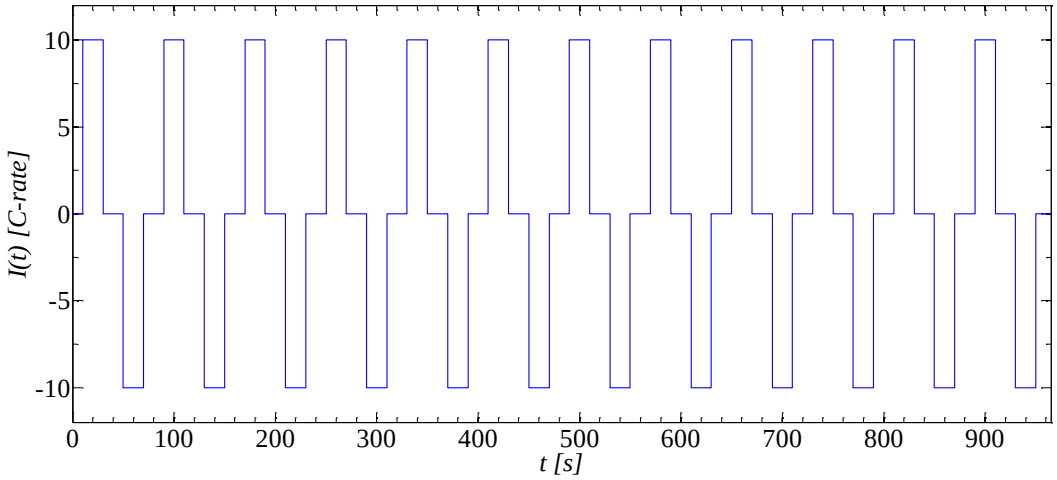

Figure 3.4. Hybrid pulse charge-discharge cycle used to create Figs. 3.5 and 3.6 (10C-rate)

Figure 3.5 shows the RMS error contour plot for the ESPM-based SOC estimator. The ESPM-based estimator operates at a constant 25^oC whereas the AutoLion-ST's temperature is changing due to adiabatic operation. The highly accurate region with less than 1% error is at low C-rate and near room temperature (25^oC). If battery operates further away from 25^oC and higher C-rate's, significant SOC estimation error is introduced.

Figure 3.6 shows the ESPM-T SOC estimation error contour plot versus battery temperature and C-rate. Besides voltage, ESPM-T-based estimator also uses battery temperature (see Fig. 3.1) to correct the model mismatch which reduces the estimation error. Unlike ESPM-based estimator (Fig. 3.5), the highly accurate region in Fig. 3.6 grows considerably for ESPM-T-based estimator. High temperature performance is specially very good, staying less than 3% for the entire high temperature range and C-rates. Cold temperature remain a problem at high C-rates. Overall, the ESPM-T estimator outperforms the ESPM estimator at low temperatures and C-rates by up to ten times. At high temperatures, the ESPM-T estimator is more than three times accurate.

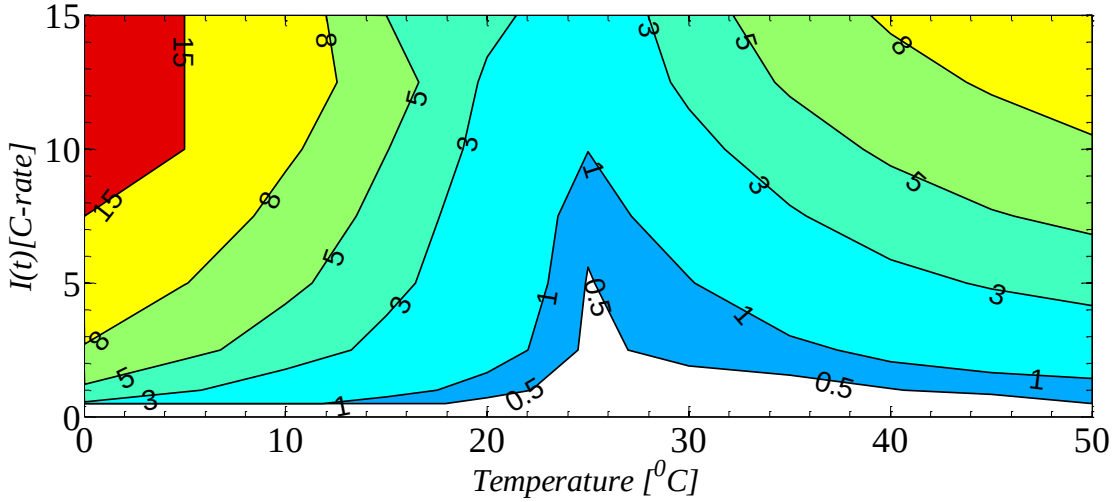

Figure 3.5. RMS SOC error of the ESPM-based observer at different operating temperatures of the AutoLion-ST

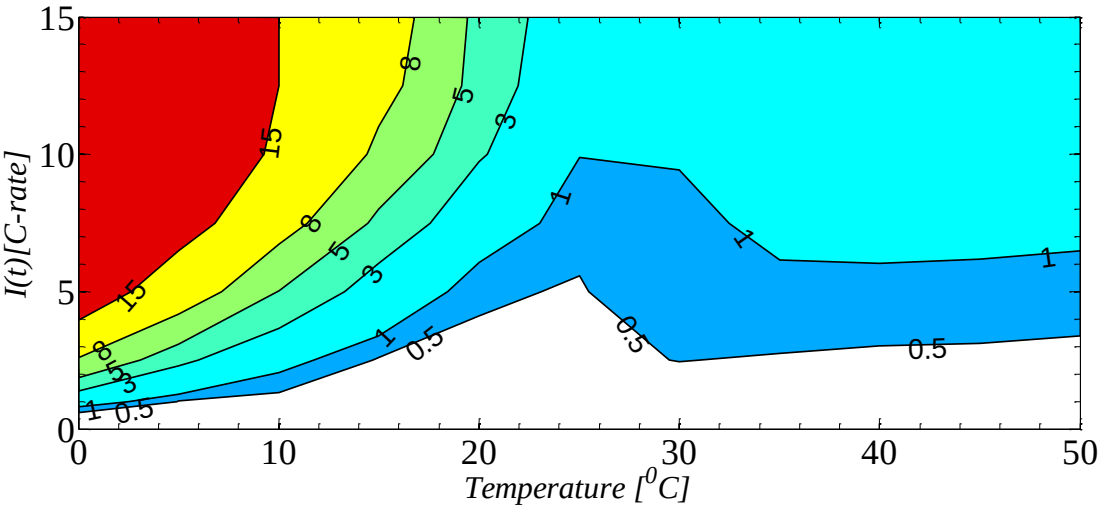

Figure 3.6. RMS SOC error of the ESPM-T-based observer at different operating temperatures of the AutoLion-ST

3.4 Conclusions

The ESPM-based observer is capable of estimating only room temperature battery SOC for aggressive HEV current inputs. Inclusion of the temperature effect in the ESPM-T model is shown to be crucially important for accurate SOC estimation in scenarios where cell temperature varies during usage. Temperature updating of the estimator state matrices provides improved SOC estimation over a wide range of temperature and C-rates. At low temperature ($< 10^oC$) and low C-rate (<0.5C), temperature measurement reduces the RMS SOC estimation error by up to ten times. For T>40^oC and $|I| \leq 15C$, temperature measurement decreases SOC estimation error by more than three times.

Chapter 4
A Nonlinear Electrolyte Enhanced Single Particle Model

4.1 Introduction

Electric Vehicle (EV) current profiles are dynamic, consisting of repeated charge and discharge pulses, and swing between a wider SOC window (95-20%). Accurate prediction of the battery response to these inputs requires models with open circuit voltage and Butler-Volmer (B-V) kinetic nonlinearities. This chapter derives a nonlinear, electrolyte-enhanced, single particle model (NESPM).The model is validated with experimental full charge, discharge, and HEV cycle from a 4.5 Ah high power and 20 Ah high energy graphite/$LiFePO_4$ cells. The NESPM is capable of operating up to $3C$ constant charge-discharge cycles and up to 25C and 10sec charge-discharge pulses within 35-65% state of charge (SOC) with less than 2% error for the 4.5 Ah high power cell. For the 20 Ah high energy cell the NESPM model is capable of operating up to $2C$ constant charge-discharge cycles and up to 10C and 10 sec charge-discharge pulses within 30-90% SOC window with 3.7% maximum error.

4.2 Nonlinear Single Particle Model with Electrolyte Diffusion Effect (NESPM) for a Graphite/$LiFePO_4$ Cell

Lithium Iron Phosphate (LFP) cathode-based Li-ion batteries possess high temperature abuse tolerance, low cost, and an environmentally benign nature [32, 33]. LFP cathodes are extremely stable due to their olivine crystalline structure.

The intercalation/deintercalation processes in LFP is thought to occur through a two phase process between a Li-poor $Li_{\epsilon}FePO_4$ phase and a Li-rich $Li_{1-\epsilon'}FePO_4$ phase [37–39]. Srinivasan and Newman [37] develop a core-shell model initially proposed by Padhi *et al.* [32] with a growing shell of $LiFePO_4$ (Li-rich phase) on a shrinking $FePO_4$ (Li-poor phase) core during discharge. This core-shell model is improved by other researchers [40–42] through tracking of multiple two-phase boundaries for repeated charge-discharge cycles but the simulation is complicated and computationally demanding. A relatively simplified phase-change diffusivity model is proposed by Thorat [43]. A phase-field model, based on the Cahn-Hilliard theory is also reported for the LFP electrode [44]. Interestingly, some recent studies also claim that the two distinct phase processes during lithiation/delithiation in a LFP cathode occur only at low currents. Large currents suppress the phase transformation [45–47] in the LFP cathode. It is also reported that LFP active material shows resistive reactant property which attributes in increasing cell impedance as charge or discharge proceeds [48, 49].

Motivated by the need of fast and accurate physics based model for offline analysis and online BMS application, this chapter extends the previous electrolyte enhanced SPM (ESPM) by incorporating non-linearities arising from the B-V kinetics and open circuit potential (OCP) of the individual electrode. The NESPM is validated against experimental constant C-rate charge-discharge and hybrid current profiles. A 4.5 Ah high power and a 20 Ah high energy gr/LFP cells are selected to conduct the experimental validations. A validated NESPM is a prerequisite of an aging model which will be discussed in chapter 5.

Table 4.1. Governing equations of a pseudo 2D Li-ion cell model.

Equations		Boundary conditions
Conservation of Li^+ in solid: $\frac{\partial c_s}{\partial t} = \frac{D_s}{r^2}\frac{\partial}{\partial r}\left(r^2 \frac{\partial c_s}{\partial r}\right)$	(4.1)	$\left(\frac{\partial c_s}{\partial r}\right)_{r=0} = 0,\ \left(D_s \frac{\partial c_s}{\partial r}\right)_{r=R_s} = \frac{-j^{Li}}{a_s F}$
Conservation of charge in solid: $\sigma^{eff}\frac{\partial^2 \phi_s}{\partial x^2} = j^{Li}$	(4.2)	$-\left(\sigma^{eff}\frac{\partial \phi_s}{\partial x}\right)_{x=0} = \left(\sigma^{eff}\frac{\partial \phi_s}{\partial x}\right)_{x=L} = \frac{I}{A}$ $\left(\frac{\partial \phi_s}{\partial x}\right)_{x=L_n} = \left(\frac{\partial \phi_s}{\partial x}\right)_{x=L_n+L_s} = 0$
Conservation of Li^+ in electrolyte : $\varepsilon_e \frac{\partial c_e}{\partial t} = D_e^{eff}\frac{\partial^2 c_e}{\partial x^2} + \frac{1-t_+^0}{F} j^{Li}$	(4.3)	$\left(\frac{\partial c_e}{\partial x}\right)_{x=0} = 0,\ \left(\frac{\partial c_e}{\partial x}\right)_{x=L} = 0$
Conservation of charge in electrolyte: $\kappa^{eff}\frac{\partial^2 \phi_e}{\partial x^2} + \kappa_d^{eff}\frac{\partial^2 c_e}{\partial x^2} + j^{Li} = 0$	(4.4)	$\left(\frac{\partial \phi_e}{\partial x}\right)_{x=0} = 0,\ \left(\frac{\partial \phi_e}{\partial x}\right)_{x=L} = 0$
Butler-Volmer (B-V) kinetics:	$j^{Li} = a_s i_0 \left[\exp\left(\frac{\alpha_a F \eta}{RT}\right) - \exp\left(\frac{-\alpha_c F \eta}{RT}\right)\right]$	(4.5)
Overpotential:	$\eta = \phi_s - \phi_e - U(c_{s,e})$	(4.6)
Cell voltage:	$V(t) = \phi_s(L,t) - \phi_s(0,t) - \frac{Rc}{A} I(t)$	(4.7)

4.3 Electrochemical Model

The fundamental governing equations of a Li-ion cell are listed in Table 4.1. Conservation of Li-ion (Li^+) and conservation of charge (e^-) in both the solid and electrolyte phases (Eq. (4.1)- Eq. (4.4)) govern the electrochemical dynamics of a Li-ion cell. The nonlinear B-V kinetic Eq. (4.5) couples the four field variables $c_{s,e}$, c_e, ϕ_s and ϕ_e representing solid particle surface concentration, electrolyte concentration, solid phase potential, and electrolyte phase potential, respectively. Overpotential in Eq. (4.6) drives the electrochemical reaction rate. Finally, the cell voltage can be evaluated from Eq. (4.7).

4.4 Derivation of the Reduced Order NESPM

The assumptions to derive the NESPM are: (i) infinite solid phase conductivity in the individual electrodes resulting in no ohmic loss in the solid electrode matrix, (ii) uniform current distribution in the individual electrode, (iii) the active material particles within each electrode are assumed to be in parallel and thus a single particle in each electrode is used to solve the associated solid phase diffusion equations, and (iv) all properties are evaluated at average electrolyte concentration at 50% SOC. Assuming infinite solid phase conductivity, Eq. (4.2) simplifies by integrating in each electrode domain to obtain the uniform current distributions

$$\frac{J_n^{Li}}{I(s)} = \frac{1}{A_n L_n}, \tag{4.8}$$

$$\frac{J_p^{Li}}{I(s)} = -\frac{1}{A_p L_p}, \tag{4.9}$$

where $J_n^{Li}(s) = \frac{1}{L_n}\int_0^{L_n} J^{Li}(x,s)\mathrm{d}x$ and $J_p^{Li}(s) = \frac{1}{L_p}\int_{L_n+L_s}^{L} J^{Li}(x,s)\mathrm{d}x$. Subscripts/superscripts 'n', 's', and 'p' represent negative, separator, and positive electrodes, respectively. Capital letters indicate Laplace transformed variables.

Taking the Laplace transformation of Eq. (4.1) and applying the associated boundary conditions provides a transcendental transfer function [60] of solid particle surface Li concentration $c_{s,e}$ in both electrodes. This transcendental transfer function is discretized using a 3^{rd} order Padé approximation [61] to produce

$$\frac{C_{s,e}^n(s)}{I(s)} = \frac{-21\left[\frac{s^2}{a_s^n F A_n R_s^n L_n} + \frac{60 D_s^n s}{a_s^n F A_n [R_s^n]^3 L_n} + \frac{495[D_s^n]^2}{a_s^n F A_n [R_s^n]^5 L_n}\right]}{s^3 + \frac{189 D_s^n}{[R_s^n]^2} s^2 + \frac{3465[D_s^n]^2}{[R_s^n]^4} s}, \tag{4.10}$$

$$\frac{C_{s,e}^p(s)}{I(s)} = \frac{21\left[\frac{s^2}{a_s^p F A_p R_s^p L_p} + \frac{60 D_s^p s}{a_s^p F A_p \left[R_s^p\right]^3 L_p} + \frac{495\left[D_s^p\right]^2}{a_s^p F A_p \left[R_s^p\right]^5 L_p}\right]}{s^3 + \frac{189 D_s^p}{\left[R_s^p\right]^2} s^2 + \frac{3465\left[D_s^p\right]^2}{\left[R_s^p\right]^4} s}, \tag{4.11}$$

where $a_s = \frac{3\varepsilon}{R_s}$ is specific interfacial area, F is Faraday constant, and the other parameters are given in Table 4.2 and Table 4.3 for the high power and high energy cells, respectively.

Table 4.2. Model parameters of the commercial 4.5 Ah high power gr/LFP Li-ion cell [67, 69]

Parameter	Neg. electrode	Separator	Pos. electrode
Thickness, L (cm)	3.40×10^{-3}	2.50×10^{-3}	7.0×10^{-3}
Particle radius, R_s (cm)	3.5×10^{-4}		3.65×10^{-6}
Active material volume fraction, ε_s	0.55		0.41
Porosity (electrolyte phase volume fraction), ε_e	0.332	0.4	0.33
Maximum solid phase concentration, $c_{s,max}$ (mol cm^{-3})	31.07×10^{-3}		22.806×10^{-3}
Stoichiometry at 0% SOC, $x_{0\%}$, $y_{0\%}$	0		0.76
Stoichiometry at 100% SOC, $x_{100\%}$, $y_{100\%}$	0.80		0.03
Average electrolyte concentration, $c_{e,avg}$ (mol cm^{-3})		1.2×10^{-3}	
Exchange current density, $i_{0,ref}$ (A cm^{-2})	$^{*}1.85 \times 10^{-4}$		$^{*}8.18 \times 10^{-5}$
Activation energy of i_0 (kJ mol^{-1})	$^{*}40$		$^{*}25$
Charge transfer coefficient, α_a, α_c	0.5, 0.5		0.5, 0.5
Li^+ transference number, t_0^+		0.38	
Solid phase Li diffusion coefficient, $D_{s,ref}$ (cm^2 s^{-1})	$^{**}5.29\times10^{-11}$		1.18×10^{-14}
Activation energy of D_s (kJ mol^{-1})	4		20
Area, A (cm^2)	3580		3487
Contact resistance, R_c (Ω cm^2)		6	

* Tuned,** Estimated

Assuming symmetric anodic and cathodic reaction charge transfer coefficients ($\alpha_a = \alpha_c$), the nonlinear B-V Eq. (4.5) is inverted to obtain

$$\eta_n = \frac{RT}{\alpha_n F} \sinh^{-1}\left(\frac{j_n^{Li}}{2a_s^n i_0^n}\right), \tag{4.12}$$

$$\eta_p = \frac{RT}{\alpha_p F} \sinh^{-1}\left(\frac{j_p^{Li}}{2a_s^p i_0^p}\right). \tag{4.13}$$

The cell voltage

Table 4.3. Model parameters of the commercial 20 Ah high energy gr/LFP Li-ion cell

Parameter	Neg. electrode	Separator	Pos. electrode
Thickness, L (cm)	3.91×10^{-3}	2.50×10^{-3}	8.05×10^{-3}
Particle radius, R_s (cm)	10.15×10^{-4}		10.5×10^{-6}
Active material volume fraction, ε_s	0.57		0.43
Porosity (electrolyte phase volume fraction), ε_e	0.332	0.4	0.33
Maximum solid phase concentration, $c_{s,max}$ (mol cm^{-3})	31.07×10^{-3}		22.806×10^{-3}
Stoichiometry at 0% SOC, $x_{0\%}$, $y_{0\%}$	0		0.76
Stoichiometry at 100% SOC, $x_{100\%}$, $y_{100\%}$	0.80		0.03
Average electrolyte concentration, $c_{e,avg}$ (mol cm^{-3})		1.2×10^{-3}	
Exchange current density, $i_{0,ref}$ (A cm^{-2})	$^{*}2.05 \times 10^{-4}$		$^{*}8.73 \times 10^{-5}$
Activation energy of i_0 (kJ mol^{-1})	$^{*}40$		$^{*}25$
Charge transfer coefficient, α_a, α_c	0.5, 0.5		0.5, 0.5
Li^+ transference number, t_0^+		0.38	
Solid phase Li diffusion coefficient, $D_{s,ref}$ (cm^2 s^{-1})	$^{*}24.0\times10^{-11}$		$^{*}3\times10^{-14}$
Activation energy of D_s (kJ mol^{-1})	4		20
Area, A (cm^2)	13762		13048
Contact resistance, R_c (Ω cm^2)		5.25	

* Tuned

$$V(t) \;=\; \eta_p(L,t) - \eta_n(0,t) + \Delta\phi_e(L,t) + U_p(c^p_{s,e}) - U_n(c^n_{s,e}) - \frac{R_c}{A}I(t), \quad (4.14)$$

where R_c (Ωcm^2) is the contact resistance. U_p and U_n are the open circuit potentials (OCPs) of the positive and negative electrodes, respectively, and can be found from the empirically measured OCP [69]. Electrolyte dynamics is solved using the IMA approximation method and discussed in detail in chapter 2.

4.5 Results and Discussion

Commercial 4.5 Ah high power cylindrical cells and 20 Ah high energy pouch cells were selected to carry out the experimental validations of the NESPM. Arbin BT-2000 battery cycler ($\pm 200A/20V$) is used to conduct the standard capacity and hybrid current tests. The capacity at $1C$ rate was measured in four steps: (1) charging to 3.6V at 1C constant current; (2) holding a constant voltage at 3.6V until the current dropped to C/20; (3) resting for 30 mins; (4) discharging at $1C$ rate to a cut-off voltage of 2.0V; (5) resting for 30 mins. The steps followed to conduct the hybrid current tests are : (1) charging to 3.6V at 1C constant current; (2) holding a constant voltage at 3.6V until the current dropped to C/20; (3) resting for 30 mins; (4) discharging at $1C$ rate to the desired SOC;(5) resting for 1hr; (6) starting the hybrid current test.

4.5.1 Experimental Validation With Constant Charge and Discharge Currents

Figures (4.1) and (4.2) compare the voltage responses of the experiments and NESPM simulations at 22^0C ambient temperature with constant current charge-discharge at 0.1C to 3C for the 4.5 Ah and 20 Ah gr/LFP cells. The conventional SPM without electrolyte dynamics performs well up to 1C rate for high power cells and up to 0.5C rate for high energy cells [70]. Adding the IMA approximated electrolyte dynamics, non-linear B-V kinetics and OCPs with the SPM extends the NESPM's operating range up to constant 3C charge-discharge currents for the 4.5 Ah high power cell. The voltage response with the NESPM for the high energy 20 Ah cell matches very well up to 2C charge-discharge rates. NESPM matches the experimental voltage response very well during the mid SOC operating range. The experimental voltage responses at the end of charge and discharge cycles do not match the NESPM as well, possibly due to the simplifying assumptions in the NESPM model. Operating the battery at very high/low SOC is usually avoided in vehicle applications due to the sharp voltage changes.

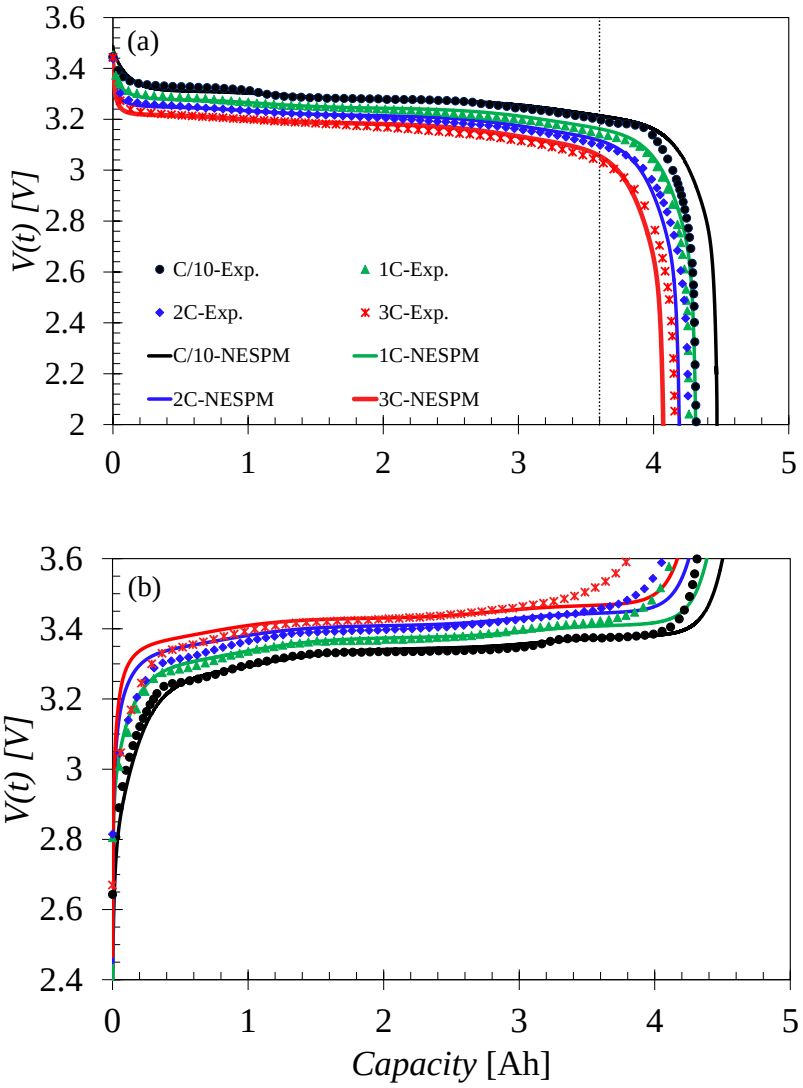

Figure 4.1. Experimental and NESPM voltage responses of a 4.5 Ah gr/LFP cell at 22^oC ambient temperature: (a) discharge, (b) charge. Vertical dotted line in Figure 4.1(a) is showing 80% of nominal capacity (3.6 Ah) line.

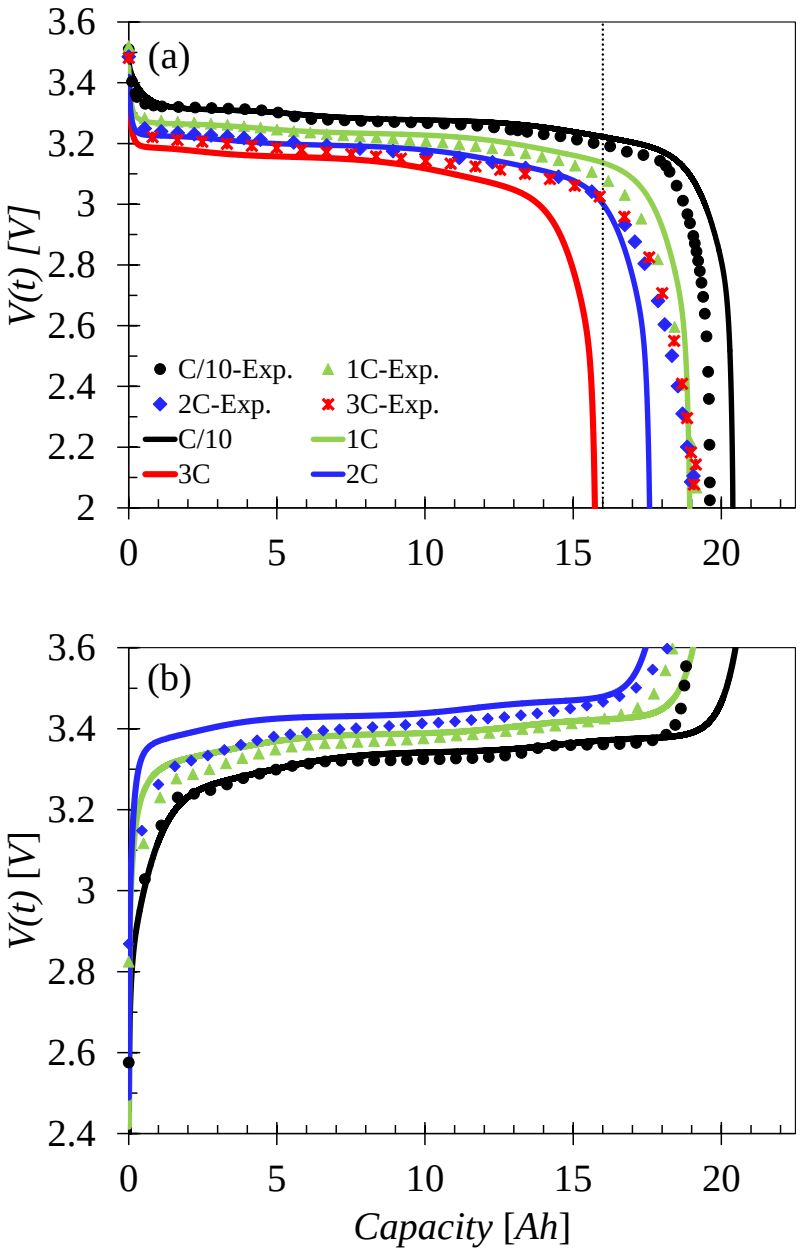

Figure 4.2. Experimental and NESPM voltage responses of a 20 Ah high energy gr/LFP cell at 22^oC ambient temperature: (a) discharge, (b) charge. Vertical dotted line in Figure 4.2(a) is showing 80% of nominal capacity (16 Ah) line.

4.5.2 Experimental Validation With Hybrid Current Profile

Figures 4.3(a)-(c) compare the conventional SPM without electrolyte dynamics, NESPM, and experimental voltage responses of the high power 4.5 Ah cell corresponding to the charge sustaining hybrid current input profile in Fig. 4.3(e). The hybrid pulse train contains up to 25C and 10 sec charge and discharge pulses and swings between 35-65% SOC (see Fig. 4.3(c)), typical of HEV applications. The cell rested for 1 hr to reach electrochemical and thermal equilibrium at an ambient 22^oC before starting the pulse current test. The cell surface temperature increases to 33^oC at the end of the hybrid cycle due to self heating. The SPM and NESPM models are, however, simulated at an average 30^oC. The zoomed in Fig. 4.3(a) shows that the SPM response deviates significantly from the NESPM and experimental voltage responses, even at lower C-rates ($\pm$7.5C). One can tune the contact resistance in the SPM to obtain a good voltage match at low C-rates but that would introduce significant voltage overshoot at higher C-rates [29]. An aging model based on the SPM will therefore be relatively inaccurate. The IMA approximated electrolyte dynamics significantly improve the NESPM's performance at low and high C-rates (see zoomed in view in Fig. 4.3(b)). The maximum voltage error of the NESPM remains less than 2% at the beginning of the hybrid cycle due to the lower initial cell temperature which, however, decreases as the cell warms up. A maximum error of 2% is observed during the most aggressive 25C and 10 sec charge-discharge pulses in the hybrid cycle.

Figures 4.4(a)-(c) compare the conventional SPM without electrolyte dynamics, NESPM, and experimental voltage responses of the high energy 20 Ah cell corresponding to charge sustaining pulse current inputs profile in Fig. 4.4(d) at three representative SOCs *e.g.* 90%, 60%, and 30%. NESPM's maximum voltage error remains within 1.3% for the 7.5C-10sec charge-discharge pulses at 90% and 60% SOCs, but increased to 3.6% at 30% SOC. The maximum voltage error for the 10C-10sec charge-discharge pulses are 2.19%, 1.24%, and 3.7% at 90%, 60%, and 30% SOCs, respectively.

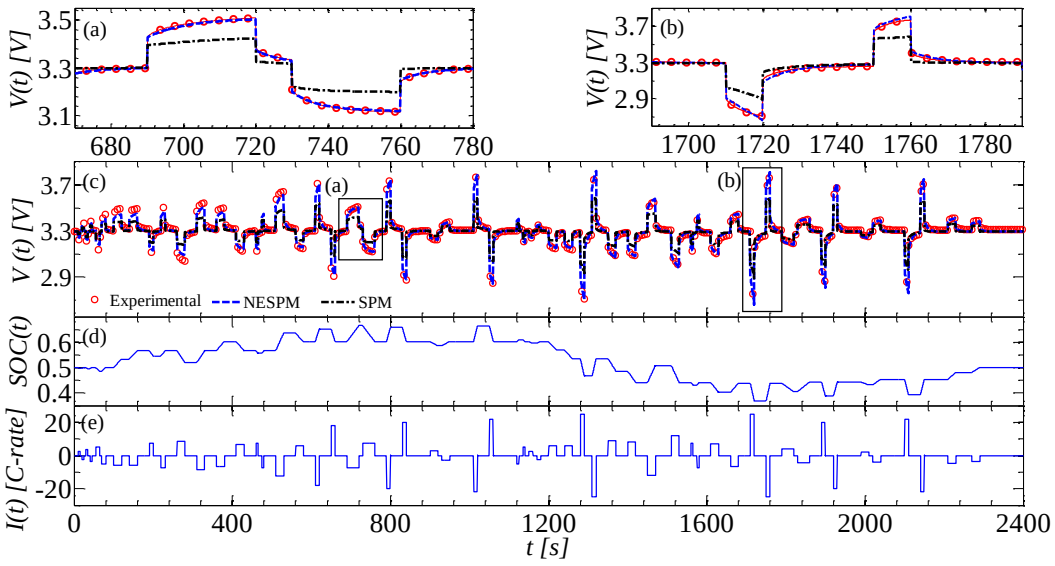

Figure 4.3. Experimental, NESPM, SPM voltage responses at 30^oC: (a) magnified voltage during $\pm 7.5C$ pulses (left box in Fig. 4.3(c)), magnified voltage during $\pm 25C$ pulses (right box of Fig. 4.3(c)), (c) voltage response, (d) SOC swing, and (e) pulse current input.

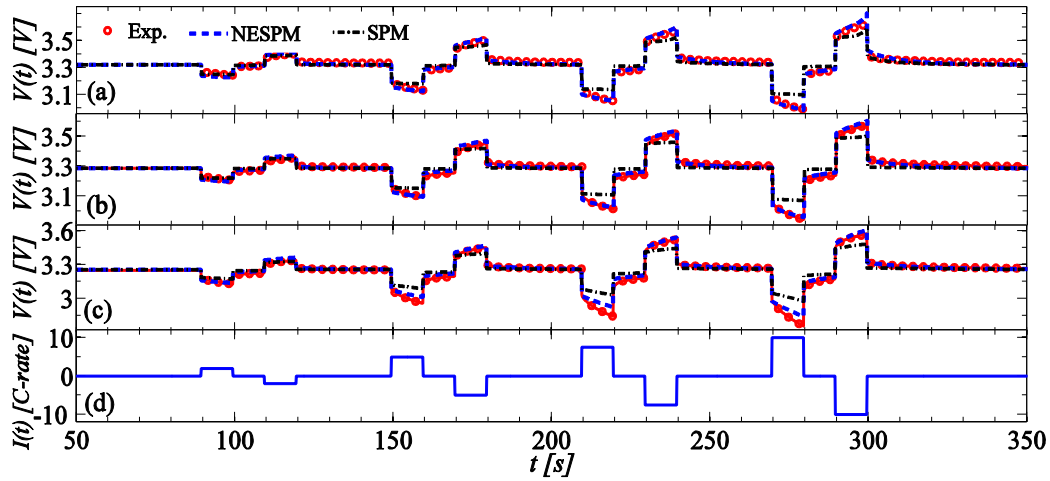

Figure 4.4. Experimental, NESPM, SPM voltage responses of the 20 Ah cell at 25^oC: (a) 90% SOC, (b) 60% SOC, (c) 30% SOC, and (d) pulse current input.

4.6 Conclusion

Inclusion of electrolyte dynamics, nonlinear kinetics, and nonlinear OCPs in the conventional SPM significantly improve the models operating range. Comparison with experimental voltage responses of the high power 4.5 Ah cell shows that the NESPM model is capable of operating up to $3C$ constant charge-discharge cycles and up to 25C and 10sec charge-discharge pulses within 35-65% SOC with 2% maximum error. For the 20 Ah high energy cell, the NESPM model is capable of operating up to $2C$ constant charge-discharge cycles and up to 10C and 10 sec charge-discharge pulses within 30-90% SOC window with 3.7% maximum error.

Chapter 5
Aging Formula for Lithium Ion Batteries with Solid Electrolyte Interphase Layer Growth

5.1 Introduction

Hybrid Electric Vehicle (HEV) current profiles are dynamic, consisting of repeated charge and discharge pulses. Accurate prediction of the battery response to these inputs requires models with open circuit voltage and Butler-Volmer kinetic nonlinearities. This chapter includes aging due to solid electrolyte interphase layer growth with the previously developed NESPM model. The NESPM aging model is then simplified to obtain explicit formulas for capacity fade and impedance rise that depend on the battery parameters and current input history. The formulas show that aging increases with SOC, operating temperature, time, and root mean square (RMS) current. The formula predicts that HEV current profiles with the (i) same average SOC, (ii) small SOC swing, (iii) same operating temperature, (iv) same cycle length, and (v) same RMS current, will have the same cell capacity fade.

5.2 Model-Based Lithium Ion Battery Aging Prediction

Lithium ion (Li-ion) batteries are well suited for electric vehicles (EVs), PHEVs, and HEVs [5]. The challenge is to choose the best cells for a specific application and optimal pack size to maximize fuel economy at minimum cost, taking into consideration the fact that batteries age and their performance degrades. It is very important to understand usage associated with a specific application influences cell degradation. Accurate modeling and prediction of the battery State of Health (SOH) is crucially important for the battery management system (BMS) to perform efficiently and economically control, manage, and estimate the pack to prevent unexpected performance deterioration and premature battery end of life (EOL).

A typical HEV current profile is complex, consisting of repeated charge and discharge pulses, operating around a narrow SOC window [5, 56]. Sharp edged, sloped, and smooth current pulses are possible. HEV pulse trains have different timings, shapes, and polarities. A clear understanding of the controlling parameters for cell aging associated with different HEV current profiles would enable system engineers to optimally design and operate HEV battery packs to enhance life within a desired performance window.

Mathematical models of the cycleable lithium consumption in the negative electrode that contributes to solid electrolyte interphase (SEI) growth are reported by many researchers [50–52]. Ramadass *et al.* [53] first propose a simplified control-oriented incremental aging model of the negative electrode in conjunction with a 1D full order electrochemical model. Randall *et al.* [54] further reduce this aging model and propose an iterative approach to calculate the SEI side reaction current density to quantify cell aging.

In this study, the control-oriented anode SEI aging model in [53] is coupled with the nonlinear electrochemical model developed in chapter 4 for gr/LFP cells. More specifically, this study (i) couples the SEI aging model of the negative electrode with the NESPM, (ii) further simplifies the NESPM aging model to an analytic aging formula to identify the controlling parameters of cell aging for HEV applications, (iii) compares the NESPM aging and aging formula for two different HEV current profiles, and (iv) experimentally validates the aging predictions. Commercially

available 4.5 Ah gr/LFP cylindrical cells are used in the experimental studies.

5.2.1 SEI Aging Model of a Gr/LFP Cell

A Li-ion battery degrades/ages with time through capacity and power fade. Capacity fade is associated with the loss of cycleable Li-ions and power fade is associated with the increase in cell impedance. The SEI aging model used for the present study is based on [53] and [54]. In this study, we coupled the SEI aging model with the NESPM, assuming aging during both charge and discharge conditions as dictated by a side reaction Tafel equation.

Ethylene carbonate (EC) is widely used as the main organic solvent of the Li-ion batteries and the EC reduction reaction is

$$S + 2Li^{+} + 2e^{-} \rightarrow P, \tag{5.1}$$

where S refers to the solvent and P is the product which is a mixture of organic and inorganic Li-ion based compounds. This side reaction is assumed to be irreversible. Table 5.1 lists the SEI aging model's governing equations coupled with the intercalation model.

Table 5.1. Governing equations of the SEI growth model coupled with the electrochemical model

Total volumetric current density of the negative electrode:	$j_n^{Li} = j_n^I + j_n^{sei}$	(5.2)
Cathodic Tafel equation of the SEI reaction:	$j_n^{sei} = -a_s^n i_{0,sei} \exp\left(-\frac{\alpha_n F}{RT}\eta_{sei}\right)$	(5.3)
Side reaction overpotential:	$\eta_{sei} = \phi_s^n - \phi_e - U_{sei}^{ref} - \frac{j_n^{Li}}{a_s^n} R_{sei}$	(5.4)
B-V kinetics for intercalation reaction:	$\eta_n = \frac{RT}{\alpha_n F} \sinh^{-1}\left(\frac{j_n^I}{2a_s^n i_0^n}\right)$	(5.5)
Intercalation reaction overpotential:	$\eta_n = \phi_s^n - \phi_e - U_n\left(c_{s,e}^n\right) - \frac{j_n^{Li}}{a_s^n} R_{sei}$	(5.6)
Capacity loss:	$\frac{\partial Q_{Loss}}{\partial t} = -\int_0^{L_n} j_n^{sei} A_n dx$	(5.7)
Impedance rise:	$\frac{\partial \delta_{sei}}{\partial t} = -\frac{M_{sei}}{a_s^n \rho_{sei} F} j_n^{sei}$	(5.8)

The total volumetric current density of the negative electrode is the sum of intercalation current (j_n^I) and side reaction current (j_n^{sei}) densities represented by Eq. (5.2). Cathodic Tafel approximation Eq. (5.3) describes the irreversible side reaction current density j_n^{sei} driven by the side reaction overpotential η_{sei} in Eq. (5.4). B-V kinetics for the intercalation reaction is represented by the nonlinear Eq. (5.5) governed by the overpotential in Eq. (5.6). Finally, capacity loss and impedance rise are calculated from Eqs. (5.7) and (5.8), respectively.

From Eqs. (5.4) and (5.6) we can see the coupled nature of the SEI aging and electrochemical intercalation models. To predict aging, one must calculate

$$\eta_{sei} = \eta_n + U_n(c_{s,e}^n) - U_{sei}^{ref}, \tag{5.9}$$

which depends on the overpotential and surface concentration in the negative electrode. Table 5.2 lists the aging model parameters. j_n^{sei} is assumed to be zero at the first time step to avoid the time consuming iterative scheme employed in [54]. This approximation is valid as j_n^{sei} is very small compared to j_n^I.

5.2.2 Aging Formula Derivation

Linearizing the B-V kinetic Eq. (4.5) at an equilibrium we get

$$\frac{\eta_n(s)}{J_n^I(s)} = \frac{R_{ct}^n}{a_s^n}, \tag{5.10}$$

where $R_{ct}^n = \frac{RT}{i_0^n(\alpha_a+\alpha_c)F}$, R=universal gas constant, and T=temperature. Linearizing Eq. (5.9),

$$\eta_{sei} = \bar{\eta}_{sei} + \widetilde{\eta}_{sei} = \bar{U}_n - U_{sei}^{ref} + \eta_n + \widetilde{U}_n. \tag{5.11}$$

The average SEI overpotential $\bar{\eta}_{sei} = \bar{U}_n - U_{sei}^{ref}$ at equilibrium and combining Eq. (5.10) and Eq. (5.11) produces

$$\widetilde{\eta}_{sei} = \eta_n + \widetilde{U}_n = \frac{R_{ct}}{a_s^n} {j_n}^I(t) + \frac{\partial U_n}{\partial c_{s,e}} \widetilde{c}_{s,e}^n(t), \tag{5.12}$$

where $\widetilde{c}_{s,e}^n = c_{s,e}^n - \bar{c}_{s,e}^n$ with $\bar{c}_{s,e}^n$ = average concentration at equilibrium SOC. Tilde indicates a small perturbation from the equilibrium condition. A 1^{st} order Padé approximation of the transcendental equation of the negative electrode particle diffusion Eq. (4.1) is

$$\widetilde{c}_{s,e}^n = g_1 \int j_n^I(t)\mathrm{d}t + g_2 j_n^I(t), \tag{5.13}$$

where $g_1 = \frac{-3}{FR_s^n a_s^n}$ and $g_2 = \frac{-R_s^n}{5D_s^n F a_s^n}$. As $j_n^I >> j_n^{sei}$, we approximate $j_n^I = j_n^{Li} = \frac{I(t)}{A_n L_n}$ in Eqs. (5.12)-(5.13). Substituting Eq. (5.13) into (5.12) and simplifying,

$$\widetilde{\eta}_{sei} = C_1 I(t) + C_2 \int I(t)dt, \tag{5.14}$$

where $C_1 = \left[\frac{R_{ct}}{a_s^n A_n L_n} + \frac{\partial U_n}{\partial c_{s,e}} \frac{g_2}{A_n L_n}\right]$ and $C_2 = \frac{g_1}{A_n L_n} \frac{\partial U_n}{\partial c_{s,e}}$. Rewriting Eq. (5.3)

$$j_n^{sei} = -a_s^n i_{0,sei} \exp\left[-\frac{\alpha_n F}{RT}\bar{\eta}_{sei}\right] \exp\left[-\frac{\alpha_n F}{RT}\widetilde{\eta}_{sei}\right]. \tag{5.15}$$

Substituting Eq. (5.14) into Eq. (5.15), we obtain

$$j_n^{sei} = -a_s^n i_{0,sei} \exp\left[-\frac{\alpha_n F}{RT}\bar{\eta}_{sei}\right] \exp\left[-\frac{\alpha_n F}{RT}\left(C_1 I(t) + C_2 \int I(\tau)d\tau\right)\right]. \tag{5.16}$$

Substituting Eq. (5.16) into Eq. (5.7) gives the capacity fade for a given cycle,

Table 5.2. Aging parameters of the commercial 4.5 Ah gr/LFP Li-ion cell [52, 53]

Parameter	Value
Side reaction equilibrium potential, U_{sei}^{ref} (V)	0.4
Side reaction exchange current density , $i_{0,sei}$ (A cm^{-2})	$^{*}4.5 \times 10^{-12}$
SEI layer Molar mass, M_{sei} (kg mol^{-1})	0.162
SEI layer density, ρ_{sei} (kg cm^{-3})	$1690{\times}10^{-6}$
SEI ionic conductivity, κ_{sei} (S cm^{-1})	0.0575
Side reaction activation energy, $E_{a,sei}$ (J mol^{-1})	$6{\times}10^{4}$

*Tuned

$$Q_{Loss} = a_s^n i_{0,sei} A_n L_n \exp\left[-\frac{\alpha_n F}{RT}\bar{\eta}_{sei}\right] \int_0^t \exp\left[-\frac{\alpha_n F}{RT}\left(C_1 I(\tau) + C_2 \int_0^t I(\tau) d\tau\right)\right] d\tau, \tag{5.17}$$

where, t is the HEV current profile's cycle time. In a charge conserving cycle, $\int_0^t I(\tau)d\tau = 0$ simplifies to

$$Q_{Loss} = a_s^n i_{0,sei} A_n L_n \exp\left[-\frac{\alpha_n F}{RT}\bar{\eta}_{sei}\right] \int_0^t \exp\left[-\frac{\alpha_n F C_1}{RT} I(\tau)\right] d\tau. \tag{5.18}$$

Taylor expanding the exponential in Eq. (5.18) up to 3^{rd} order, using $\int_0^t I(\tau)d\tau = 0$ for a charge conserving cycle, and simplifying produces the capacity fade formula,

$$Q_{Loss} = a_s^n i_{0,sei} A_n L_n t \exp\left[-\frac{\alpha_n F}{RT}\bar{\eta}_{sei}\right] \left\{1 + \left[\frac{I_{rms}}{I_a}\right]^2\right\}, \tag{5.19}$$

where the RMS current, $I_{rms} = \sqrt{\frac{1}{t}\left\{\int_0^t \left[I(\tau)\right]^2 d\tau\right\}}$ in Amps and $I_a = \left[\frac{\sqrt{2}RT}{\alpha_n F C_1}\right]$ in Amps. Similarly, the impedance rise due to the SEI layer growth is

$$R_{sei} = R_{sei,0} + \frac{\delta_{sei}}{\kappa_{sei}}, \tag{5.20}$$

where SEI layer thickness

$$\delta_{sei} = \frac{M_{sei} i_{0,sei} t}{\rho_{sei} F} \exp\left[-\frac{\alpha_n F}{RT}\bar{\eta}_{sei}\right] \left\{1 + \left[\frac{I_{rms}}{I_a}\right]^2\right\}. \tag{5.21}$$

and $R_{sei,0}$ is the initial film resistance. The aging formula (Eq. (5.19)) predicts several well-known features of Li-ion cell aging. First, aging occurs even for batteries at rest (I=0) (calendar aging) and follows a linearly with time. Sarasketa-Zabala

et al. [71], Prada *et al.* [72], Safari *et al.* [73], and Broussely *et al.* [74] also observe a linear calendar aging with time, except a short break of period at the beginning. Ploehn *et al.* [51], however, propose a one dimensional solvent diffusion model with one adjustable parameter which predicts that calendar aging increases with the square root of time. According to the aging formula, aging rate increases with increasing OCV/SOC through $\bar{\eta}_{sei}$ and increasing $i_{0,sei}$. Exchange current density follows Arrhenius behavior with temperature so higher temperature produces faster aging.

Battery usage aging also increases linearly with time which agrees well with literature [72, 73, 75–77] except at the very beginning of life. Battery usage increases aging proportional to the square of the RMS current. Thus, I_{rms} is a metric for the aggressiveness of HEV current profiles with respect to battery aging. The aging formula (5.19) shows that the sensitivity to usage aging depends on the aging current, I_a. Substitutions simplify $I_a = \frac{30\sqrt{2}A_n L_n D_s^n RT\epsilon i_0}{R_s^n(5D_s^n RT - R_s^n i_0^n \frac{\partial U_n}{\partial c_{s,e}})}$, where $\frac{\partial U_n}{\partial c_{s,e}} < 0$. So the aging current is proportional to the negative electrodes volume, porosity, and exchange current density. Large particles have a smaller I_a. The maximum I_a (and minimum usage aging) occurs when the slope of the OCP curve is small (near 50% SOC). As shown in Fig. 5.1 at a fixed temperature, I_a increases linearly with SOC, peaks near 50% SOC, and then decreases. Thus, cells are more sensitive to usage aging at high and low SOCs. Figure 5.1 also shows that cells are less sensitive to usage aging at higher temperatures as I_a increases with temperature at a specific SOC. Total aging as shown in Eq. (5.19), however, increases at higher temperatures due to strong Arrhenius type temperature dependance of $i_{0,sei}$.

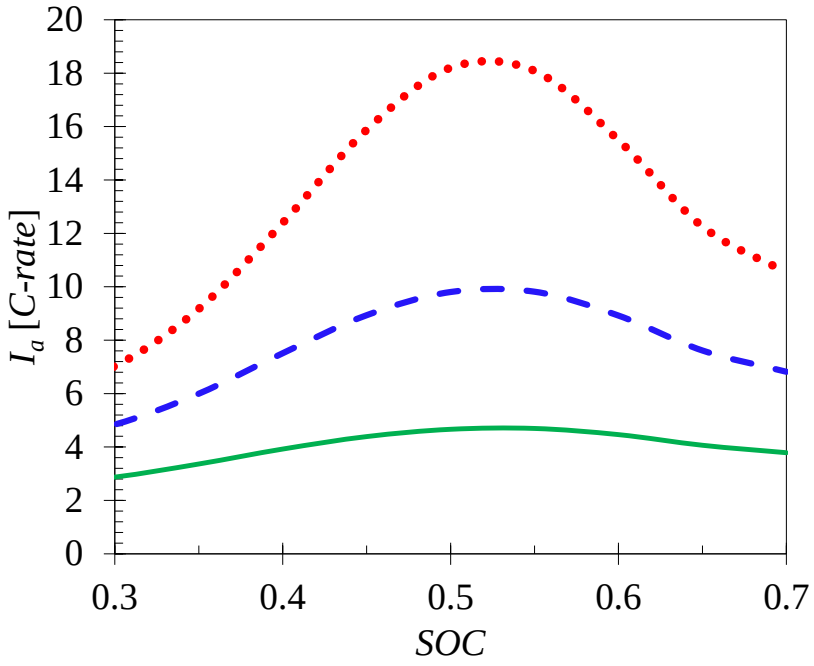

Figure 5.1. Aging current I_a versus SOC at 15^oC (solid), 30^oC (dashed), and 45^oC (dotted).

5.3 Aging Model Validation

Commercial 4.5 Ah gr/LFP cylindrical cells were cycled at 22^oC ambient temperature with aggressive HEV current profiles consisting of $\pm 25C$ pulses in an Arbin BT-2000 battery cycler ($\pm 200A/20V$). The cycling was interrupted at specific intervals for characterization tests (capacity and electrochemical impedance spectroscopy (EIS)). The capacity at $1C$ rate was measured in four steps: (1) charging to 3.6V at 1C constant current; (2) holding a constant voltage at 3.6V until the current dropped to C/20; (3) resting for 30 mins; (4) discharging at $1C$ rate to a cut-off voltage of 2.0V; (5) resting for 30 mins. A Solartron SI 1287 electrochemical interface and Solartron SI 1255B frequency response analyzer (FRA) were coupled for EIS measurements. The EIS was carried out at 70% SOC with an AC voltage amplitude of 5 mV over a frequency range of 50000 to 0.005 Hz (10 points per decade of frequency), after removing 30% of the full capacity at $1C$ rate and resting the cell for 1 hour.

A charge sustaining 4180 sec long HEV current profile (Baseline profile) was

cycled for about 4 months at 22^oC ambient temperature to tune the NESPM aging model. The side reaction exchange current density, $i_{0,sei}$ and SEI layer conductivity, κ_{sei} are obtained from experimental fitting of this data. The Baseline profile has an RMS value of 6C, swings between 38-48% SOC with maximum 21C discharge and 13.5C charge pulses, and throughput 11 Ah.

A second profile is created by combining rectangular and triangular pulses (Modified profile). The average consecutive discharge rate equals the Baseline profile average discharge rate to ensure the same cell surface temperature during cycling. The Modified profile is more aggressive with maximum 26C charging rate but average discharge rate, SOC swing, RMS current, cycle time, and average SOC are the same as as the Baseline profile. Figure 5.2 compares the SOCs of the Baseline and Modified profiles.

Figure 5.3 compares the experimentally measured and theoretically predicted cell capacity versus number of cycles for the Baseline and Modified profiles. The cell capacities are normalized with the initial, fresh cell capacity. The Baseline experimental data is used to tune the model parameters to obtain a good fit between the theoretical aging curve and the experiment. Other than a short break of periods at the beginning, the experimental data shows a fairly linear degradation trend, matching the theory with less than 1% error. The cell capacity faded 5.1% during the four months of cycling with the Baseline HEV current profile.

The charge transfer resistance and solid particle diffusion resistance are obtained from EIS testing [73]. The resistances changed less than 1 $m\Omega$, indicating a non-resistive SEI layer formation. This insignificant change in cell internal resistance is also observed in the time response. Safari *et al.* [73] also observed fairly constant impedance for room temperature cycling of gr/LFP cells.

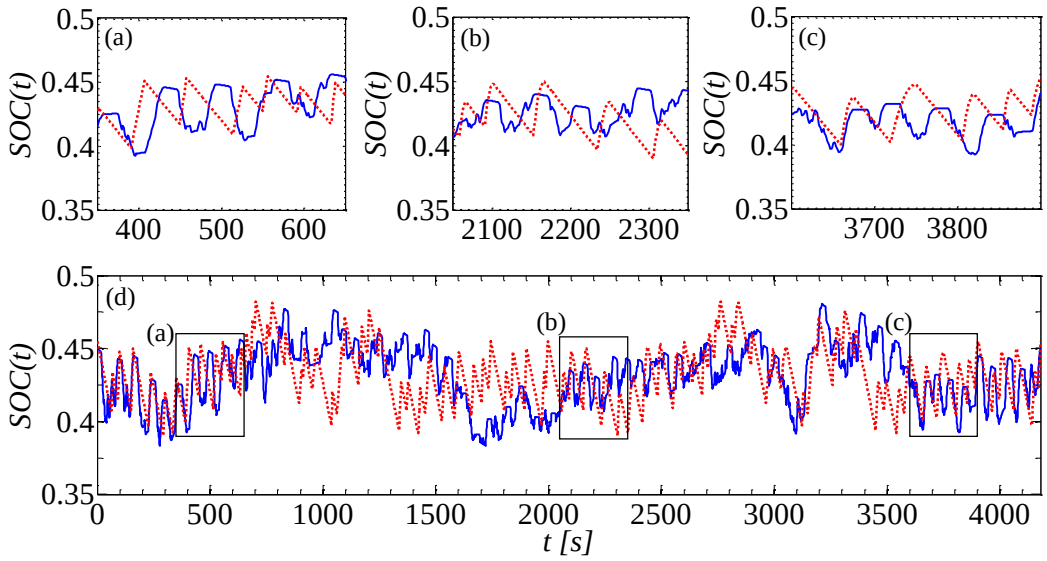

Figure 5.2. Comparison of Baseline (solid) and Modified (dotted) SOCs: (a) magnified view at the beginning (left box in Fig. 5.2(d)), (b) magnified view in the middle (middle box in Fig. 5.2(d)), (c) magnified view at the end (right box in Fig. 5.2(d)), and (d) complete cycles.

Figure 5.3 also shows that the normalized capacities versus cycles for the Modified profile. Despite the Modified cycle's very different profile, the cycling test follows the same trend as the Baseline and the NESPM aging models predictions, with less than 1% error. Unlike the Baseline profile test, the capacities during

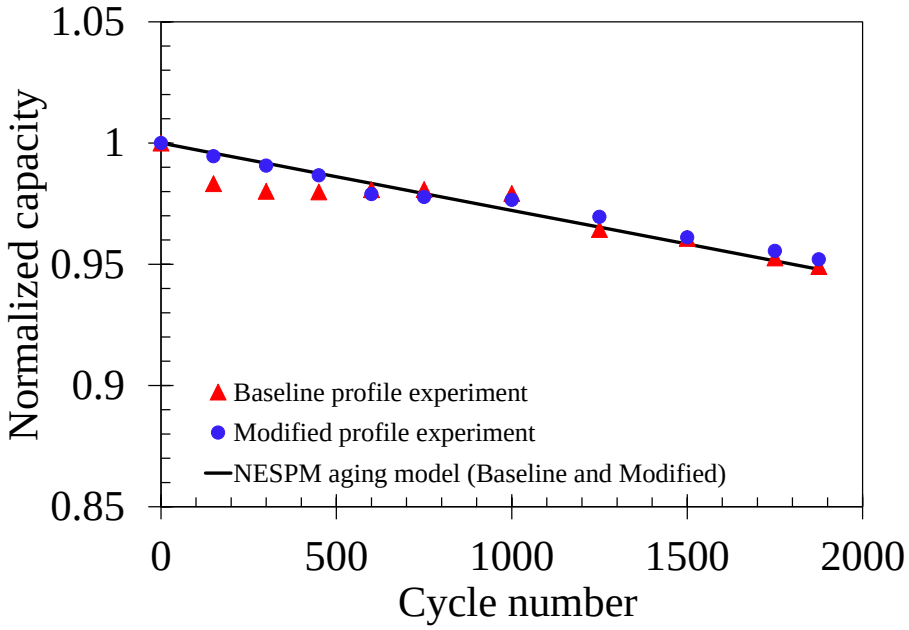

Figure 5.3. Comparison of experimental and model predicted normalized capacities characterized at 1C and at 22 ^oC.

the Modified profile test does not show any initial break in capacity fade. This may be due to the fact that the test cell for the Modified HEV profile test was four months older than the Baseline test cell when the test began. The linear decreasing trend in capacity is more noticeable with the Modified HEV current profile. Capacities from both cycling tests follow the theoretically predicted slope. The average cell surface temperature in the modified cycle test was 33.2^oC, very close to the baseline cycling test's average temperature which was 33^oC. The closely matched experimental results with the NESPM aging model's predictions provide significant proof that for cycles satisfying five conditions (*e.g.* (i) same average operating SOC, (ii) small SOC swing, (iii) same temperature, (iv) same cycle time, and (v) same RMS current (I_{rms})), then cell aging will be independent of HEV current profile.

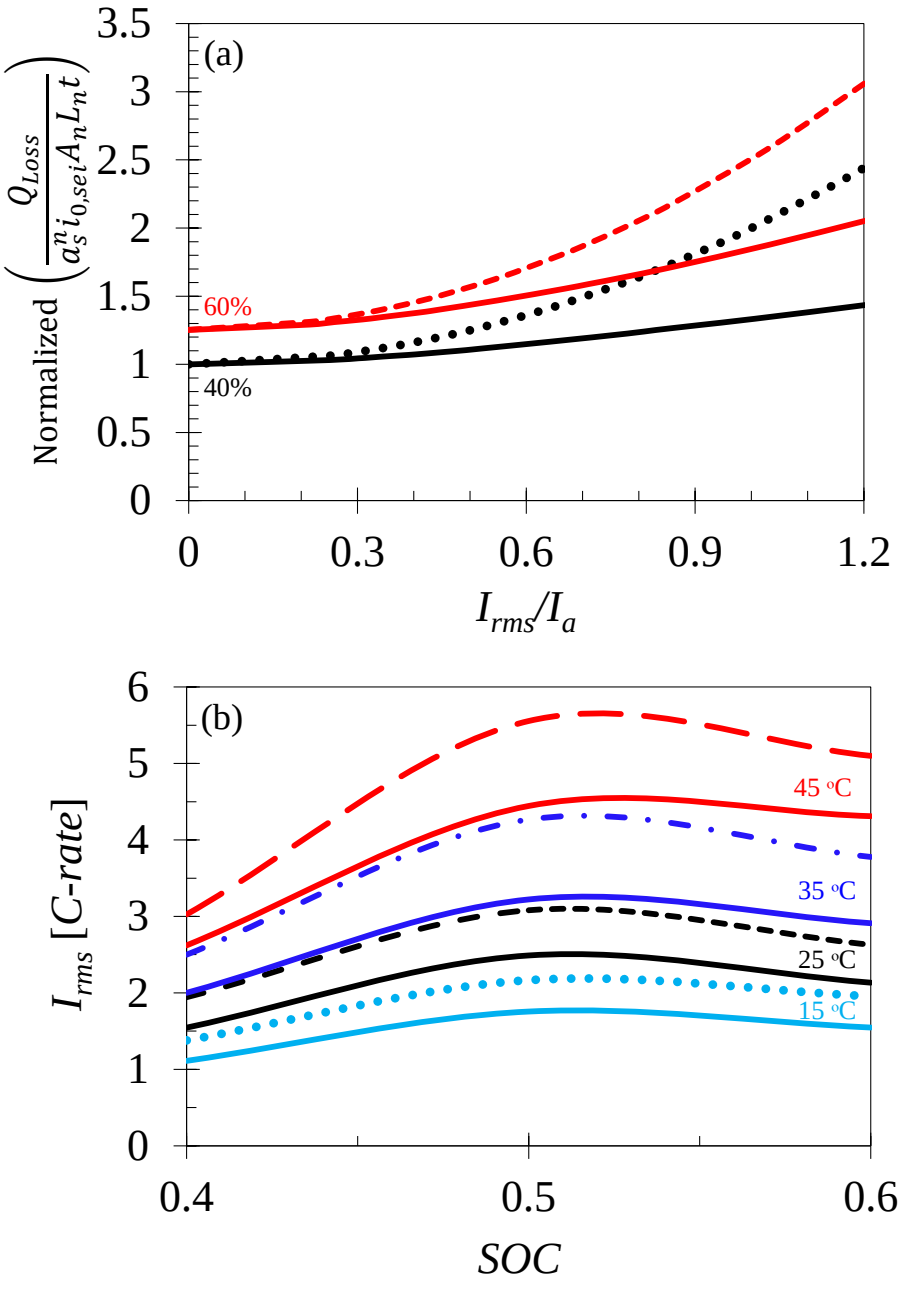

Figure 5.4. Comparison of aging formula and NESPM aging model: (a) normalized capacity fades of NESPM aging (solid) and aging formula (dashed) at 25^oC, (b) I_{rms} of the aging formula with 3% (solid) and 5% (dashed) capacity fade errors.

5.4 Accuracy of the Aging Formula

Figure 5.4(a) plots the normalized capacity fades predicted by the NESPM aging model and aging formula (Eq. (5.19)) versus $\frac{I_{rms}}{I_a}$ at two different average SOCs for the Baseline profile. Capacity is normalized by the capacity fade at 40% SOC and $I_{rms} = 0$. This is also the calendar capacity fade at 40% SOC. The NESPM aging model and aging formula match well at low I_{rms}. Both predict that the calendar capacity fade is much larger than the usage capacity fade for $I_{rms} < I_a$. Both models also predict higher degradation at higher SOC operation. The aging formula overpredicts the NESPM aging model when $\frac{I_{rms}}{I_a} > 0.35$ due to the limits of linearization. For the example cells cycled in this study, $I_a \approx 9C$ so current profiles with $I_{rms} \approx 3C$ will be accurately predicted with the aging formula.

The ratio $\frac{I_{rms}}{I_a}$ decreases at higher temperatures and near 50% SOC due to increased value of I_a (see Fig. 5.1) allowing the aging formula to be less sensitive to I_{rms} currents. Figure 5.4(b) summarizes the I_{rms} currents at which the aging formula predicts capacity fade with 3% and 5% errors relative to the NESPM aging model.

5.5 Conclusion

The anode SEI growth aging model coupled with the NESPM successfully predicts the experimental capacity fade within 1.3% error resulting from four months of cycling with two HEV current profiles. A simple explicit aging formula derived in this study follows the NESPM aging model's predicted capacity fade for less aggressive HEV current profiles. The aging formula provides insight into the main controlling parameters of cell aging for HEV applications. Accurate operating range of the aging formula at different temperature and SOC is determined.

Analysis conducted by both aging models on the two HEV current profiles showed that calendar life capacity fade significantly dominates the total capacity fade compared to usage capacity. Cell aging is shown to be independent of HEV current profiles satisfying the following five conditions: (i) same average operating SOC, (ii) small SOC swing, (iii) same operating temperature, (iv) same cycle length, and (v) same RMS current.

Chapter 6
Life-Extending Thermal Management for Heterogeneous Lithium ion Battery Packs in Hybrid Electric Vehicles

6.1 Introduction

A pack model with three cells in parallel is developed in this chapter to investigate the effects of pack mismatch and elevated temperature on pack performance and life for HEV applications. The pack model predicts the voltage, individual cell current, and degradation for an input pack current with different capacity and/or impedance cells operating at different temperatures and SOC set points. The cell level ESPM-T is experimentally validated with the 4.5 Ah graphite/$LiFePO_4$ cell which shows a maximum voltage error of 1% up to 25C and 10 sec charge-discharge pulses within a 35-65% SOC window and 25^oC to 40^oC temperature range. The SEI aging model is experimentally validated with an aggressive HEV cycle running for 4 months with less than 1% error. Battery End of Life (EOL) is defined as the cycle number when the battery voltage hits 3.6V/2V (maximum/minimum) voltage limits. Simulations show that operating cells at 35^oC increases their life by 45% compared to room temperature operation. If the cell temperature is increased stepwise, then battery life is increased 85% more with a 50^oC (max) cell temperature at EOL. Pack mismatch shown to reduce pack life and is more severe at lower temperatures.

A heterogeneous temperature management strategy reduces pack mismatch at EOL but also results in reduced pack life.

This study (i) linearizes and couples the control-oriented anode SEI aging model in [53] with the ESPM-T model derived in chapter 2. The model uses measured temperature data to adjust the model parameters using Arrhenius-type relations but does not predict the cell temperature, (ii) extends the cell model to a pack model with three cells in parallel. Pack voltage limits are implemented that limit the current and prevents over and undercharge in the simulation. The pack model simulates the individual cell performance and aging for a specific current input to the pack. The individual cells can have different capacity and/or impedance, different temperature, and SOC set point. The pack model is analyzed for different combinations of cooling conditions and cell capacities, (iii) simulates the pack with uniform cells (baseline case) to find an optimum operating temperature that maximizes EOL for an aggressive HEV cycle. Simulates the pack with different levels of capacity mismatch and compares the results with the baseline case to identify the effect of cell mismatch on pack performance and life, and, (iv) develops thermal management strategies to increase pack life without sacrificing performance for both uniform and mismatch packs.

6.2 A Three Cell Performance, Thermal, and Aging (PTA) Model

From Eq. (2.56), the ESPM impedance of a single cell is

$$Z_i = \frac{\widetilde{V}_i(s)}{I_i(s)} = K_k + \frac{K_{k,1} + K_{k,2}}{s} + \frac{b_{k,0}s^6 + b_{k,1}s^5 + b_{k,2}s^4 + b_{k,3}s^3 + b_{k,4}s^2 + b_{k,5}s + b_{k,6}}{s^6 + a_{k,1}s^5 + a_{k,2}s^4 + a_{k,3}s^3 + a_{k,4}s^2 + a_{k,5}s + a_{k,6}}, \tag{6.1}$$

where i=cell number, 1,2,3, and k=i-1. The individual cells can have different capacity and/or impedance, temperature, and SOC set point. The impedance of the three cell pack in parallel is

$$Z_{pack} = \frac{\widetilde{V}_{pack}}{I_{pack}} = \frac{Z_1 Z_2 Z_3}{Z_1 Z_2 + Z_1 Z_3 + Z_2 Z_3}, \tag{6.2}$$

where $\widetilde{V}_{pack}$ is the pack voltage ($\widetilde{V}_{pack} = \widetilde{V}_1 = \widetilde{V}_2 = \widetilde{V}_3$) and I_{pack} is the pack input current. Combining Eqs. (6.1) and (6.2) in MuPAD provides the 21^{st} order impedance transfer function

$$Z_{pack} = \frac{\widetilde{V}_{pack}}{I_{pack}} = \frac{E_{00}s^{21} + E_{01}s^{20} + \ldots + E_{20}s + E_{21}}{s\left(s^{20} + A_{01}s^{19} + \ldots + A_{19}s + A_{20}\right)}, \tag{6.3}$$

where the coefficients $E_{00} \ldots A_{20}$ are given in Appendix C. The individual cell currents are calculated from the 27^{th} order impedance

$$H_i = \frac{I_i}{I_{pack}} = \frac{Z_{pack}}{Z_i} = \frac{M_{k,0}s^{27} + M_{k,1}s^{26} + \ldots + M_{k,26}s + M_{k,27}}{\left(s^{27} + N_{k,1}s^{26} + \ldots + N_{k,26}s + N_{k,27}\right)}, \tag{6.4}$$

where the co-efficients $M_{0,0} \ldots N_{2,27}$ are also given in Appendix C.

6.3 SEI Aging Model

From chapter 5, the SEI layer overpotential,

$$\eta_{sei} = \eta_n + U_n(c^n_{s,e}) - U^{ref}_{sei}, \tag{6.5}$$

depends on the overpotential and surface concentration in the negative electrode of a cell. Linearizing Eq. (6.5),

$$\eta_{sei} = \bar{\eta}_{sei} + \widetilde{\eta}_{sei} = \bar{U}_n - U^{ref}_{sei} + \eta_n + \widetilde{U}_n. \tag{6.6}$$

The average SEI overpotential at equilibrium provides

$$\bar{\eta}_{sei} = \bar{U}_n - U^{ref}_{sei}. \tag{6.7}$$

The volumetric current density at the negative electrode

$$\frac{J^{Li}_n(s)}{I(s)} = \frac{1}{A_n L_n}. \tag{6.8}$$

The linearized B-V kinetic equation at the negative electrode

$$\frac{\eta_n(s)}{J^I_n(s)} = \frac{R^n_{ct}}{a^n_s}, \tag{6.9}$$

where $R^n_{ct} = \frac{RT}{i^n_0(\alpha_a+\alpha_c)F}$. Combining Eqs. (6.6), (6.7) and (6.8) produces

$$\widetilde{\eta}_{sei} = \eta_n + \widetilde{U}_n = \frac{R^n_{ct}}{a^n_s} {j_n}^I(t) + \frac{\partial U_n}{\partial c_{s,e}} \widetilde{c}^n_{s,e}(t), \tag{6.10}$$

where $\widetilde{c}^n_{s,e}(t)$ is calculated from the 3^{rd} order Padé approximated transfer function

$$\frac{\widetilde{C}^n_{s,e}(s)}{I(s)} = -\frac{21\left[\frac{1}{a^n_s F A_n R^n_s L_n} s^2 + \frac{60 D^n_s}{a^n_s F A_n [R^n_s]^3 L_n} s + \frac{495[D^n_s]^2}{a^n_s F A_n [R^n_s]^5 L_n}\right]}{s^3 + \frac{189 D^n_s}{[R^n_s]^2} s^2 + \frac{3465[D^n_s]^2}{[R^n_s]^4} s}, \tag{6.11}$$

with $\widetilde{c}^n_{s,e} = c^n_{s,e} - \bar{c}^n_{s,e}$ with $\bar{c}^n_{s,e}$ = average concentration and $\eta_n = \widetilde{\eta}_n$ at an equilibrium SOC. As $j^I_n >> j^{sei}_n$, we approximate $j^I_n = j^{Li}_n = \frac{I(t)}{A_n L_n}$ in Eq. (6.10). The Tafel

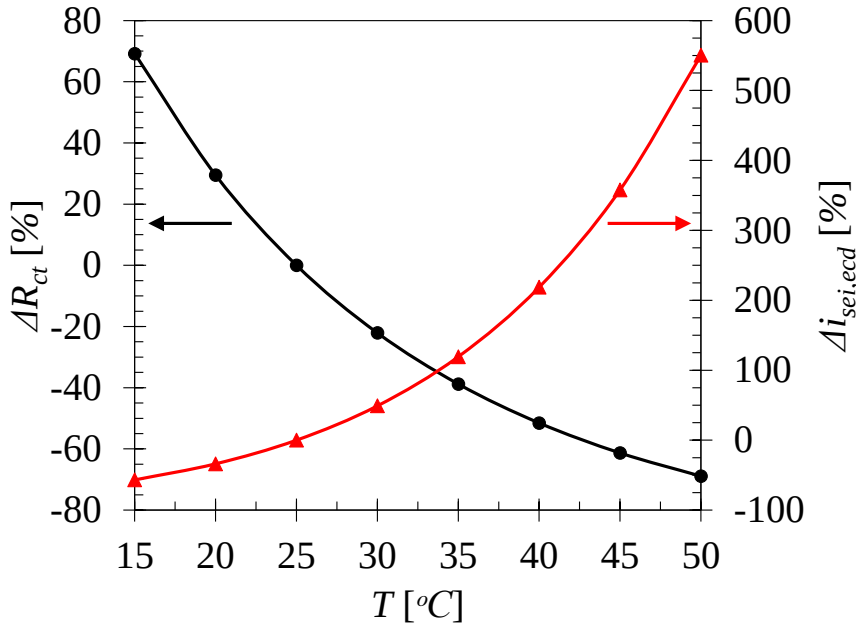

Figure 6.1. Effect of temperature on performance (charge transfer resistance) and life (side reaction current density) of Li-ion batteries with respect to 25^oC.

equation,

$$j_n^{sei} = -a_s^n i_{0,sei} \exp\left[-\frac{\alpha_n F}{RT}\eta_{sei}\right], \tag{6.12}$$

evaluates the side reaction volumetric current using Eqs. (6.7), (6.10), and (6.11). j_n^{sei} is assumed to be zero at the first time step to avoid the time consuming iterative scheme employed in [54]. The aging model parameters are listed in Table 5.2. The capacity loss

$$Q_{Loss} = -A_n L_n \int_0^t j_n^{sei} d\tau \tag{6.13}$$

and SEI layer thickness

$$\delta_{sei} = -\frac{M_{sei}}{a_s^n \rho_{sei} F} \int_0^t j_n^{sei} d\tau, \tag{6.14}$$

where t is the cycle time. The impedance rise due to the SEI layer growth

$$R_{sei} = R_{sei,0} + \frac{\delta_{sei}}{\kappa_{sei}}, \tag{6.15}$$

where $R_{sei,0}$ is the initial SEI resistance.

Figure 6.1 shows the effect of temperature on performance and aging of Li-ion cells with respect to a reference 25^oC. R_{ct} is inversely proportional to exchange current densities i_0 $\left(R_{ct} = \frac{RT}{i_0(\alpha_a+\alpha_c)F}\right)$ and capacity fade and impedance rise are proportional to $i_{0,sei}$ (Eqs. (6.12), (6.13), and (6.14)). Exchange current densities i_0 and $i_{0,sei}$ follow Arrhenius behavior so higher temperature reduces charge transfer resistance R_{ct} (due to increased i_0) which improves performance. Higher temperature also increases $i_{0,sei}$, accelerating capacity fade and impedance rise.

Figure 6.2(a) compares the voltages of a fresh cell with nominal capacity ($Q = 4.5$Ah) at 25^oC, a 20% aged cell at 25^oC, and a 20% aged cell at 35^oC in response to the pulse current profile in Fig. 6.2(b). The fresh cell's voltage at 25^oC remains below the upper voltage limit ($3.6V$). The aged cell at 25^oC hits the upper voltage limit, and cannot deliver the desired performance, so it has exceeded its EOL. Operating the aged cell at 35^oC, however, provides the desired performance without hitting the voltage limit due to reduced cell impedance. Thus elevating the cell temperature has extended the life of this cell.

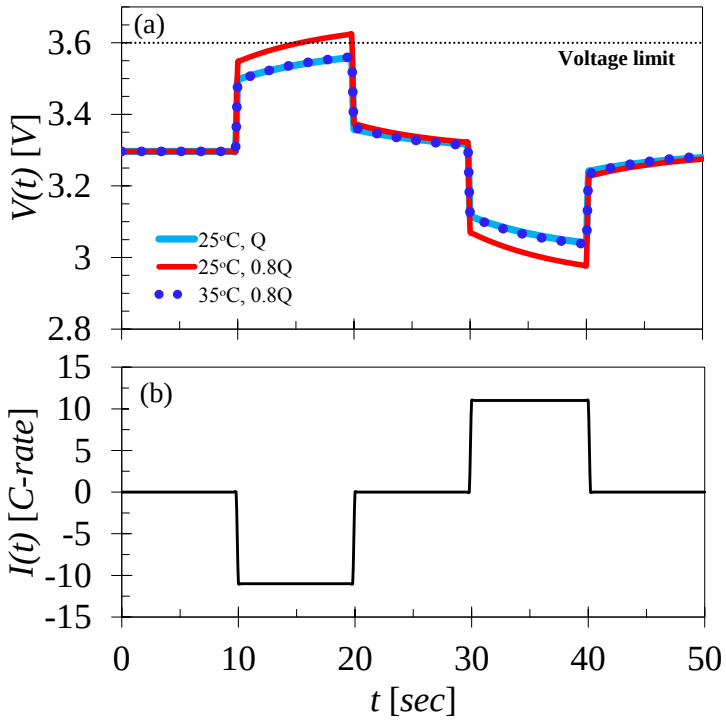

Figure 6.2. Effect of temperature on cell performance of lithium ion batteries at 50% SOC: (a) voltage response and (b) pulse current input.

6.4 Results and Discussions

Commercially available automotive grade 4.5 Ah gr/LFP cylindrical cells are chosen for the simulation studies. The cell level electrochemical and aging models are validated with these cells. Heterogeneous cells in parallel are simulated to predict current distribution, including temperature effects. Then, thermal control strategies are developed to maximize the power output of mismatched cells in parallel without causing over-aging. The outputs of the proposed study include: A novel temperature actuated control algorithm that maximizes power and minimizes degradation in mismatched parallel packs, and a new thermal management methodology that can be used in other applications and with different cell chemistry.

6.4.1 Improved Voltage Prediction by Using Measured Cell Surface Temperature in the ESPM-T Model

Figure 6.3(d) compares the voltage responses of the isothermal ESPM and non-isothermal ESPM-T models with the experimental voltage response of an aggressive 5100 sec long HEV current profile in Fig. 6.3(g). The ESPM model is simulated at an isothermal 25^oC whereas the measured cell surface temperature updates the internal cell physio-chemical parameters at every time step in the ESPM-T model. The maximum cell surface temperature reaches to 38^oC from 25^oC during the test as shown in Fig. 6.3(f) and the SOC swing remains within 35-65% shown in Fig. 6.3(e). Zoomed in Figs. 6.3(a), 6.3(b), and 6.3(c) show a voltage error of 1.15%, 2.1%, and 4.5% with the isothermal ESPM model at $\pm 6C$, $\pm 22C$, and $\pm 25C$ pulses, respectively. ESPM-T, however, is able to reduce the voltage error to 1.1%, 0.1%, and 1% for the same pulses. This test underscores the limitations of isothermal models prediction capabilities where cell temperature is not tightly controlled. Comparisons of ESPM and ESPM-T in wider temperature zones (-10^oC to 50^oC) are presented in chapter 2 with a pseudo 2D full order model. The on-board measured cell surface temperature can easily be fed back into the ESPM-T to improve the model's performance in a wider temperature zone.

6.4.2 Aging Model Tuning

A charge sustaining 4180 sec long HEV current profile was cycled for 4 months at 22^oC ambient temperature to tune the aging model. The profile swings between 38-48% SOC with maximum 21C discharge and 13.5C charge pulses and throughputs 11 Ah/cycle. The steady state average cell surface temperature reached 33^oC during the test. The side reaction exchange current density, $i_{0,sei}$ is obtained from experimental fitting of this data.

Figure 6.4 compares the experimentally measured and theoretically predicted cell capacity versus number of cycles. The cell capacities are normalized by the initial, fresh cell capacity. The experimental data is used to tune the model parameters to obtain a good fit between the theoretical aging curve and the experiment. Other than a short period of time at the beginning, the experimental data shows a fairly linear degradation trend, matching the theory with less than 1% error. The cell capacity faded 5.1% during the four months of cycling with the HEV current profile.

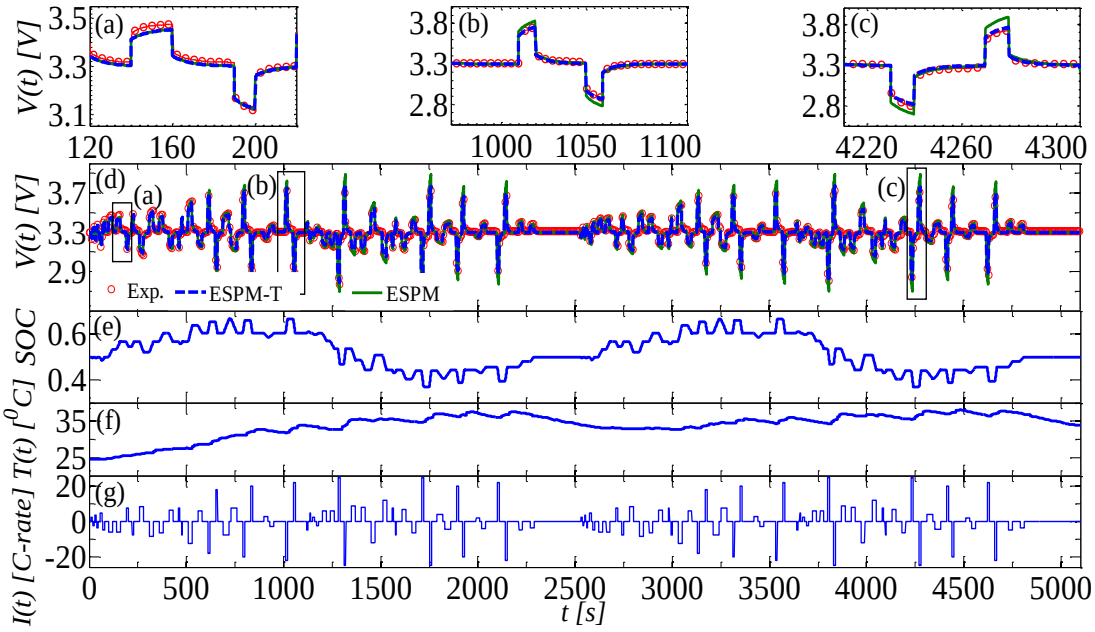

Figure 6.3. Voltage responses of experimental, ESPM at 25^oC, and ESPM-T: (a) magnified voltage during ±6C pulses (left box in Fig. 6.3(d)), (b) magnified voltage during ±22C pulses (middle box in Fig. 6.3(d)), (c) magnified voltage during ±25C pulses (right box in Fig. 6.3(d)), (d) voltage responses, (e) SOC, (f) cell surface temperature, and (g) pulse current input.

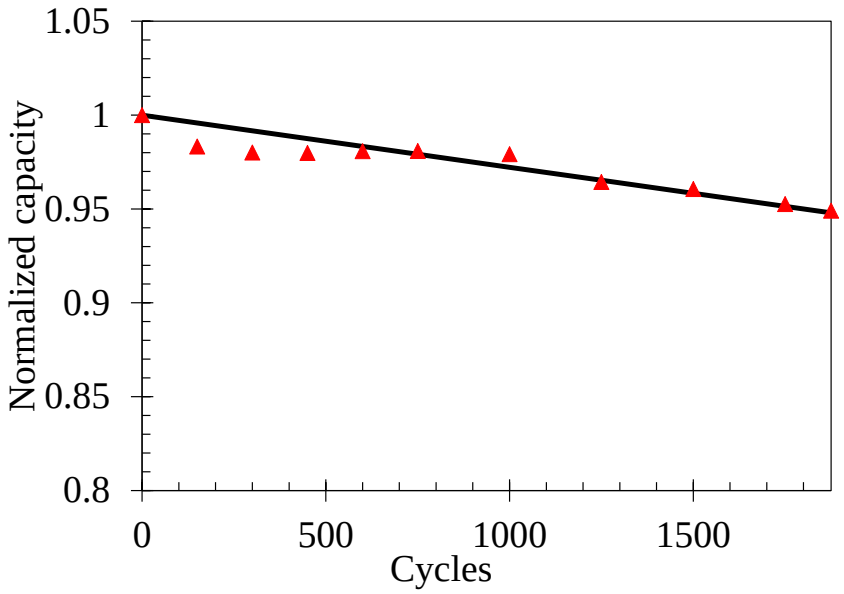

Figure 6.4. Comparison of experimental (dotted) and model predicted (solid) normalized capacities characterized at 1C and 22^oC.

The charge transfer resistance and solid particle diffusion resistance are obtained from EIS testing [73]. The resistances changed less than 1 $m\Omega$, indicating a non-resistive SEI layer formation. This insignificant change in cell internal resistance is also observed in the time response. Insignificant increase in resistance due to SEI formation has also been observed in experiments conducted by [71, 73, 77, 78] for gr/LFP cells. The substantially open structure of the SEI layer is attributed to the negligible increase in SEI resistance. Thus, the impedance rise is dominated by the capacity fade and not by an interfacial resistance.

6.5 Thermal Management Strategies for Li-ion Batteries that Optimize Life and Performance

In this section, three thermal management strategies are simulated using the PTA pack model. A 4280 sec charge sustaining Urban Dynamometer Driving Schedule (UDDS) initialized at 56% SOC for an hybrid electric mid-size passenger car is used for the simulation study [22]. In Strategy I, the pack is cycled at an elevated temperature until the voltage exceeds either its upper 3.6V limit or lower 2V limit. Effect of cell mismatch within the pack is analyzed by introducing different levels of capacity mismatch *e.g.* 4%, 6%, and 10%. In Strategy II, the pack (both uniform and mismatched) operating temperature is increase by 2.5^oC when the battery exceeds a voltage limit. In Strategy III, the pack (mismatched) operating temperature is increase by 2.5^oC when the battery exceeds a voltage limit but the weaker cell is kept at 2.5^oC lower than the stronger cells. Impedance rise due to SEI layer growth is not included in this study as explained in section 6.4.2. Thus, capacity fade is the sole contributor of increased impedance.

6.5.1 Strategy I: Optimum Battery Operating Temperature

Figure 6.5 shows the normalized capacity of an uniform pack with respect to cycle number at different operating temperatures. Every cell in the pack experiences the same aging due to cell uniformity. A pack operating at 25^oC reaches its EOL before reaching 80% of its initial capacity, USABC defined battery EOL. Increased pack temperature causes faster aging (steeper slope) but also improves the reaction kinetics, resulting in an extended EOL. The pack can provide the

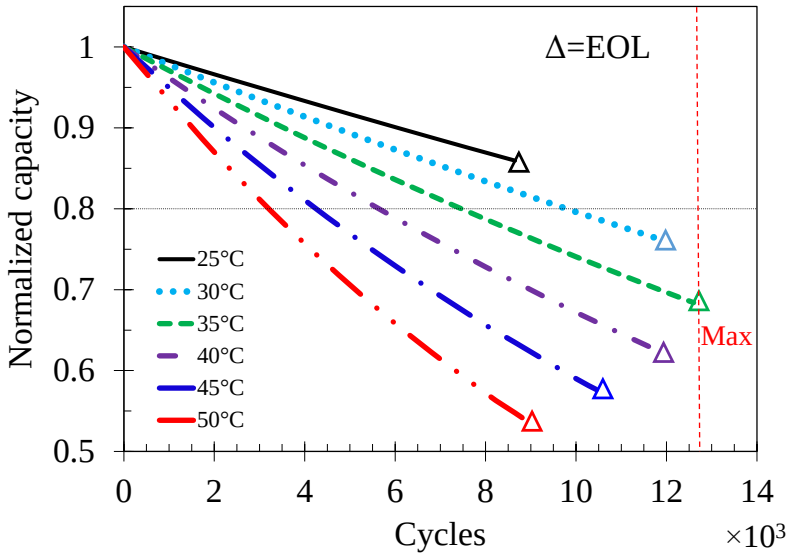

Figure 6.5. Strategy I: Capacity loss versus number of cycles for isothermal operation of a Li-ion battery under the UDDS driving cycle.

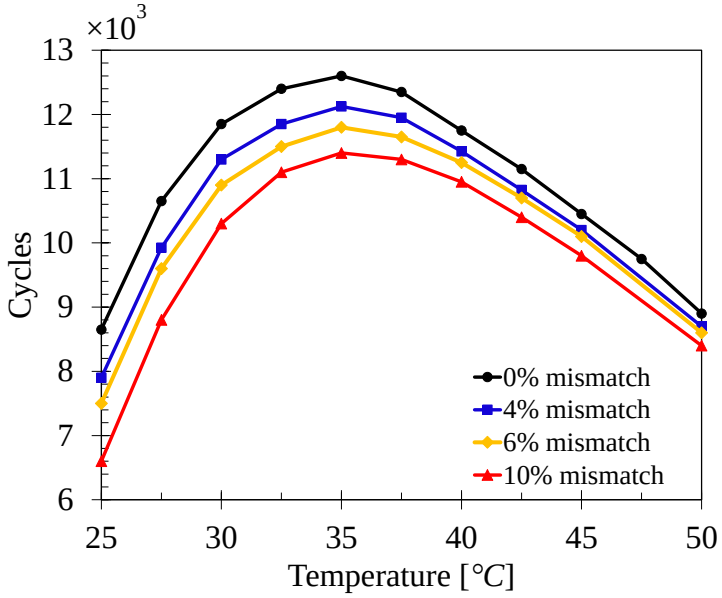

Figure 6.6. Cycles for EOL versus temperature for Strategy I: Isothermal operation of a Li-ion battery with different levels of cell mismatch under the UDDS driving cycles.

desired performance at higher temperatures even after reaching USABC defined EOL of 80% capacity fade. The optimum cell temperature is around 35^oC which increases battery EOL by 45% compared to 25^oC isothermal operation.

Figure 6.6 shows the effect of capacity mismatch on pack EOL. The simulations are performed by introducing one mismatched cell with 4%, 6%, and 10% reduced capacity in the three cell pack. Battery life under Strategy I increases with temperature, maximizes around 35^oC, and then reduces. Introducing mismatch in the pack reduces pack life compared to uniform pack but follows the same trend as the uniform case. Increased mismatch shortens pack life and is more severe at lower temperatures. A 10% mismatch reduces the battery life by 24% at 25^oC but only 9.5% at 35^oC.

6.5.2 Strategy II: Adaptive Temperature Set Point

Figure 6.5 also shows that a stepwise increase in battery temperature whenever the voltage limits are exceeded can further increase the battery life. In Strategy II, the pack temperature is increased by 2.5^oC whenever the voltage limits are reached. Figure 6.7 shows the normalized capacity and cell temperature plots of the uniform pack. The slope of the normalized capacity plot becomes steeper with increasing temperature due to increased aging rate. The reduced impedance caused by increased temperature in Strategy II, however, significantly increases EOL.

Figure 6.8 compares Strategy I and Strategy II in terms of cycle number for different levels of mismatch. The step wise temperature increase in Strategy II further extends battery life for both uniform and mismatched packs. The uniform pack life can be increased by 43% with a maximum temperature of 35^oC compared to isothermal operation at 35^oC. If the cell temperature is allowed to increase up to 50^oC, an 85% life extension is possible compared to isothermal operation at 35^oC. As in Strategy I, a mismatched pack has a shorter life and increasing mismatch accelerates aging (see Fig. 6.8).

6.5.3 Strategy III: Adaptive Temperature Set Point with Heterogeneous Temperature Management

The goal of Strategy III is to homogenize an initially heterogeneous pack through differential temperature set points. This is achieved by reducing the relative

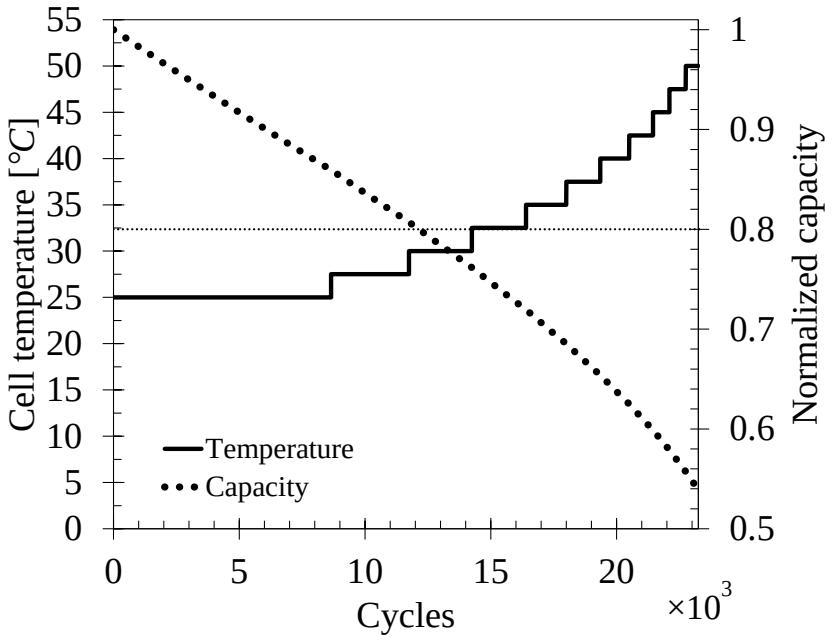

Figure 6.7. Normalized capacity and pack temperature versus UDDS cycling under Strategy II.

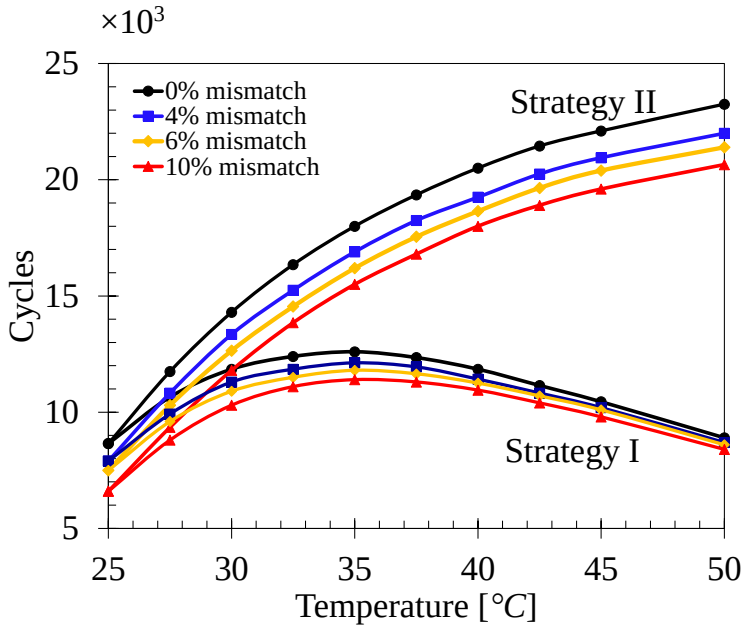

Figure 6.8. Cycle life versus temperature for heterogeneous 3-cell packs under Strategy I and Strategy II.

temperature of the weak cell so it has higher impedance, lower current throughput, and slower aging. In Strategy III, the weak cell's temperature is kept 2.5^oC lower than the strong cells and the pack temperature is increased stepwise by 2.5^oC every time the pack hits the voltage limit. This is essentially Strategy II with the weaker cells at a lower temperature than the stronger cells in the pack.

Figure 6.9 compares Strategy II and Strategy III in terms of cycle number for different levels of mismatch. Operating the weaker cell at lower temperature increases its internal resistance. This degrades the pack performance and the EOL voltage limit is reached earlier which reflects in terms of shorter life compared to Strategy II as shown in Fig. 6.9. Life shortens slightly more at lower temperature than higher temperature. Figure 6.10 compares the capacity difference between the strong and weak cells in Strategy II and Strategy III over the life of the pack. The capacity difference remains the same in Strategy II, indicating a same rate of capacity fade of each cell in the pack. The capacity difference in Strategy III reduces significantly with usage. The weaker cell operates at low temperature (higher internal resistance) and shares less current which reduces its aging rate. The stronger cells share more current and experience faster aging. Thus, faster aging of the stronger cells and slower aging of the weaker cell eventually reduces the capacity mismatch at a faster rate in Strategy III. If a relatively uniform pack is the goal at the EOL for secondary applications, Strategy III is a viable option with the expense of slightly reduced life.

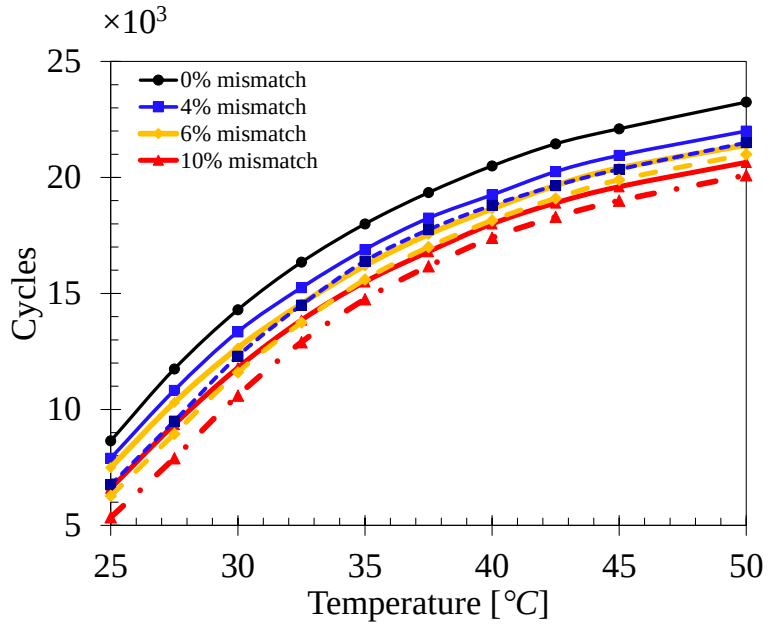

Figure 6.9. UDDS cycles to EOL versus temperature for Strategy II (solid) and Strategy III (dashed).

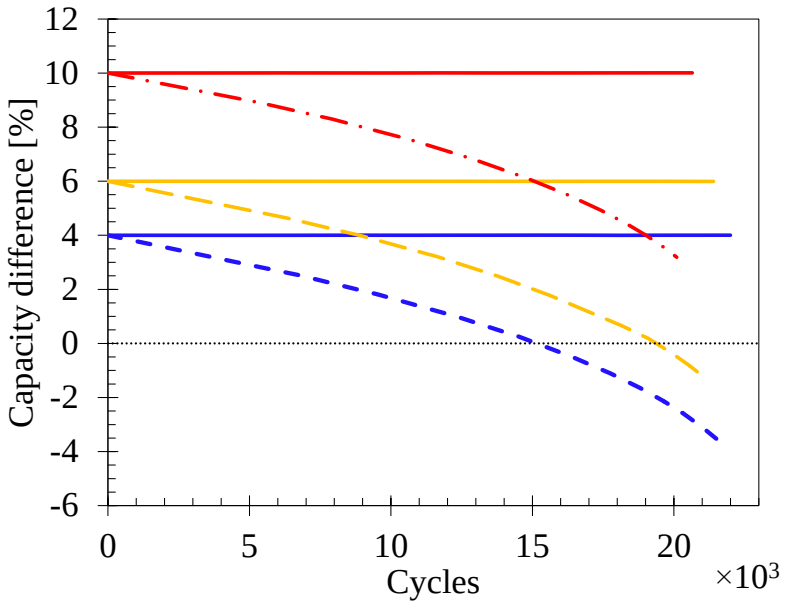

Figure 6.10. Capacity difference versus UDDS cycles for Strategy II (solid), and Strategy III (dashed).)

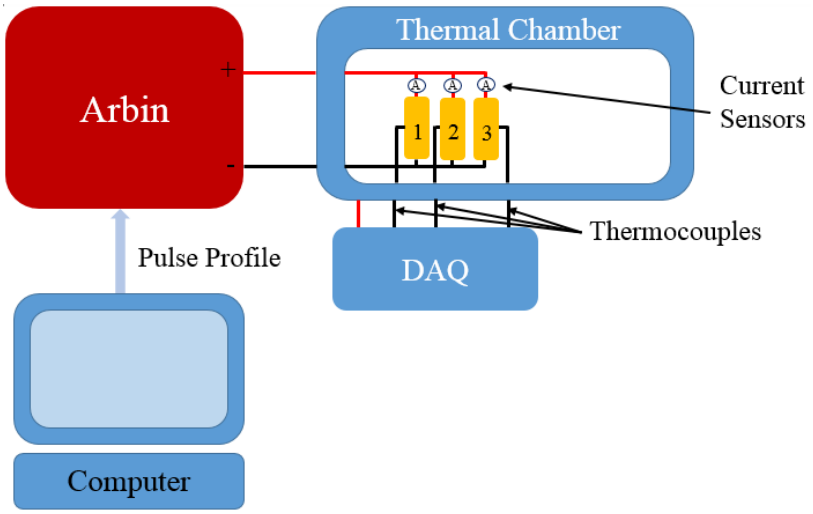

Figure 6.11. Schematic of the experimental setup.

6.6 Experimental Validation

Figure 6.11 shows the schematic view of the experimental setup to validate the proposed thermal management strategies. The setup includes a three cell pack with a pack holder, thermal chamber, and an Arbin BT-2000 battery cycler. Current sensors and thermocouples monitor individual cell current and skin temperatures, respectively. Figure 6.12(a) shows the battery holder design with current sensors installed and Fig. 6.12(b) shows the battery pack placed inside the thermal chamber. Commercially available automotive grade 4.5 Ah gr/LFP cells are selected to conduct the experimental validations.

Aging tests are time consuming and expensive. For example, only 5.1% capacity fade of the single cell is observed after four months of continuous cycling at 33^oC (see Fig.6.4). Validation of all three thermal management strategies for all the simulated conditions will take years of experimentation which is beyond the project time and budget. To reduce the experimental time, two tests are proposed as shown in 6.13. In Test 1, the three cell pack with one 10% capacity mismatched cell is cycled isothermally at 42.5^oC up to 1500 cycles. Characterization tests *e.g.* static capacity, PPC and EIS will be conducted at regular cycle intervals. Simulation predicts insignificant change in capacity reduction within the pack at this cycling condition (see Fig. 6.10). The maximum/minimum voltage at 1500 cycles will be

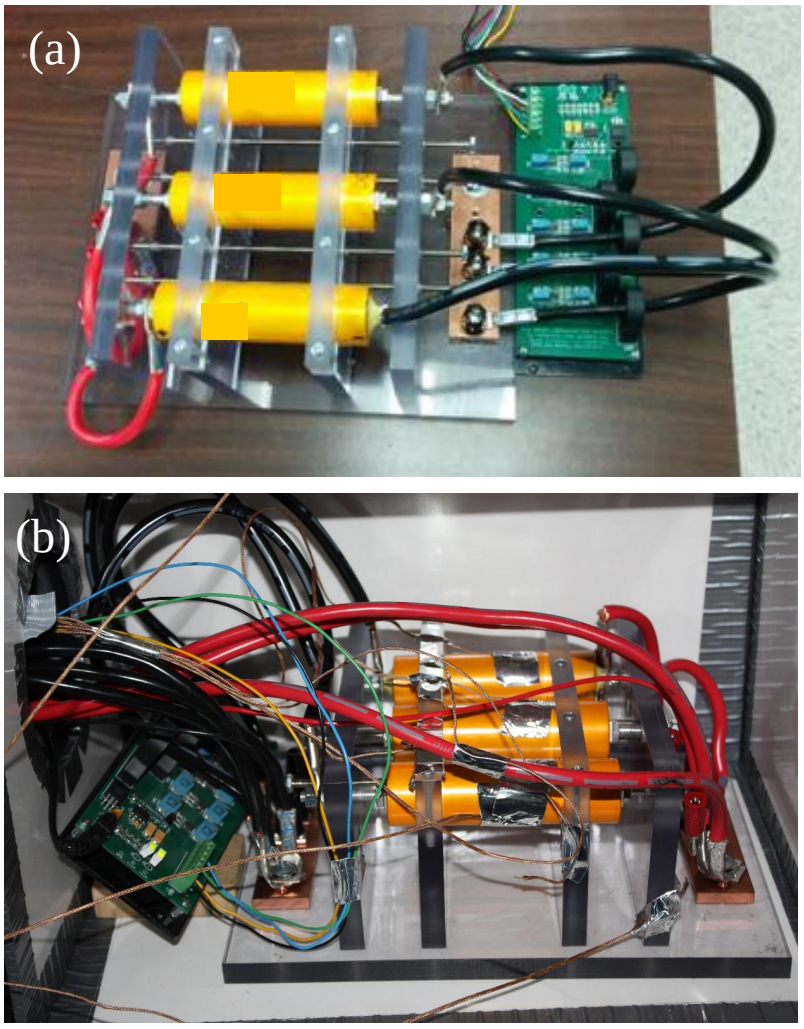

Figure 6.12. Experimental set up: (a) battery holder with current sensors installed and (b) pack placed in the thermal chamber.

defined as the EOL voltage instead of 3.6V/2V to reduce total test time. Next, the pack temperature will be increase stepwise by 2.5^oC up to 50^oC every time the pack voltage reaches the EOL voltage defined at 1500 cycles. Additional number of cycles without hitting the EOL voltage will quantify percentage increase of pack life due to elevated temperature operation.

In Test 2, the 10% capacity mismatched cell in the pack will be kept at a relatively lower temperature *e.g.* ΔT 5^oC and will be cycled until the EOL is reached defined in Test 1. Temperature will be increased stepwise by 2.5^oC up

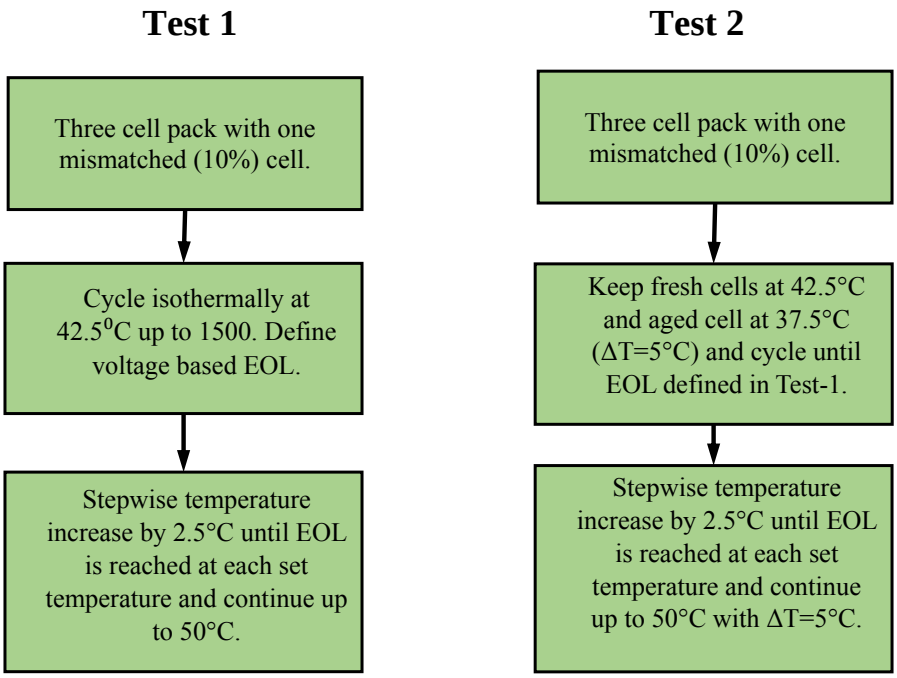

Figure 6.13. Design of planned experiments.

to 50^oC as performed in the Test 1. Simulation predicts that the heterogeneous temperature management will have reduced pack life compared to isothermal operation in Test 1 but capacity mismatch within the pack will reduce much faster at the EOL.

6.7 Conclusion

Including cell surface temperature effects in a ESPM increases the voltage response fidelity, enabling more reliable model based battery management and control. The control oriented linearized SEI growth model can be implemented in online battery management systems to estimate battery SOH for HEV applications.

A maximum/minimum voltage based battery EOL definition for HEV applications and three thermal management strategies are simulated which show that elevated temperature operation can significantly extend battery life/reduce battery size without sacrificing performance. Cell mismatch in a parallel connected pack significantly reduces pack life. Heterogeneous temperature management of a mis-

matched pack reduces pack life compared to isothermal temperature management but significantly reduces the mismatch at the EOL, resulting a more uniform pack at the EOL which can be used in secondary applications.

We are currently working on extending these temperature set point strategies for dynamic HEV current profiles along with experimental validations.

Chapter 7
Conclusions and Future Work

7.1 Conclusions

- The traditional SPM neglects electrolyte diffusion only provides satisfactory performance over narrow C-rate and temperature range. Using only seven states, the ESPM developed in chapter 2 includes an IMA model of electrolyte diffusion and matches the commercially available finite volume based gr/NCM lithium ion battery model's (AutoLion-ST) pulse response up to 20C-10 sec at room temperature with 3% error. The ESPM linearized at 50% SOC, has slightly higher voltage error (4.3%) for wider SOC swing (35 - 65%). The ESPM-T model updates the ESPM parameters with temperature, maintaining the voltage response to 30 sec pulse charge-discharge current inputs to within 5% of the AutoLion-ST for $25^oC < T < 50^oC$ at 12.5C and $-10^oC < T < 50^oC$ at 1C.

- The ESPM-based observer is capable of estimating only room temperature battery SOC for aggressive HEV current inputs. Inclusion of the temperature effect in the ESPM-T model is shown to be crucially important in chapter 3 for accurate SOC estimation in scenarios where cell temperature varies during usage. Temperature updating of the estimator state matrices provides improved SOC estimation over a wide range of temperature and C-rates. At low temperature ($< 10^oC$) and low C-rate (<0.5C), temperature measurement reduces the RMS SOC estimation error by up to ten times. For T>40^oC and $|I| \leq 15C$, temperature measurement decreases SOC estimation error by more than three times.

- A nonlinear, electrolyte-enhanced, single particle model (NESPM) is derived in chapter 4 by including nonlinearities associated with open circuit voltage and Butler-Volmer kinetics. The model is validated with experimental full charge, discharge, and HEV cycle from a 4.5 Ah high power and 20 Ah high energy graphite gr/LFP cells. Comparison with experimental voltage responses of the high power 4.5 Ah cell shows that the NESPM model is capable of operating up to $3C$ constant charge-discharge cycles and up to 25C and 10 sec charge-discharge pulses within 35-65% SOC with 2% maximum error. For the 20 Ah high energy cell the NESPM model is capable of operating up to $2C$ constant charge-discharge cycles and up to 10C and 10 sec charge-discharge pulses within 30-90% SOC window with 3.7% maximum error.

- An aging model due to SEI layer growth has been included with the NESPM model in chapter 5. The NESPM aging model is then simplified to obtain explicit formulas for capacity fade and impedance rise that depend on the battery parameters and current input history. The anode SEI growth aging model coupled with the NESPM successfully predicts the experimental capacity fade within 1.3% error resulting from four months of cycling with two HEV current profiles. A simple explicit aging formula is also derived which follows the NESPM aging model's predicted capacity fade for less aggressive HEV current profiles. The aging formula provides insight into the main controlling parameters of cell aging for HEV applications. Accurate operating range of the aging formula at different temperature and SOC is determined. Analysis conducted by both aging models on the two HEV current profiles showed that calendar life capacity fade significantly dominates the total capacity fade compared to usage capacity. Cell aging is shown to be independent of HEV current profiles satisfying the following five conditions: (i) same average operating SOC, (ii) small SOC swing, (iii) same operating temperature, (iv) same cycle length, and (v) same RMS current.

- The single cell ESPM-T and aging models have been extended to a pack model with three cells in parallel in chapter 6 to develop thermal management strategies to extend battery life within a desired performance window. Battery End of Life (EOL) is defined as the cycle number when the battery voltage

hits 3.6V/2V (maximum/minimum) voltage limits. The pack model simulates different combination of cells with different capacity operating at different temperature and SOC set points. So, effect of cell mismatch, temperature mismatch, and SOC mismatch can be easily analyzed.

The ESPM-T and aging models are experimentally validated with 4.5 Ah high power gr/LFP cell test data to obtain reliable pack model predictions. Experimental validation shows that the ESPM-T is capable of simulating up to 25C and 10 sec charge-discharge pulses within a 35-65% SOC window and 25^oC to 40^oC temperature range with less than 1% voltage error. The SEI aging model is tuned with 4 months of test data with an aggressive HEV cycle at 33^oC. The Arrhenius temperature dependence on aging at higher temperatures which extends up to 50^oC is simulated using literature data.

The optimum pack temperature is shown to be around 35^oC which increases battery EOL by 45% compared to 25^oC isothermal operation for the UDDS current profile investigated. If the cell temperature is increased stepwise, then battery life is increased 85% more with a 50^oC cell temperature at EOL. Introducing mismatch in the pack reduces pack life compared to uniform pack but follows the same trend as the uniform case. The effect of mismatch on life reduction is more severe at lower temperatures compared to higher temperatures. A 10% mismatch reduces the battery life by 24% at 25^oC but only 9.5% at 35^oC. Heterogeneous temperature management by keeping the weaker cell at a lower temperature within the mismatched pack reduces pack life compared to isothermal temperature management. Heterogeneous temperature management, however, reduces the pack mismatch at the EOL, resulting a more uniform pack at the EOL which can be used in secondary applications.

Pack level experimental test setup with the three cells in parallel has been built. Two tests (Test 1 and Test 2) have been finalized to validate the thermal management strategies developed in chapter 6. Test 1 has been started on July, 2015. It is expected to take 12 months to complete the tests.

7.2 Future Work

- **Develop a real-time battery thermal management algorithm based on dynamic HEV current profile**

  The thermal management strategies developed in chapter 6 is based on a specific current profile (assuming a vehicle is driving around a fixed route *e.g.* a commuter bus). It is necessary to generalized these strategies for all HEV applications and all load conditions. The battery load will vary depending on the types of vehicles (small/medium/large), driving style, commuters on-board, *etc.* The pack voltage might hit the limit and increase the temperature set point which does not necessarily mean EOL of the pack. A real-time pack thermal management algorithm based on a dynamic HEV current profile must avoid these scenarios by increasing the temperature during higher power demand as well as reducing the pack temperature during lower/normal operating conditions. Moving average of the maximum and minimum voltages of dynamic HEV current profiles can be used to decide the temperature set point in the real-time thermal management strategies. The pack model will be an important tool to develop, virtual implement, and test these thermal management strategies.

  This study does not calculate the battery heating load required to warm up and maintain the battery up to a specific temperature. Battery heating load depends on ambient temperature, current profile, battery chemistry, pack design, and cooling and/or heating conditions and is highly variable depending on the type of HEV. Additional heat may come from the internal combusion engine, dedicated heaters, and regen during braking. A complete heat and energy balance of the whole system is necessary before practical implementation of the thermal management strategies proposed in this study.

- **Experimental validations of the thermal management strategies**

  The ESPM-T model is experimentally validated up to 25C and 10 sec charge-discharge pulses within a 35-65% SOC window and 25^oC to 40^oC temperature range with less than 1% voltage error. The aging model is tuned with experimental test data of 4 month's of aging test at 33^oC. The Arrhenius temperature dependence on aging at higher temperatures which extends up

to 50^oC is simulated using literature data. So it is very important to test the simulation results proposed in chapter 6. Results obtained from the proposed tests described in Section 6.6 should also be used to tune the aging model parameters at higher temperatures.

- **Case studies to identify the best or mixed strategy between temperature and current control in a parallel connected battery pack**

  Case studies can be simulated where individual cell/string current in a mismatch pack will be controlled to optimize life and performance in parallel packs. The pack model can be simulated along with pulse width modulated individual cell current controllers. Individual string current control along with thermal control will give more control to manage the pack to satisfy desired performance and life goals.

- **Novel hybrid battery systems**

  The pack model can be extended to a novel hybrid battery systems in which cells with different chemistry and strengths can be integrated. Control and management strategies of such hybrid packs can be developed to enhance performance, lifetime, and cost of the pack utilizing the unique features of different electrochemistry.

- **Adding other aging mechanisms**

  This study assumed that SEI layer growth is the main aging mechanism of gr/LFP Li-ion battery. Gr/LFP chemistry has a stable olivine crystalline cathode and operates at a lower operating voltage compared to other Li-ion chemistry. Resistance increase due to SEI layer growth is negligible and capacity fade is the main cause of impedance increase of gr/LFP chemistry. These assumptions might not be true for other Li-ion chemistry *e.g.* gr/LCO, gr/LMO, gr/NCM, and gr/NCA where a passive layer can also be formed on the positive electrode particle surface and increase the cell impedance [79]. It is important to test the proposed thermal management strategies for other Li-ion battery chemistry with experimental validation. Other aging mechanisms such as coupled mechanical chemical degradation of electrodes [80, 81] can also be incorporated along with SEI aging.

Appendix A
Sub-Model Coefficients

A.1 Coefficients of the electrolyte concentration profile in Eqs. (2.46) - (2.48)

$$q_{1,n} = 36D_nD_pD_s^2\left(\varepsilon_nL_n + \varepsilon_sL_s + \varepsilon_pL_p\right),$$

$$q_{2,n} = 12D_nD_s^2L_p^2\varepsilon_p\left(L_n\varepsilon_n + L_s\varepsilon_s\right) + 12D_s^2D_pL_n^2\varepsilon_n(L_s\varepsilon_s + L_p\varepsilon_p) + 12D_nD_sD_pL_s^2\varepsilon_s \left(L_n\varepsilon_n + L_p\varepsilon_p\right) + 36D_nD_sD_p\varepsilon_n\varepsilon_pL_nL_sL_p,$$

$$q_{3,n} = L_nL_sL_p\varepsilon_n\varepsilon_s\varepsilon_p\left[3D_nD_pL_s^2 + 4D_s^2L_nL_p + 4D_sL_s\left(D_nL_p + D_pL_n\right)\right],$$

$$p_{0,n} = p_{0,s} = p_{0,p} = 36D_nD_pD_s^2(L_nb_1 - L_pb_2),$$

$$p_{1,n} = 12D_nD_sL_nL_pb_1\varepsilon_p\left(D_sL_p + 3D_pL_s\right) + 12D_nD_sL_s^2\varepsilon_s\left(L_nb_1 + L_pb_2\right) + \left[18D_s^2D_pb_1\left(L_s\varepsilon_s + L_p\varepsilon_p\right) + 6D_s^2D_pL_pb_2\varepsilon_n\right]\left(L_n^2 - x^2\right),$$

$$p_{2,n} = L_pL_s\varepsilon_s[D_nL_nL_sb_1\varepsilon_p\left(4D_sL_p + 3D_pL_s\right) + 6D_sb_1\varepsilon_p\left(D_sL_p + D_pL_s\right)\left(L_n^2 - x^2\right)] + D_pD_sL_sb_2\varepsilon_n\left(3x^2 - L_n^2\right),$$

$$p_{1,s} = 6D_s[3D_nD_pL_nb_1\varepsilon_s\left(L_n^2 - x^2\right) + 6D_nD_pL_n^2b_1\varepsilon_s\left(L_s - x\right) + D_nD_pL_pb_2\varepsilon_s \left(L_s^2 - 3x^2\right) + 2D_nD_pL_sb_1\varepsilon_s\left(L_s - 3x\right) + 3D_nD_pL_nL_pb_2\varepsilon_s\left(2x - L_n\right) - 2D_pD_sL_n^2L_pb_2\varepsilon_n + 6D_nD_pL_nL_p\left(b_2\varepsilon_n + b_1\varepsilon_p\right)\left(L_n - x\right) + 2D_nL_nL_pb_1\varepsilon_p\left(D_sL_p + 3D_pL_s\right)],$$

$$p_{2,s} = L_nL_p\varepsilon_s[3D_nD_pL_sb_1\varepsilon_p(L_s^2 + 3x^2) + 6D_nD_p\left(L_n - x\right)\left(L_s^2b_1\varepsilon_p - L_s^2b_2\varepsilon_n\right) + 3\left(L_n^2 + x^2\right)\left(2D_nD_pL_pb_1\varepsilon_p - 2D_sD_pL_nb_2\varepsilon_n - 3D_nD_pL_sb_2\varepsilon_n\right) - \left\{12D_nD_sL_pb_1\varepsilon_p\left(L_s + L_n\right) + 18D_nD_pL_nL_s\left(b_2\varepsilon_n + b_1\varepsilon_p\right)\right\}x + 2D_pD_sL_nb_2\varepsilon_n\left(6L_nx + L_s^2\right) + D_nb_1\varepsilon_p\{4D_sL_pL_s\left(3L_n + L_s\right) + 9D_pL_n^2L_s\}],$$

$$
\begin{aligned}
p_{1,p} = {} & 18D_s^2L_nL_p(D_nL_pb_1\varepsilon_p - D_pL_nb_2\varepsilon_n) - 6D_nD_pD_sL_nL_s(b_1L_s\varepsilon_s + 6L_pb_2\varepsilon_n) \\
& +18D_nD_s^2[2b_2\left(L_n - x\right)\left(L_nL_p\varepsilon_n + L_s^2\varepsilon_s\right) + 2\left(L_s - x\right) \\
& \left(L_n^2b_2\varepsilon_n + L_n^2b_1\varepsilon_p + L_nL_pb_1\varepsilon_s + L_sL_pb_2\varepsilon_p\right) + 2L_nL_sb_2\left(L_p - x\right) \\
& \left(\varepsilon_n + \varepsilon_s\right) + L_n\left(b_2\varepsilon_n + b_1\varepsilon_p\right)\left(L_n^2 + x^2\right) + L_sb_2\varepsilon_s\left(b_2\varepsilon_n + b_1\varepsilon_p\right)\left(L_s^2 + x^2\right) \\
& +L_nL_s\left(L_nb_2\varepsilon_s + L_sb_2\varepsilon_n + L_sb_1\varepsilon_p\right)],
\end{aligned}
$$

$$
\begin{aligned}
p_{2,p} = {} & L_nL_s\varepsilon_s[3D_nL_sb_2\varepsilon_n(2D_sL_n^2 - D_pL_pL_s) + 2D_sL_nL_sb_2\varepsilon_n(3D_sL_s - 2D_pL_p) \\
& -D_nD_sL_sb_1\varepsilon_p\left(2L_p^2 + 3L_s^2\right) + 6D_nD_sL_s\left(2L_pb_2\varepsilon_n - L_sb_1\varepsilon_p\right)\left(L_n - x\right) \\
& +6D_nD_sL_s\left(2L_nb_2\varepsilon_n - L_pb_1\varepsilon_p\right)\left(L_s - x\right) + (12D_s^2L_n^2b_2\varepsilon_n + 12D_s^2L_nL_sb_2\varepsilon_n \\
& +12D_nD_sL_s^2b_2\varepsilon_n - 6D_nD_sL_nL_sb_1\varepsilon_p)\left(L_p - x\right) + \ 12D_s^2L_nb_2\varepsilon_n\left(L_nL_s - xL_p\right) \\
& +(L_n^2 + x^2)\left(6D_s^2L_nb_2\varepsilon_n - 3D_nD_sL_sb_1\varepsilon_p\right) + 6D_nD_sL_sb_2\varepsilon_n\left(L_s^2 + x^2\right)].
\end{aligned}
$$

A.2 Coefficients of electrolyte phase potential difference in Eq. (2.55)

$$
L_0 = 72D_nD_pD_s^2\kappa_n\kappa_p\kappa_s\left(L_n\varepsilon_n + L_s\varepsilon_s + L_p\varepsilon_p\right),
$$

$$
\begin{aligned}
L_1 = {} & 24D_s\kappa_n\kappa_p\kappa_s[D_pD_s\ \varepsilon_nL_n^2\left(\varepsilon_pL_p + \varepsilon_sL_s\right) + D_n\varepsilon_n\varepsilon_pL_nL_p\left(D_sL_p + 3D_pL_s\right) \\
& +D_n\varepsilon_p\varepsilon_sL_pL_s\left(D_sL_p + D_pL_s\right) + D_nD_p\varepsilon_n\varepsilon_sL_nL_s^2],
\end{aligned}
$$

$$
L_2 = 2L_nL_pL_s\varepsilon_n\varepsilon_s\varepsilon_p\kappa_n\kappa_p\kappa_s(3D_nD_pL_s^2 + 4D_s^2L_nL_p + 4D_nD_sL_pL_s + 4D_pD_sL_nL_s),
$$

$$
\begin{aligned}
R_0 = {} & 36D_nD_pD_s^2L_n^2b_3\kappa_p\kappa_s\left(L_n\varepsilon_n + L_s\varepsilon_s + L_p\varepsilon_p\right) - 36D_nD_pD_s^2L_p^2b_4\kappa_s\kappa_n^2 \\
& \left(L_n\varepsilon_n + L_s\varepsilon_s + L_p\varepsilon_p\right) + 36D_nD_s^2L_p^2b_2\kappa_{d,p}\kappa_n\kappa_s\left(L_n\varepsilon_n + L_s\varepsilon_s\right) \\
& +36D_pD_s^2L_n^2b_1\kappa_{d,n}\kappa_p\kappa_s\left(L_p\varepsilon_p + L_s\varepsilon_s\right) \\
& +36D_s^2L_nL_p\kappa_s\left(D_pL_nb_2\varepsilon_n\kappa_{d,n}\kappa_p + D_nL_pb_1\varepsilon_p\kappa_{d,p}\kappa_n\right) \\
& +36D_nD_pD_sL_s^2\varepsilon_s\kappa_{d,s}\kappa_n\kappa_p(b_1L_n + b_2L_p) \\
& -72(D_nD_pD_s^2L_pL_sb_4\kappa_n^2\kappa_p + D_nD_pD_s^2L_nL_pb_4\kappa_n\kappa_p\kappa_s)(L_n\varepsilon_n + L_s\varepsilon_s + L_p\varepsilon_p) \\
& +72D_nD_pD_sL_nL_pL_s\kappa_{d,s}\kappa_n\kappa_p(b_2\varepsilon_n + b_1\varepsilon_p),
\end{aligned}
$$

$$
\begin{aligned}
R_1 = {} & 12D_pD_s^2L_n^2\varepsilon_n\kappa_s\left(L_n^2b_3\kappa_p - L_p^2b_4\kappa_n\right)\left(L_p\varepsilon_p + L_s\varepsilon_s\right) + 12D_nD_s^2L_p^2\kappa_s \\
& \left(L_n^2b_3\kappa_p\varepsilon_n - L_p^2b_4\kappa_n\varepsilon_p\right)\left(L_p\varepsilon_p + L_s\varepsilon_s\right) \\
& +12D_nD_pD_sL_s^2\varepsilon_s\kappa_s\left(L_n^2b_3\kappa_p - L_p^2b_4\kappa_n\right)\left(L_n\varepsilon_n + L_p\varepsilon_p\right) \\
& -24D_s^2L_nL_p^2b_4\varepsilon_n\varepsilon_p\kappa_p\left(L_s\kappa_n + L_p\kappa_s\right)\left(D_nL_p + D_pL_n\right) \\
& -24D_nD_sL_sL_p^2b_4\varepsilon_p\varepsilon_s\kappa_p\left(L_n\kappa_s + L_s\kappa_n\right)\left(D_sL_p + D_pL_s\right) \\
& -24D_pD_sL_nL_pL_sb_4\varepsilon_n\varepsilon_s\kappa_p\left(L_n\kappa_s + L_s\kappa_n\right)\left(D_sL_n + D_nL_s\right) \\
& -72D_nD_pD_sL_nL_p^2L_sb_4\varepsilon_n\varepsilon_p\kappa_p\left(L_s\kappa_n + L_n\kappa_s\right)
\end{aligned}
$$

$$
\begin{aligned}
&+12D_sL_nL_pL_s^2\varepsilon_{_s}\kappa_{d,s}\kappa_n\kappa_p\left(D_pL_{_n}b_2\varepsilon_n+D_nL_pb_1\varepsilon_p\right)\\
&+12D_s^2L_n^2L_sL_p^2\varepsilon_{_s}\kappa_s\left(b_2\varepsilon_n\kappa_n\kappa_{d,p}+b_1\varepsilon_p\kappa_{d,n}\kappa_{_p}\right)\\
&+36D_nD_pD_sL_nL_p\varepsilon_n\varepsilon_p\kappa_s\left(L_n^2b_3\kappa_n-L_p^2b_4\kappa_p\right)\\
&+6D_nD_pL_nL_pL_s^3\varepsilon_{_s}\kappa_{d,s}\kappa_n\kappa_p\left(b_2\varepsilon_n+b_1\varepsilon_p\right)\\
&+6D_nD_sL_nL_p^2L_s^2\varepsilon_{_s}\kappa_{d,p}\kappa_n\kappa_s\left(2b_2\varepsilon_n-b_1\varepsilon_p\right)\\
&-6D_pD_sL_n^2L_pL_s^2b_{_2}\varepsilon_n\varepsilon_s\kappa_{d,n}\kappa_p\kappa_s,
\end{aligned}
$$

$$
\begin{aligned}
R_2=&-L_nL_pL_s\varepsilon_n\varepsilon_s\varepsilon_p[(-b_3\kappa_p\kappa_sL_n^2+2b_4\kappa_p\kappa_s\kappa_nL_nL_p+b_4\kappa_s\kappa_n^2L_p^2\\
&+2b_4\kappa_p\kappa_n^2L_sL_p)(3D_nD_pL_s^2+4D_s^2L_nL_p\\
&+4D_nD_sL_pL_s+4D_pD_sL_nL_s)].
\end{aligned}
$$

Appendix B
ESPM Impedance Transfer Function Derivation

Substituting Eqs. (2.33), (2.34), (2.35), (2.36), and (2.37) into Eq. (2.39) we obtain,

$$\frac{\tilde{V}(s)}{I(s)} = K + \frac{R_2 s^2 + R_1 s + R_0}{L_2 s^2 + L_1 s + L_0} + \frac{\alpha_1 s^2 + 60\alpha_1\alpha_2 s + 495\alpha_1\alpha_2^2}{s^3 + 189\alpha_2 s^2 + 3465\alpha_2^2 s} + \frac{\beta_1 s^2 + 60\beta_1\beta_2 s + 495\beta_1\beta_2^2}{s^3 + 189\beta_2 s^2 + 3465\beta_2^2 s}, \tag{B.1}$$

where,

$$\begin{aligned}
K &= -\left[\frac{R_{ct}^p}{a_s^p}\frac{1}{AL_p} + \frac{R_{ct}^n}{a_s^n}\frac{1}{AL_n} + \frac{R_c}{A}\right],\\
C^p &= 21\frac{\partial U_p}{\partial c_{s,e}},\\
C^n &= 21\frac{\partial U_n}{\partial c_{s,e}},\\
\alpha_1 &= \frac{C^p}{a_s^p F A R_s^p L_p},\\
\alpha_2 &= \frac{D_s^p}{\left[R_s^p\right]^2},\\
\beta_1 &= \frac{C^n}{a_s^n F A R_s^n L_n},\\
\beta_2 &= \frac{D_s^n}{[R_s^n]^2}.
\end{aligned}$$

Simplifying Eq. (B.1)

$$\frac{\tilde{V}(s)}{I(s)} = K + \frac{E_0 s^2 + E_1 s + E_2}{s^2 + F_1 s + F_2} + \frac{A_2 s^2 + A_1 s + A_0}{s(s^2 + B_2 s + B_1)} + \frac{C_2 s^2 + C_1 s + C_0}{s(s^2 + D_2 s + D_1)}, \tag{B.2}$$

where,

$E_0 = \frac{R_2}{L_2}$,
$E_1 = \frac{R_1}{L_2}$,
$E_2 = \frac{R_0}{L_2}$,
$F_1 = \frac{L_1}{L_2}$,
$F_2 = \frac{L_0}{L_2}$,
$A_0 = 495\alpha_1\alpha_2^2$,
$A_1 = 60\alpha_1\alpha_2$,
$A_2 = \alpha_1$,
$B_1 = 3465\alpha_2^2$,
$B_2 = 189\alpha_2$,
$C_0 = 495\beta_1\beta_2^2$,
$C_1 = 60\beta_1\beta_2$,
$C_2 = \beta_1$,
$D_1 = 3465\beta_2^2$,
$D_2 = 189\beta_2$.

Factoring out one integrator, Eq. (B.2) can be written as:

$$\frac{\tilde{V}(s)}{I(s)} = K + \frac{K_1 + K_2}{s} + \frac{E_0 s^2 + E_1 s + E_2}{s^2 + F_1 s + F_2} + \frac{g_1 s^3 + g_2 s^2 + g_3 s + g_4}{s^4 + h_1 s^3 + h_2 s^2 + h_3 s + h_4}, \quad \text{(B.3)}$$

where,

$K_1 = \frac{A_0}{B_1}$,
$e_0 = \frac{A_1 B_1 - A_0 B_2}{B_1}$,
$e_1 = \frac{A_2 B_1 - A_0}{B_1}$,
$K_2 = \frac{C_0}{D_1}$,
$f_0 = \frac{C_1 D_1 - C_0 D_2}{D_1}$,
$f_1 = \frac{C_2 D_1 - C_0}{D_1}$,
$g_1 = e_1 + f_1$,
$g_2 = e_0 + e_1 D_2 + f_0 + f_1 B_2$,
$g_3 = e_0 D_2 + e_1 D_1 + f_0 B_2 + f_1 B_1$,
$g_4 = e_0 D1 + f_0 B1$,
$h_1 = B_2 + D_2$,
$h_2 = B_1 + B_2 D_2 + D_1$,

$h_3 = B_1 D_2 + B_2 D_1,$
$h_4 = B_1 D_1.$

After further manipulation of Eq. (B.3), the final equation suitable for state space realization can be written as follows:

$$\frac{\tilde{V}(s)}{I(s)} = K + \frac{K_1 + K_2}{s} + \frac{b_{00}s^6 + b_{01}s^5 + b_{02}s^4 + b_{03}s^3 + b_{04}s^2 + b_{05}s + b_{06}}{s^6 + a_{01}s^5 + a_{02}s^4 + a_{03}s^3 + a_{04}s^2 + a_{05}s + a_{06}}, \quad \text{(B.4)}$$

where,

$b_{00} = E_0,$
$b_{01} = E_1 + g_1 + E_0 h_1,$
$b_{02} = E_2 + g_2 + E_0 h_2 + E_1 h_1 + F_1 g_1,$
$b_{03} = g_3 + E_0 h_3 + E_1 h_2 + E_2 h_1 + F_1 g_2 + F_2 g_1,$
$b_{04} = g_4 + E_0 h_4 + E_1 h_3 + E_2 h_2 + F_1 g_3 + F_2 g_2,$
$b_{05} = E_1 h_4 + E_2 h_3 + F_1 g_4 + F_2 g_3,$
$b_{06} = E_2 h_4 + F_2 g_4,$
$a_{01} = F_1 + h_1,$
$a_{02} = F_2 + h_2 + F_1 h_1,$
$a_{03} = h_3 + F_1 h_2 + F_2 h_1,$
$a_{04} = h_4 + F_1 h_3 + F_2 h_2,$
$a_{05} = F_1 h_4 + F_2 h_3,$
$a_{06} = F_2 h_4.$

Appendix C
Pack Model Coefficients

Considering first two cells in parallel, the equivalent impedance transfer function is

$$G_1 = \frac{Z_1 Z_2}{Z_1 + Z_2} = \frac{C_{00}s^{14} + C_{01}s^{13} + \ldots + C_{13}s + C_{14}}{s\left(D_{00}s^{13} + D_{01}s^{12} + \ldots + D_{12}s + D_{13}\right)}, \tag{C.1}$$

The impedance transfer function of the pack model with three cells in parallel is

$$Z_{pack} = \frac{\widetilde{V}_{pack}}{I_{pack}} = \frac{Z_1 Z_2 Z_3}{Z_1 Z_2 + Z_1 Z_3 + Z_2 Z_3} = \frac{G_1 Z_3}{G_1 + Z_3}. \tag{C.2}$$

The final pack model impedance transfer function is

$$Z_{pack} = \frac{E_{00}s^{21} + E_{01}s^{20} + \ldots + E_{20}s + E_{21}}{s\left(s^{20} + A_{01}s^{19} + \ldots + A_{19}s + A_{20}\right)}. \tag{C.3}$$

The individual cell current is calculated from the 27^{th} order impedance transfer function solved in MuPAD:

$$H_i = \frac{I_i}{I_{pack}} = \frac{Z_{pack}}{Z_i} = \frac{M_{k,0}s^{27} + M_{k,1}s^{26} + \ldots + M_{k,26}s + M_{k,27}}{\left(s^{27} + N_{k,1}s^{26} + \ldots + N_{k,26}s + N_{k,27}\right)}, \tag{C.4}$$

where i=cell number, 1,2,3, and k=i-1. The coefficients of Eqs. (C.1)-(C.4) are given below:

$$C_{00} = K_2 b_{00} + K_1 b_{01} + b_{00} b_{10} + K_1 K_2,$$

$$C_{01} = K_2 b_{01} + K_1 b_{11} + K_{01} b_{10} + K_{11} b_{00} + K_{02} b_{10} + K_{12} b_{00} + b_{00} b_{11} + b_{01} b_{10} + K_2 K_{01} + K_2 K_{02} + K_1 K_{11} + K_1 K_{12} + K_1 K_2 a_{01} + K_1 K_2 a_{11} + K_1 a_{01} b_{10} + K_2 a_{11} b_{00},$$

$$C_{02} = K_2b_{02} + K_1b_{12} + K_{01}b_{11} + K_{11}b_{01} + K_{02}b_{11} + K_{12}b_{01} + b_{00}b_{12} + b_{01}b_{11} + b_{02}b_{10} + K_{01}K_{11} + K_{01}K_{12} + K_{02}K_{11} + K_{02}K_{12} + K_1K_2a_{02} + K_1K_2a_{12} + K_2K_{01}a_{01} + K_2K_{02}a_{01} + K_1K_{11}a_{01} + K_1K_{12}a_{01} + K_2K_{01}a_{11} + K_2K_{02}a_{11} + K_1K_{11}a_{11} + K_1K_{12}a_{11} + K_1a_{01}b_{11} + K_1a_{02}b_{10} + K_2a_{11}b_{01} + K_2a_{12}b_{00} + K_{01}a_{01}b_{10} + K_{02}a_{01}b_{10} + K_{11}a_{11}b_{00} + K_{12}a_{11}b_{00} + K_1K_2a_{01}a_{11},$$

$$C_{03} = K_2b_{03} + K_1b_{13} + K_{01}b_{12} + K_{11}b_{02} + K_{02}b_{12} + K_{12}b_{02} + b_{00}b_{13} + b_{01}b_{12} + b_{02}b_{11} + b_{03}b_{10} + K_1K_2a_{03} + K_1K_2a_{13} + K_2K_{01}a_{02} + K_2K_{02}a_{02} + K_1K_{11}a_{02} + K_1K_{12}a_{02} + K_2K_{01}a_{12} + K_2K_{02}a_{12} + K_1K_{11}a_{12} + K_1K_{12}a_{12} + K_{01}K_{11}a_{01} + K_{01}K_{12}a_{01} + K_{02}K_{11}a_{01} + K_{02}K_{12}a_{01} + K_{01}K_{11}a_{11} + K_{01}K_{12}a_{11} + K_{02}K_{11}a_{11} + K_{02}K_{12}a_{11} + K_1a_{01}b_{12} + K_1a_{02}b_{11} + K_1a_{03}b_{10} + K_2a_{11}b_{02} + K_2a_{12}b_{01} + K_2a_{13}b_{00} + K_{01}a_{01}b_{11} + K_{01}a_{02}b_{10} + K_{02}a_{01}b_{11} + K_{02}a_{02}b_{10} + K_{11}a_{11}b_{01} + K_{11}a_{12}b_{00} + K_{12}a_{11}b_{01} + K_{12}a_{12}b_{00} + K_1K_2a_{01}a_{12} + K_1K_2a_{02}a_{11} + K_2K_{01}a_{01}a_{11} + K_2K_{02}a_{01}a_{11} + K_1K_{11}a_{01}a_{11} + K_1K_{12}a_{01}a_{11},$$

$$C_{04} = K_2b_{04} + K_1b_{14} + K_{01}b_{13} + K_{11}b_{03} + K_{02}b_{13} + K_{12}b_{03} + b_{00}b_{14} + b_{01}b_{13} + b_{02}b_{12} + b_{03}b_{11} + b_{04}b_{10} + K_1K_2a_{04} + K_1K_2a_{14} + K_2K_{01}a_{03} + K_2K_{02}a_{03} + K_1K_{11}a_{03} + K_1K_{12}a_{03} + K_2K_{01}a_{13} + K_2K_{02}a_{13} + K_1K_{11}a_{13} + K_1K_{12}a_{13} + K_{01}K_{11}a_{02} + K_{01}K_{12}a_{02} + K_{02}K_{11}a_{02} + K_{02}K_{12}a_{02} + K_{01}K_{11}a_{12} + K_{01}K_{12}a_{12} + K_{02}K_{11}a_{12} + K_{02}K_{12}a_{12} + K_1a_{01}b_{13} + K_1a_{02}b_{12} + K_1a_{03}b_{11} + K_1a_{04}b_{10} + K_2a_{11}b_{03} + K_2a_{12}b_{02} + K_2a_{13}b_{01} + K_2a_{14}b_{00} + K_{01}a_{01}b_{12} + K_{01}a_{02}b_{11} + K_{01}a_{03}b_{10} + K_{02}a_{01}b_{12} + K_{02}a_{02}b_{11} + K_{02}a_{03}b_{10} + K_{11}a_{11}b_{02} + K_{11}a_{12}b_{01} + K_{11}a_{13}b_{00} + K_{12}a_{11}b_{02} + K_{12}a_{12}b_{01} + K_{12}a_{13}b_{00} + K_1K_2a_{01}a_{13} + K_1K_2a_{02}a_{12} + K_1K_2a_{03}a_{11} + K_2K_{01}a_{01}a_{12} + K_2K_{01}a_{02}a_{11} + K_2K_{02}a_{01}a_{12} + K_2K_{02}a_{02}a_{11} + K_1K_{11}a_{01}a_{12} + K_1K_{11}a_{02}a_{11} + K_1K_{12}a_{01}a_{12} + K_1K_{12}a_{02}a_{11} + K_{01}K_{11}a_{01}a_{11} + K_{01}K_{12}a_{01}a_{11} + K_{02}K_{11}a_{01}a_{11} + K_{02}K_{12}a_{01}a_{11},$$

$$C_{05} = K_2b_{05} + K_1b_{15} + K_{01}b_{14} + K_{11}b_{04} + K_{02}b_{14} + K_{12}b_{04} + b_{00}b_{15} + b_{01}b_{14} + b_{02}b_{13} + b_{03}b_{12} + b_{04}b_{11} + b_{05}b_{10} + K_1K_2a_{05} + K_1K_2a_{15} + K_2K_{01}a_{04} + K_2K_{02}a_{04} + K_1K_{11}a_{04} + K_1K_{12}a_{04} + K_2K_{01}a_{14} + K_2K_{02}a_{14} + K_1K_{11}a_{14} + K_1K_{12}a_{14} + K_{01}K_{11}a_{03} + K_{01}K_{12}a_{03} + K_{02}K_{11}a_{03} + K_{02}K_{12}a_{03} + K_{01}K_{11}a_{13} + K_{01}K_{12}a_{13} + K_{02}K_{11}a_{13} + K_{02}K_{12}a_{13} + K_1a_{01}b_{14} + K_1a_{02}b_{13} + K_1a_{03}b_{12} + K_1a_{04}b_{11} + K_1a_{05}b_{10} + K_2a_{11}b_{04} + K_2a_{12}b_{03} + K_2a_{13}b_{02} + K_2a_{14}b_{01} + K_2a_{15}b_{00} + K_{01}a_{01}b_{13} + K_{01}a_{02}b_{12} + K_{01}a_{03}b_{11} + K_{01}a_{04}b_{10} + K_{02}a_{01}b_{13} + K_{02}a_{02}b_{12} + K_{02}a_{03}b_{11} + K_{02}a_{04}b_{10} + K_{11}a_{11}b_{03} + K_{11}a_{12}b_{02} + K_{11}a_{13}b_{01} + K_{11}a_{14}b_{00} + K_{12}a_{11}b_{03} + K_{12}a_{12}b_{02} + K_{12}a_{13}b_{01} + K_{12}a_{14}b_{00} + K_1K_2a_{01}a_{14} +$$

$K_1K_2a_{02}a_{13}+K_1K_2a_{03}a_{12}+K_1K_2a_{04}a_{11}+K_2K_{01}a_{01}a_{13}+K_2K_{01}a_{02}a_{12}+K_2K_{01}a_{03}a_{11}+$
$K_2K_{02}a_{01}a_{13}+K_2K_{02}a_{02}a_{12}+K_2K_{02}a_{03}a_{11}+K_1K_{11}a_{01}a_{13}+K_1K_{11}a_{02}a_{12}+K_1K_{11}a_{03}a_{11}+$
$K_1K_{12}a_{01}a_{13}+K_1K_{12}a_{02}a_{12}+K_1K_{12}a_{03}a_{11}+K_{01}K_{11}a_{01}a_{12}+K_{01}K_{11}a_{02}a_{11}+K_{01}K_{12}a_{01}a_{12}+$
$K_{01}K_{12}a_{02}a_{11} + K_{02}K_{11}a_{01}a_{12} + K_{02}K_{11}a_{02}a_{11} + K_{02}K_{12}a_{01}a_{12} + K_{02}K_{12}a_{02}a_{11},$

$C_{06} = K_2b_{06}+K_1b_{16}+K_{01}b_{15}+K_{11}b_{05}+K_{02}b_{15}+K_{12}b_{05}+b_{00}b_{16}+b_{01}b_{15}+b_{02}b_{14}+$
$b_{03}b_{13} + b_{04}b_{12} + b_{05}b_{11} + b_{06}b_{10} + K_1K_2a_{06} + K_1K_2a_{16} + K_2K_{01}a_{05} + K_2K_{02}a_{05} +$
$K_1K_{11}a_{05}+K_1K_{12}a_{05}+K_2K_{01}a_{15}+K_2K_{02}a_{15}+K_1K_{11}a_{15}+K_1K_{12}a_{15}+K_{01}K_{11}a_{04}+$
$K_{01}K_{12}a_{04} + K_{02}K_{11}a_{04} + K_{02}K_{12}a_{04} + K_{01}K_{11}a_{14} + K_{01}K_{12}a_{14} + K_{02}K_{11}a_{14} +$
$K_{02}K_{12}a_{14} + K_1a_{01}b_{15} + K_1a_{02}b_{14} + K_1a_{03}b_{13} + K_1a_{04}b_{12} + K_1a_{05}b_{11} + K_1a_{06}b_{10} +$
$K_2a_{11}b_{05} + K_2a_{12}b_{04} + K_2a_{13}b_{03} + K_2a_{14}b_{02} + K_2a_{15}b_{01} + K_2a_{16}b_{00} + K_{01}a_{01}b_{14} +$
$K_{01}a_{02}b_{13} + K_{01}a_{03}b_{12} + K_{01}a_{04}b_{11} + K_{01}a_{05}b_{10} + K_{02}a_{01}b_{14} + K_{02}a_{02}b_{13} + K_{02}a_{03}b_{12} +$
$K_{02}a_{04}b_{11} + K_{02}a_{05}b_{10} + K_{11}a_{11}b_{04} + K_{11}a_{12}b_{03} + K_{11}a_{13}b_{02} + K_{11}a_{14}b_{01} + K_{11}a_{15}b_{00} +$
$K_{12}a_{11}b_{04}+K_{12}a_{12}b_{03}+K_{12}a_{13}b_{02}+K_{12}a_{14}b_{01}+K_{12}a_{15}b_{00}+K_1K_2a_{01}a_{15}+K_1K_2a_{02}a_{14}+$
$K_1K_2a_{03}a_{13}+K_1K_2a_{04}a_{12}+K_1K_2a_{05}a_{11}+K_2K_{01}a_{01}a_{14}+K_2K_{01}a_{02}a_{13}+K_2K_{01}a_{03}a_{12}+$
$K_2K_{01}a_{04}a_{11}+K_2K_{02}a_{01}a_{14}+K_2K_{02}a_{02}a_{13}+K_2K_{02}a_{03}a_{12}+K_2K_{02}a_{04}a_{11}+K_1K_{11}a_{01}a_{14}+$
$K_1K_{11}a_{02}a_{13}+K_1K_{11}a_{03}a_{12}+K_1K_{11}a_{04}a_{11}+K_1K_{12}a_{01}a_{14}+K_1K_{12}a_{02}a_{13}+K_1K_{12}a_{03}a_{12}+$
$K_1K_{12}a_{04}a_{11} + K_{01}K_{11}a_{01}a_{13} + K_{01}K_{11}a_{02}a_{12} + K_{01}K_{11}a_{03}a_{11} + K_{01}K_{12}a_{01}a_{13} +$
$K_{01}K_{12}a_{02}a_{12} + K_{01}K_{12}a_{03}a_{11} + K_{02}K_{11}a_{01}a_{13} + K_{02}K_{11}a_{02}a_{12} + K_{02}K_{11}a_{03}a_{11} +$
$K_{02}K_{12}a_{01}a_{13} + K_{02}K_{12}a_{02}a_{12} + K_{02}K_{12}a_{03}a_{11},$

$C_{07} = K_{01}b_{16}+K_{11}b_{06}+K_{02}b_{16}+K_{12}b_{06}+b_{01}b_{16}+b_{02}b_{15}+b_{03}b_{14}+b_{04}b_{13}+b_{05}b_{12}+$
$b_{06}b_{11} + K_2K_{01}a_{06} + K_2K_{02}a_{06} + K_1K_{11}a_{06} + K_1K_{12}a_{06} + K_2K_{01}a_{16} + K_2K_{02}a_{16} +$
$K_1K_{11}a_{16}+K_1K_{12}a_{16}+K_{01}K_{11}a_{05}+K_{01}K_{12}a_{05}+K_{02}K_{11}a_{05}+K_{02}K_{12}a_{05}+K_{01}K_{11}a_{15}+$
$K_{01}K_{12}a_{15}+K_{02}K_{11}a_{15}+K_{02}K_{12}a_{15}+K_1a_{01}b_{16}+K_1a_{02}b_{15}+K_1a_{03}b_{14}+K_1a_{04}b_{13}+$
$K_1a_{05}b_{12} + K_1a_{06}b_{11} + K_2a_{11}b_{06} + K_2a_{12}b_{05} + K_2a_{13}b_{04} + K_2a_{14}b_{03} + K_2a_{15}b_{02} +$
$K_2a_{16}b_{01} + K_{01}a_{01}b_{15} + K_{01}a_{02}b_{14} + K_{01}a_{03}b_{13} + K_{01}a_{04}b_{12} + K_{01}a_{05}b_{11} + K_{01}a_{06}b_{10} +$
$K_{02}a_{01}b_{15} + K_{02}a_{02}b_{14} + K_{02}a_{03}b_{13} + K_{02}a_{04}b_{12} + K_{02}a_{05}b_{11} + K_{02}a_{06}b_{10} + K_{11}a_{11}b_{05} +$
$K_{11}a_{12}b_{04} + K_{11}a_{13}b_{03} + K_{11}a_{14}b_{02} + K_{11}a_{15}b_{01} + K_{11}a_{16}b_{00} + K_{12}a_{11}b_{05} + K_{12}a_{12}b_{04} +$
$K_{12}a_{13}b_{03}+K_{12}a_{14}b_{02}+K_{12}a_{15}b_{01}+K_{12}a_{16}b_{00}+K_1K_2a_{01}a_{16}+K_1K_2a_{02}a_{15}+K_1K_2a_{03}a_{14}+$
$K_1K_2a_{04}a_{13}+K_1K_2a_{05}a_{12}+K_1K_2a_{06}a_{11}+K_2K_{01}a_{01}a_{15}+K_2K_{01}a_{02}a_{14}+K_2K_{01}a_{03}a_{13}+$
$K_2K_{01}a_{04}a_{12}+K_2K_{01}a_{05}a_{11}+K_2K_{02}a_{01}a_{15}+K_2K_{02}a_{14}+K_2K_{02}a_{03}a_{13}+K_2K_{02}a_{04}a_{12}+$
$K_2K_{02}a_{05}a_{11}+K_1K_{11}a_{01}a_{15}+K_1K_{11}a_{02}a_{14}+K_1K_{11}a_{03}a_{13}+K_1K_{11}a_{04}a_{12}+K_1K_{11}a_{05}a_{11}+$
$K_1K_{12}a_{01}a_{15}+K_1K_{12}a_{02}a_{14}+K_1K_{12}a_{03}a_{13}+K_1K_{12}a_{04}a_{12}+K_1K_{12}a_{05}a_{11}+K_{01}K_{11}a_{01}a_{14}+$

$K_{01}K_{11}a_{02}a_{13} + K_{01}K_{11}a_{03}a_{12} + K_{01}K_{11}a_{04}a_{11} + K_{01}K_{12}a_{01}a_{14} + K_{01}K_{12}a_{02}a_{13} +$
$K_{01}K_{12}a_{03}a_{12} + K_{01}K_{12}a_{04}a_{11} + K_{02}K_{11}a_{01}a_{14} + K_{02}K_{11}a_{02}a_{13} + K_{02}K_{11}a_{03}a_{12} +$
$K_{02}K_{11}a_{04}a_{11} + K_{02}K_{12}a_{01}a_{14} + K_{02}K_{12}a_{02}a_{13} + K_{02}K_{12}a_{03}a_{12} + K_{02}K_{12}a_{04}a_{11},$

$C_{08} = b_{02}b_{16} + b_{03}b_{15} + b_{04}b_{14} + b_{05}b_{13} + b_{06}b_{12} + K_{01}K_{11}a_{06} + K_{01}K_{12}a_{06} +$
$K_{02}K_{11}a_{06} + K_{02}K_{12}a_{06} + K_{01}K_{11}a_{16} + K_{01}K_{12}a_{16} + K_{02}K_{11}a_{16} + K_{02}K_{12}a_{16} +$
$K_1a_{02}b_{16} + K_1a_{03}b_{15} + K_1a_{04}b_{14} + K_1a_{05}b_{13} + K_1a_{06}b_{12} + K_2a_{12}b_{06} + K_2a_{13}b_{05} +$
$K_2a_{14}b_{04} + K_2a_{15}b_{03} + K_2a_{16}b_{02} + K_{01}a_{01}b_{16} + K_{01}a_{02}b_{15} + K_{01}a_{03}b_{14} + K_{01}a_{04}b_{13} +$
$K_{01}a_{05}b_{12} + K_{01}a_{06}b_{11} + K_{02}a_{01}b_{16} + K_{02}a_{02}b_{15} + K_{02}a_{03}b_{14} + K_{02}a_{04}b_{13} + K_{02}a_{05}b_{12} +$
$K_{02}a_{06}b_{11} + K_{11}a_{11}b_{06} + K_{11}a_{12}b_{05} + K_{11}a_{13}b_{04} + K_{11}a_{14}b_{03} + K_{11}a_{15}b_{02} + K_{11}a_{16}b_{01} +$
$K_{12}a_{11}b_{06} + K_{12}a_{12}b_{05} + K_{12}a_{13}b_{04} + K_{12}a_{14}b_{03} + K_{12}a_{15}b_{02} + K_{12}a_{16}b_{01} + K_1K_2a_{02}a_{16} +$
$K_1K_2a_{03}a_{15} + K_1K_2a_{04}a_{14} + K_1K_2a_{05}a_{13} + K_1K_2a_{06}a_{12} + K_2K_{01}a_{01}a_{16} + K_2K_{01}a_{02}a_{15} +$
$K_2K_{01}a_{03}a_{14} + K_2K_{01}a_{04}a_{13} + K_2K_{01}a_{05}a_{12} + K_2K_{01}a_{06}a_{11} + K_2K_{02}a_{01}a_{16} + K_2K_{02}a_{02}a_{15} +$
$K_2K_{02}a_{03}a_{14} + K_2K_{02}a_{04}a_{13} + K_2K_{02}a_{05}a_{12} + K_2K_{02}a_{06}a_{11} + K_1K_{11}a_{01}a_{16} + K_1K_{11}a_{02}a_{15} +$
$K_1K_{11}a_{03}a_{14} + K_1K_{11}a_{04}a_{13} + K_1K_{11}a_{05}a_{12} + K_1K_{11}a_{06}a_{11} + K_1K_{12}a_{01}a_{16} + K_1K_{12}a_{02}a_{15} +$
$K_1K_{12}a_{03}a_{14} + K_1K_{12}a_{04}a_{13} + K_1K_{12}a_{05}a_{12} + K_1K_{12}a_{06}a_{11} + K_{01}K_{11}a_{01}a_{15} + K_{01}K_{11}a_{02}a_{14} +$
$K_{01}K_{11}a_{03}a_{13} + K_{01}K_{11}a_{04}a_{12} + K_{01}K_{11}a_{05}a_{11} + K_{01}K_{12}a_{01}a_{15} + K_{01}K_{12}a_{02}a_{14} +$
$K_{01}K_{12}a_{03}a_{13} + K_{01}K_{12}a_{04}a_{12} + K_{01}K_{12}a_{05}a_{11} + K_{02}K_{11}a_{01}a_{15} + K_{02}K_{11}a_{02}a_{14} +$
$K_{02}K_{11}a_{03}a_{13} + K_{02}K_{11}a_{04}a_{12} + K_{02}K_{11}a_{05}a_{11} + K_{02}K_{12}a_{01}a_{15} + K_{02}K_{12}a_{02}a_{14} +$
$K_{02}K_{12}a_{03}a_{13} + K_{02}K_{12}a_{04}a_{12} + K_{02}K_{12}a_{05}a_{11},$

$C_{09} = b_{03}b_{16} + b_{04}b_{15} + b_{05}b_{14} + b_{06}b_{13} + K_1a_{03}b_{16} + K_1a_{04}b_{15} + K_1a_{05}b_{14} + K_1a_{06}b_{13} +$
$K_2a_{13}b_{06} + K_2a_{14}b_{05} + K_2a_{15}b_{04} + K_2a_{16}b_{03} + K_{01}a_{02}b_{16} + K_{01}a_{03}b_{15} + K_{01}a_{04}b_{14} +$
$K_{01}a_{05}b_{13} + K_{01}a_{06}b_{12} + K_{02}a_{02}b_{16} + K_{02}a_{03}b_{15} + K_{02}a_{04}b_{14} + K_{02}a_{05}b_{13} + K_{02}a_{06}b_{12} +$
$K_{11}a_{12}b_{06} + K_{11}a_{13}b_{05} + K_{11}a_{14}b_{04} + K_{11}a_{15}b_{03} + K_{11}a_{16}b_{02} + K_{12}a_{12}b_{06} + K_{12}a_{13}b_{05} +$
$K_{12}a_{14}b_{04} + K_{12}a_{15}b_{03} + K_{12}a_{16}b_{02} + K_1K_2a_{03}a_{16} + K_1K_2a_{04}a_{15} + K_1K_2a_{05}a_{14} +$
$K_1K_2a_{06}a_{13} + K_2K_{01}a_{02}a_{16} + K_2K_{01}a_{03}a_{15} + K_2K_{01}a_{04}a_{14} + K_2K_{01}a_{05}a_{13} + K_2K_{01}a_{06}a_{12} +$
$K_2K_{02}a_{02}a_{16} + K_2K_{02}a_{03}a_{15} + K_2K_{02}a_{04}a_{14} + K_2K_{02}a_{05}a_{13} + K_2K_{02}a_{06}a_{12} + K_1K_{11}a_{02}a_{16} +$
$K_1K_{11}a_{03}a_{15} + K_1K_{11}a_{04}a_{14} + K_1K_{11}a_{05}a_{13} + K_1K_{11}a_{06}a_{12} + K_1K_{12}a_{02}a_{16} + K_1K_{12}a_{03}a_{15} +$
$K_1K_{12}a_{04}a_{14} + K_1K_{12}a_{05}a_{13} + K_1K_{12}a_{06}a_{12} + K_{01}K_{11}a_{01}a_{16} + K_{01}K_{11}a_{02}a_{15} + K_{01}K_{11}a_{03}a_{14} +$
$K_{01}K_{11}a_{04}a_{13} + K_{01}K_{11}a_{05}a_{12} + K_{01}K_{11}a_{06}a_{11} + K_{01}K_{12}a_{01}a_{16} + K_{01}K_{12}a_{02}a_{15} +$
$K_{01}K_{12}a_{03}a_{14} + K_{01}K_{12}a_{04}a_{13} + K_{01}K_{12}a_{05}a_{12} + K_{01}K_{12}a_{06}a_{11} + K_{02}K_{11}a_{01}a_{16} +$
$K_{02}K_{11}a_{02}a_{15} + K_{02}K_{11}a_{03}a_{14} + K_{02}K_{11}a_{04}a_{13} + K_{02}K_{11}a_{05}a_{12} + K_{02}K_{11}a_{06}a_{11} +$
$K_{02}K_{12}a_{01}a_{16} + K_{02}K_{12}a_{02}a_{15} + K_{02}K_{12}a_{03}a_{14} + K_{02}K_{12}a_{04}a_{13} + K_{02}K_{12}a_{05}a_{12} +$

$K_{02}K_{12}a_{06}a_{11}$,

$C_{10} = b_{04}b_{16} + b_{05}b_{15} + b_{06}b_{14} + K_1a_{04}b_{16} + K_1a_{05}b_{15} + K_1a_{06}b_{14} + K_2a_{14}b_{06} + K_2a_{15}b_{05} + K_2a_{16}b_{04} + K_{01}a_{03}b_{16} + K_{01}a_{04}b_{15} + K_{01}a_{05}b_{14} + K_{01}a_{06}b_{13} + K_{02}a_{03}b_{16} + K_{02}a_{04}b_{15} + K_{02}a_{05}b_{14} + K_{02}a_{06}b_{13} + K_{11}a_{13}b_{06} + K_{11}a_{14}b_{05} + K_{11}a_{15}b_{04} + K_{11}a_{16}b_{03} + K_{12}a_{13}b_{06} + K_{12}a_{14}b_{05} + K_{12}a_{15}b_{04} + K_{12}a_{16}b_{03} + K_1K_2a_{04}a_{16} + K_1K_2a_{05}a_{15} + K_1K_2a_{06}a_{14} + K_2K_{01}a_{03}a_{16} + K_2K_{01}a_{04}a_{15} + K_2K_{01}a_{05}a_{14} + K_2K_{01}a_{06}a_{13} + K_2K_{02}a_{03}a_{16} + K_2K_{02}a_{04}a_{15} + K_2K_{02}a_{05}a_{14} + K_2K_{02}a_{06}a_{13} + K_1K_{11}a_{03}a_{16} + K_1K_{11}a_{04}a_{15} + K_1K_{11}a_{05}a_{14} + K_1K_{11}a_{06}a_{13} + K_1K_{12}a_{03}a_{16} + K_1K_{12}a_{04}a_{15} + K_1K_{12}a_{05}a_{14} + K_1K_{12}a_{06}a_{13} + K_{01}K_{11}a_{02}a_{16} + K_{01}K_{11}a_{03}a_{15} + K_{01}K_{11}a_{04}a_{14} + K_{01}K_{11}a_{05}a_{13} + K_{01}K_{11}a_{06}a_{12} + K_{01}K_{12}a_{02}a_{16} + K_{01}K_{12}a_{03}a_{15} + K_{01}K_{12}a_{04}a_{14} + K_{01}K_{12}a_{05}a_{13} + K_{01}K_{12}a_{06}a_{12} + K_{02}K_{11}a_{02}a_{16} + K_{02}K_{11}a_{03}a_{15} + K_{02}K_{11}a_{04}a_{14} + K_{02}K_{11}a_{05}a_{13} + K_{02}K_{11}a_{06}a_{12} + K_{02}K_{12}a_{02}a_{16} + K_{02}K_{12}a_{03}a_{15} + K_{02}K_{12}a_{04}a_{14} + K_{02}K_{12}a_{05}a_{13} + K_{02}K_{12}a_{06}a_{12}$,

$C_{11} = b_{05}b_{16} + b_{06}b_{15} + K_1a_{05}b_{16} + K_1a_{06}b_{15} + K_2a_{15}b_{06} + K_2a_{16}b_{05} + K_{01}a_{04}b_{16} + K_{01}a_{05}b_{15} + K_{01}a_{06}b_{14} + K_{02}a_{04}b_{16} + K_{02}a_{05}b_{15} + K_{02}a_{06}b_{14} + K_{11}a_{14}b_{06} + K_{11}a_{15}b_{05} + K_{11}a_{16}b_{04} + K_{12}a_{14}b_{06} + K_{12}a_{15}b_{05} + K_{12}a_{16}b_{04} + K_1K_2a_{05}a_{16} + K_1K_2a_{06}a_{15} + K_2K_{01}a_{04}a_{16} + K_2K_{01}a_{05}a_{15} + K_2K_{01}a_{06}a_{14} + K_2K_{02}a_{04}a_{16} + K_2K_{02}a_{05}a_{15} + K_2K_{02}a_{06}a_{14} + K_1K_{11}a_{04}a_{16} + K_1K_{11}a_{05}a_{15} + K_1K_{11}a_{06}a_{14} + K_1K_{12}a_{04}a_{16} + K_1K_{12}a_{05}a_{15} + K_1K_{12}a_{06}a_{14} + K_{01}K_{11}a_{03}a_{16} + K_{01}K_{11}a_{04}a_{15} + K_{01}K_{11}a_{05}a_{14} + K_{01}K_{11}a_{06}a_{13} + K_{01}K_{12}a_{03}a_{16} + K_{01}K_{12}a_{04}a_{15} + K_{01}K_{12}a_{05}a_{14} + K_{01}K_{12}a_{06}a_{13} + K_{02}K_{11}a_{03}a_{16} + K_{02}K_{11}a_{04}a_{15} + K_{02}K_{11}a_{05}a_{14} + K_{02}K_{11}a_{06}a_{13} + K_{02}K_{12}a_{03}a_{16} + K_{02}K_{12}a_{04}a_{15} + K_{02}K_{12}a_{05}a_{14} + K_{02}K_{12}a_{06}a_{13}$,

$C_{12} = b_{06}b_{16} + K_1a_{06}b_{16} + K_2a_{16}b_{06} + K_{01}a_{05}b_{16} + K_{01}a_{06}b_{15} + K_{02}a_{05}b_{16} + K_{02}a_{06}b_{15} + K_{11}a_{15}b_{06} + K_{11}a_{16}b_{05} + K_{12}a_{15}b_{06} + K_{12}a_{16}b_{05} + K_1K_2a_{06}a_{16} + K_2K_{01}a_{05}a_{16} + K_2K_{01}a_{06}a_{15} + K_2K_{02}a_{05}a_{16} + K_2K_{02}a_{06}a_{15} + K_1K_{11}a_{05}a_{16} + K_1K_{11}a_{06}a_{15} + K_1K_{12}a_{05}a_{16} + K_1K_{12}a_{06}a_{15} + K_{01}K_{11}a_{04}a_{16} + K_{01}K_{11}a_{05}a_{15} + K_{01}K_{11}a_{06}a_{14} + K_{01}K_{12}a_{04}a_{16} + K_{01}K_{12}a_{05}a_{15} + K_{01}K_{12}a_{06}a_{14} + K_{02}K_{11}a_{04}a_{16} + K_{02}K_{11}a_{05}a_{15} + K_{02}K_{11}a_{06}a_{14} + K_{02}K_{12}a_{04}a_{16} + K_{02}K_{12}a_{05}a_{15} + K_{02}K_{12}a_{06}a_{14}$,

$C_{13} = K_{01}a_{06}b_{16} + K_{02}a_{06}b_{16} + K_{11}a_{16}b_{06} + K_{12}a_{16}b_{06} + K_2K_{01}a_{06}a_{16} + K_2K_{02}a_{06}a_{16} + K_1K_{11}a_{06}a_{16} + K_1K_{12}a_{06}a_{16} + K_{01}K_{11}a_{05}a_{16} + K_{01}K_{11}a_{06}a_{15} + K_{01}K_{12}a_{05}a_{16} + K_{01}K_{12}a_{06}a_{15} + K_{02}K_{11}a_{05}a_{16} + K_{02}K_{11}a_{06}a_{15} + K_{02}K_{12}a_{05}a_{16} + K_{02}K_{12}a_{06}a_{15}$,

$$C_{14} = K_{01}K_{11}a_{06}a_{16} + K_{01}K_{12}a_{06}a_{16} + K_{02}K_{11}a_{06}a_{16} + K_{02}K_{12}a_{06}a_{16}.$$

$$D_{00} = K_1 + K_2 + b_{00} + b_{10},$$

$$D_{01} = K_{01} + K_{02} + K_{11} + K_{12} + b_{01} + b_{11} + K_1a_{01} + K_2a_{01} + K_1a_{11} + K_2a_{11} + a_{01}b_{10} + a_{11}b_{00},$$

$$D_{02} = b_{02} + b_{12} + K_1a_{02} + K_2a_{02} + K_1a_{12} + K_2a_{12} + K_{01}a_{01} + K_{02}a_{01} + K_{01}a_{11} + K_{11}a_{01} + K_{02}a_{11} + K_{12}a_{01} + K_{11}a_{11} + K_{12}a_{11} + a_{01}b_{11} + a_{02}b_{10} + a_{11}b_{01} + a_{12}b_{00} + K_1a_{01}a_{11} + K_2a_{01}a_{11},$$

$$D_{03} = b_{03} + b_{13} + K_1a_{03} + K_2a_{03} + K_1a_{13} + K_2a_{13} + K_{01}a_{02} + K_{02}a_{02} + K_{01}a_{12} + K_{11}a_{02} + K_{02}a_{12} + K_{12}a_{02} + K_{11}a_{12} + K_{12}a_{12} + a_{01}b_{12} + a_{02}b_{11} + a_{03}b_{10} + a_{11}b_{02} + a_{12}b_{01} + a_{13}b_{00} + K_1a_{01}a_{12} + K_1a_{02}a_{11} + K_2a_{01}a_{12} + K_2a_{02}a_{11} + K_{01}a_{01}a_{11} + K_{02}a_{01}a_{11} + K_{11}a_{01}a_{11} + K_{12}a_{01}a_{11},$$

$$D_{04} = b_{04} + b_{14} + K_1a_{04} + K_2a_{04} + K_1a_{14} + K_2a_{14} + K_{01}a_{03} + K_{02}a_{03} + K_{01}a_{13} + K_{11}a_{03} + K_{02}a_{13} + K_{12}a_{03} + K_{11}a_{13} + K_{12}a_{13} + a_{01}b_{13} + a_{02}b_{12} + a_{03}b_{11} + a_{04}b_{10} + a_{11}b_{03} + a_{12}b_{02} + a_{13}b_{01} + a_{14}b_{00} + K_1a_{01}a_{13} + K_1a_{02}a_{12} + K_1a_{03}a_{11} + K_2a_{01}a_{13} + K_2a_{02}a_{12} + K_2a_{03}a_{11} + K_{01}a_{01}a_{12} + K_{01}a_{02}a_{11} + K_{02}a_{01}a_{12} + K_{02}a_{02}a_{11} + K_{11}a_{01}a_{12} + K_{11}a_{02}a_{11} + K_{12}a_{01}a_{12} + K_{12}a_{02}a_{11},$$

$$D_{05} = b_{05} + b_{15} + K_1a_{05} + K_2a_{05} + K_1a_{15} + K_2a_{15} + K_{01}a_{04} + K_{02}a_{04} + K_{01}a_{14} + K_{11}a_{04} + K_{02}a_{14} + K_{12}a_{04} + K_{11}a_{14} + K_{12}a_{14} + a_{01}b_{14} + a_{02}b_{13} + a_{03}b_{12} + a_{04}b_{11} + a_{05}b_{10} + a_{11}b_{04} + a_{12}b_{03} + a_{13}b_{02} + a_{14}b_{01} + a_{15}b_{00} + K_1a_{01}a_{14} + K_1a_{02}a_{13} + K_1a_{03}a_{12} + K_1a_{04}a_{11} + K_2a_{01}a_{14} + K_2a_{02}a_{13} + K_2a_{03}a_{12} + K_2a_{04}a_{11} + K_{01}a_{01}a_{13} + K_{01}a_{02}a_{12} + K_{01}a_{03}a_{11} + K_{02}a_{01}a_{13} + K_{02}a_{02}a_{12} + K_{02}a_{03}a_{11} + K_{11}a_{01}a_{13} + K_{11}a_{02}a_{12} + K_{11}a_{03}a_{11} + K_{12}a_{01}a_{13} + K_{12}a_{02}a_{12} + K_{12}a_{03}a_{11},$$

$$D_{06} = b_{06} + b_{16} + K_1a_{06} + K_2a_{06} + K_1a_{16} + K_2a_{16} + K_{01}a_{05} + K_{02}a_{05} + K_{01}a_{15} + K_{11}a_{05} + K_{02}a_{15} + K_{12}a_{05} + K_{11}a_{15} + K_{12}a_{15} + a_{01}b_{15} + a_{02}b_{14} + a_{03}b_{13} + a_{04}b_{12} + a_{05}b_{11} + a_{06}b_{10} + a_{11}b_{05} + a_{12}b_{04} + a_{13}b_{03} + a_{14}b_{02} + a_{15}b_{01} + a_{16}b_{00} + K_1a_{01}a_{15} + K_1a_{02}a_{14} + K_1a_{03}a_{13} + K_1a_{04}a_{12} + K_1a_{05}a_{11} + K_2a_{01}a_{15} + K_2a_{02}a_{14} + K_2a_{03}a_{13} + K_2a_{04}a_{12} + K_2a_{05}a_{11} + K_{01}a_{01}a_{14} + K_{01}a_{02}a_{13} + K_{01}a_{03}a_{12} + K_{01}a_{04}a_{11} + K_{02}a_{01}a_{14} +$$

$K_{02}a_{02}a_{13}+K_{02}a_{03}a_{12}+K_{02}a_{04}a_{11}+K_{11}a_{01}a_{14}+K_{11}a_{02}a_{13}+K_{11}a_{03}a_{12}+K_{11}a_{04}a_{11}+$
$K_{12}a_{01}a_{14}+K_{12}a_{02}a_{13}+K_{12}a_{03}a_{12}+K_{12}a_{04}a_{11},$

$D_{07}=K_{01}a_{06}+K_{02}a_{06}+K_{01}a_{16}+K_{11}a_{06}+K_{02}a_{16}+K_{12}a_{06}+K_{11}a_{16}+K_{12}a_{16}+$
$a_{01}b_{16}+a_{02}b_{15}+a_{03}b_{14}+a_{04}b_{13}+a_{05}b_{12}+a_{06}b_{11}+a_{11}b_{06}+a_{12}b_{05}+a_{13}b_{04}+a_{14}b_{03}+$
$a_{15}b_{02}+a_{16}b_{01}+K_1a_{01}a_{16}+K_1a_{02}a_{15}+K_1a_{03}a_{14}+K_1a_{04}a_{13}+K_1a_{05}a_{12}+K_1a_{06}a_{11}+$
$K_2a_{01}a_{16}+K_2a_{02}a_{15}+K_2a_{03}a_{14}+K_2a_{04}a_{13}+K_2a_{05}a_{12}+K_2a_{06}a_{11}+K_{01}a_{01}a_{15}+$
$K_{01}a_{02}a_{14}+K_{01}a_{03}a_{13}+K_{01}a_{04}a_{12}+K_{01}a_{05}a_{11}+K_{02}a_{01}a_{15}+K_{02}a_{02}a_{14}+K_{02}a_{03}a_{13}+$
$K_{02}a_{04}a_{12}+K_{02}a_{05}a_{11}+K_{11}a_{01}a_{15}+K_{11}a_{02}a_{14}+K_{11}a_{03}a_{13}+K_{11}a_{04}a_{12}+K_{11}a_{05}a_{11}+$
$K_{12}a_{01}a_{15}+K_{12}a_{02}a_{14}+K_{12}a_{03}a_{13}+K_{12}a_{04}a_{12}+K_{12}a_{05}a_{11},$

$D_{08}=a_{02}b_{16}+a_{03}b_{15}+a_{04}b_{14}+a_{05}b_{13}+a_{06}b_{12}+a_{12}b_{06}+a_{13}b_{05}+a_{14}b_{04}+$
$a_{15}b_{03}+a_{16}b_{02}+K_1a_{02}a_{16}+K_1a_{03}a_{15}+K_1a_{04}a_{14}+K_1a_{05}a_{13}+K_1a_{06}a_{12}+K_2a_{02}a_{16}+$
$K_2a_{03}a_{15}+K_2a_{04}a_{14}+K_2a_{05}a_{13}+K_2a_{06}a_{12}+K_{01}a_{01}a_{16}+K_{01}a_{02}a_{15}+K_{01}a_{03}a_{14}+$
$K_{01}a_{04}a_{13}+K_{01}a_{05}a_{12}+K_{01}a_{06}a_{11}+K_{02}a_{01}a_{16}+K_{02}a_{02}a_{15}+K_{02}a_{03}a_{14}+K_{02}a_{04}a_{13}+$
$K_{02}a_{05}a_{12}+K_{02}a_{06}a_{11}+K_{11}a_{01}a_{16}+K_{11}a_{02}a_{15}+K_{11}a_{03}a_{14}+K_{11}a_{04}a_{13}+K_{11}a_{05}a_{12}+$
$K_{11}a_{06}a_{11}+K_{12}a_{01}a_{16}+K_{12}a_{02}a_{15}+K_{12}a_{03}a_{14}+K_{12}a_{04}a_{13}+K_{12}a_{05}a_{12}+K_{12}a_{06}a_{11},$

$D_{09}=a_{03}b_{16}+a_{04}b_{15}+a_{05}b_{14}+a_{06}b_{13}+a_{13}b_{06}+a_{14}b_{05}+a_{15}b_{04}+a_{16}b_{03}+$
$K_1a_{03}a_{16}+K_1a_{04}a_{15}+K_1a_{05}a_{14}+K_1a_{06}a_{13}+K_2a_{03}a_{16}+K_2a_{04}a_{15}+K_2a_{05}a_{14}+$
$K_2a_{06}a_{13}+K_{01}a_{02}a_{16}+K_{01}a_{03}a_{15}+K_{01}a_{04}a_{14}+K_{01}a_{05}a_{13}+K_{01}a_{06}a_{12}+K_{02}a_{02}a_{16}+$
$K_{02}a_{03}a_{15}+K_{02}a_{04}a_{14}+K_{02}a_{05}a_{13}+K_{02}a_{06}a_{12}+K_{11}a_{02}a_{16}+K_{11}a_{03}a_{15}+K_{11}a_{04}a_{14}+$
$K_{11}a_{05}a_{13}+K_{11}a_{06}a_{12}+K_{12}a_{02}a_{16}+K_{12}a_{03}a_{15}+K_{12}a_{04}a_{14}+K12a_{05}a_{13}+K_{12}a_{06}a_{12},$

$D_{10}=a_{04}b_{16}+a_{05}b_{15}+a_{06}b_{14}+a_{14}b_{06}+a_{15}b_{05}+a_{16}b_{04}+K_1a_{04}a_{16}+K_1a_{05}a_{15}+$
$K_1a_{06}a_{14}+K_2a_{04}a_{16}+K_2a_{05}a_{15}+K_2a_{06}a_{14}+K_{01}a_{03}a_{16}+K_{01}a_{04}a_{15}+K_{01}a_{05}a_{14}+$
$K_{01}a_{06}a_{13}+K_{02}a_{03}a_{16}+K_{02}a_{04}a_{15}+K_{02}a_{05}a_{14}+K_{02}a_{06}a_{13}+K_{11}a_{03}a_{16}+K_{11}a_{04}a_{15}+$
$K_{11}a_{05}a_{14}+K_{11}a_{06}a_{13}+K_{12}a_{03}a_{16}+K_{12}a_{04}a_{15}+K_{12}a_{05}a_{14}+K_{12}a_{06}a_{13},$

$D_{11}=a_{05}b_{16}+a_{06}b_{15}+a_{15}b_{06}+a_{16}b_{05}+K_1a_{05}a_{16}+K_1a_{06}a_{15}+K_2a_{05}a_{16}+K_2a_{06}a_{15}+$
$K_{01}a_{04}a_{16}+K_{01}a_{05}a_{15}+K_{01}a_{06}a14+K_{02}a_{04}a_{16}+K_{02}a_{05}a_{15}+K_{02}a_{06}a_{14}+K_{11}a_{04}a_{16}+$
$K_{11}a_{05}a_{15}+K_{11}a_{06}a_{14}+K_{12}a_{04}a_{16}+K_{12}a_{05}a_{15}+K_{12}a_{06}a_{14},$

$D_{12}=a_{06}b_{16}+a_{16}b_{06}+K_1a_{06}a_{16}+K_2a_{06}a_{16}+K_{01}a_{05}a_{16}+K_{01}a_{06}a_{15}+K_{02}a_{05}a_{16}+$

$K_{02}a_{06}a_{15} + K_{11}a_{05}a_{16} + K_{11}a_{06}a_{15} + K_{12}a_{05}a_{16} + K_{12}a_{06}a_{15}$,

$D_{13} = K_{01}a_{06}a_{16} + K_{02}a_{06}a_{16} + K_{11}a_{06}a_{16} + K_{12}a_{06}a_{16}$,

$D_{14} = 0$.

$E_{00} = (C_{00}b_{20} + C_{00}K_3)/(C_{00} + D_{00}b_{20} + D_{00}K_3)$,

$E_{01} = (C_{00}b_{21} + C_{01}b_{20} + C_{01}K_3 + C_{00}K_{21} + C_{00}K_{22} + C_{00}K_3a_{21})/(C_{00} + D_{00}b_{20} + D_{00}K_3)$,

$E_{02} = (C_{00}b_{22} + C_{01}b_{21} + C_{02}b_{20} + C_{02}K_3 + C_{01}K_{21} + C_{01}K_{22} + C_{00}K_3a_{22} + C_{01}K_3a_{21} + C_{00}K_{21}a_{21} + C_{00}K_{22}a_{21})/(C_{00} + D_{00}b_{20} + D_{00}K_3)$,

$E_{03} = (C_{00}b_{23} + C_{01}b_{22} + C_{02}b_{21} + C_{03}b_{20} + C_{03}K_3 + C_{02}K_{21} + C_{02}K_{22} + C_{00}K_3a_{23} + C_{01}K_3a_{22} + C_{02}K_3a_{21} + C_{00}K_{21}a_{22} + C_{01}K_{21}a_{21} + C_{00}K_{22}a_{22} + C_{01}K_{22}a_{21})/(C_{00} + D_{00}b_{20} + D_{00}K_3)$,

$E_{04} = (C_{00}b_{24} + C_{01}b_{23}2 + C_{02}b_{22} + C_{03}b_{21} + C_{04}b_{20} + C_{04}K_3 + C_{03}K_{21} + C_{03}K_{22} + C_{00}K_3a_{24} + C_{01}K_3a_{23} + C_{02}K_3a_{22} + C_{03}K_3a_{21} + C_{00}K_{21}a_{23} + C_{01}K_{21}a_{22} + C_{02}K_{21}a_{21} + C_{00}K_{22}a_{23} + C_{01}K_{22}a_{22} + C_{02}K_{22}a_{21})/(C_{00} + D_{00}b_{20} + D_{00}K_3)$,

$E_{05} = (C_{00}b_{25} + C_{01}b_{24} + C_{02}b_{23} + C_{03}b_{22} + C_{04}b_{21} + C_{05}b_{20} + C_{05}K_3 + C_{04}K_{21} + C_{04}K_{22} + C_{00}K_3a_{25} + C_{01}K_3a_{24} + C_{02}K_3a_{23} + C_{03}K_3a_{22} + C_{04}K_3a_{21} + C_{00}K_{21}a_{24} + C_{01}K_{21}a_{23} + C_{02}K_{21}a_{22} + C_{03}K_{21}a_{21} + C_{00}K_{22}a_{24} + C_{01}K_{22}a_{23} + C_{02}K_{22}a_{22} + C_{03}K_{22}a_{21})/(C_{00} + D_{00}b_{20} + D_{00}K_3)$,

$E_{06} = (C_{00}b_{26} + C_{01}b_{25} + C_{02}b_{24} + C_{03}b_{23} + C_{04}b_{22} + C_{05}b_{21} + C_{06}b_{20} + C_{06}K_3 + C_{05}K_{21} + C_{05}K_{22} + C_{00}K_3a_{26} + C_{01}K_3a_{25} + C_{02}K_3a_{24} + C_{03}K_3a_{23} + C_{04}K_3a_{22} + C_{05}K_3a_{21} + C_{00}K_{21}a_{25} + C_{01}K_{21}a_{24} + C_{02}K_{21}a_{23} + C_{03}K_{21}a_{22} + C_{04}K_{21}a_{21} + C_{00}K_{22}a_{25} + C_{01}K_{22}a_{24} + C_{02}K_{22}a_{23} + C_{03}K_{22}a_{22} + C_{04}K_{22}a_{21})/(C_{00} + D_{00}b_{20} + D_{00}K_3)$,

$E_{07} = (C_{01}b_{26} + C_{02}b_{25} + C_{03}b_{24} + C_{04}b_{23} + C_{05}b_{22} + C_{06}b_{21} + C_{07}b_{20} + C_{07}K_3 + C_{06}K_{21} + C_{06}K_{22} + C_{01}K_3a_{26} + C_{02}K_3a_{25} + C_{03}K_3a_{24} + C_{04}K_3a_{23} + C_{05}K_3a_{22} +$

$C_{06}K_3a_{21}+C_{00}K_{21}a_{26}+C_{01}K_{21}a_{25}+C_{02}K_{21}a_{24}+C_{03}K_{21}a_{23}+C_{04}K_{21}a_{22}+C_{05}K_{21}a_{21}+C_{00}K_{22}a_{26}+C_{01}K_{22}a_{25}+C_{02}K_{22}a_{24}+C_{03}K_{22}a_{23}+C_{04}K_{22}a_{22}+C_{05}K_{22}a_{21})/(C_{00}+D_{00}b_{20}+D_{00}K_3)$,

$E_{08}=(C_{02}b_{26}+C_{03}b_{25}+C_{04}b_{24}+C_{05}b_{23}+C_{06}b_{22}+C_{07}b_{21}+C_{08}b_{20}+C_{08}K_3+C_{07}K_{21}+C_{07}K_{22}+C_{02}K_3a_{26}+C_{03}K_3a_{25}+C_{04}K_3a_{24}+C_{05}K_3a_{23}+C_{06}K_3a_{22}+C_{07}K_3a_{21}+C_{01}K_{21}a_{26}+C_{02}K_{21}a_{25}+C_{03}K_{21}a_{24}+C_{04}K_{21}a_{23}+C_{05}K_{21}a_{22}+C_{06}K_{21}a_{21}+C_{01}K_{22}a_{26}+C_{02}K_{22}a_{25}+C_{03}K_{22}a_{24}+C_{04}K_{22}a_{23}+C_{05}K_{22}a_{22}+C_{06}K_{22}a_{21})/(C_{00}+D_{00}b_{20}+D_{00}K_3)$,

$E_{09}=(C_{03}b_{26}+C_{04}b_{25}+C_{05}b_{24}+C_{06}b_{23}+C_{07}b_{22}+C_{08}b_{21}+C_{09}b_{20}+C_{09}K_3+C_{08}K_{21}+C_{08}K_{22}+C_{03}K_3a_{26}+C_{04}K_3a_{25}+C_{05}K_3a_{24}+C_{06}K_3a_{23}+C_{07}K_3a_{22}+C_{08}K_3a_{21}+C_{02}K_{21}a_{26}+C_{03}K_{21}a_{25}+C_{04}K_{21}a24+C_{05}K_{21}a_{23}+C_{06}K_{21}a_{22}+C_{07}K_{21}a_{21}+C_{02}K_{22}a_{26}+C_{03}K_{22}a_{25}+C_{04}K_{22}a_{24}+C_{05}K_{22}a_{23}+C_{06}K_{22}a_{22}+C_{07}K_{22}a_{21}/(C_{00}+D_{00}b_{20}+D_{00}K_3)$,

$E_{10}=(C_{04}b_{26}+C_{05}b_{25}+C_{06}b_{24}+C_{07}b_{23}+C_{08}b_{22}+C_{09}b_{21}+C_{10}b_{20}+C_{10}K_3+C_{09}K_{21}+C_{09}K_{22}+C_{04}K_3a_{26}+C_{05}K_3a_{25}+C_{06}K_3a_{24}+C_{07}K_3a_{23}+C_{08}K_3a_{22}+C_{09}K_3a_{21}+C_{03}K_{21}a_{26}+C_{04}K_{21}a_{25}+C_{05}K_{21}a_{24}+C_{06}K_{21}a_{23}+C_{07}K_{21}a_{22}+C_{08}K_{21}a_{21}+C_{03}K_{22}a_{26}+C_{04}K_{22}a_{25}+C_{05}K_{22}a_{24}+C_{06}K_{22}a_{23}+C_{07}K_{22}a_{22}+C_{08}K_{22}a_{21})/(C_{00}+D_{00}b_{20}+D_{00}K_3)$,

$E_{11}=(C_{05}b_{26}+C_{06}b_{25}+C_{27}b_{24}+C_{08}b_{23}+C_{09}b_{22}+C_{10}b_{21}+C_{11}b_{20}+C_{11}K_3+C_{10}K_{21}+C_{10}K_{22}+C_{05}K_3a_{26}+C_{06}K_3a_{25}+C_{07}K_3a_{24}+C_{08}K_3a_{23}+C_{09}K_3a_{22}+C_{10}K_3a_{21}+C_{04}K_{21}a_{26}+C_{05}K_{21}a_{25}+C_{06}K_{21}a_{24}+C_{07}K_{21}a_{23}+C_{08}K_{21}a_{22}+C_{09}K_{21}a_{21}+C_{04}K_{22}a_{26}+C_{05}K_{22}a_{25}+C_{06}K_{22}a_{24}+C_{07}K_{22}a_{23}+C_{08}K_{22}a_{22}+C_{09}K_{22}a_{21})/(C_{00}+D_{00}b_{20}+D_{00}K_3)$,

$E_{12}=(C_{06}b_{26}+C_{07}b_{25}+C_{08}b_{24}+C_{09}b_{23}+C_{10}b_{22}+C_{11}b_{21}+C_{12}b_{20}+C_{12}K_3+C_{11}K_{21}+C_{11}K_{22}+C_{06}K_3a_{26}+C_{07}K_3a_{25}+C_{08}K_3a_{24}+C_{09}K_3a_{23}+C_{10}K_3a_{22}+C_{11}K_3a_{21}+C_{05}K_{21}a_{26}+C_{06}K_{21}a_{25}+C_{07}K_{21}a_{24}+C_{08}K_{21}a_{23}+C_{09}K_{21}a_{22}+C_{10}K_{21}a_{21}+C_{05}K_{22}a_{26}+C_{06}K_{22}a_{25}+C_{07}K_{22}a_{24}+C_{08}K_{22}a_{23}+C_{09}K_{22}a_{22}+C_{10}K_{22}a_{21})/(C_{00}+D_{00}b_{20}+D_{00}K_3)$,

$$E_{13} = (C_{07}b_{26} + C_{08}b_{25} + C_{09}b_{24} + C_{10}b_{23} + C_{11}b_{22} + C_{14}b_{21} + C_{13}b_{20} + C_{13}K_3 + C_{12}K_{21} + C_{12}K_{22} + C_{07}K_3a_{26} + C_{08}K_3a_{25} + C_{09}K_3a_{24} + C_{10}K_3a_{23} + C_{11}K_3a_{22} + C_{12}K_3a_{21} + C_{06}K_{21}a_{26} + C_{07}K_{21}a_{25} + C_{08}K_{21}a_{24} + C_{09}K_{21}a_{23} + C_{10}K_{21}a_{22} + C_{11}K_{21}a_{21} + C_{06}K_{22}a_{26} + C_{07}K_{22}a_{25} + C_{08}K_{22}a_{24} + C_{09}K_{22}a_{23} + C_{10}K_{22}a_{22} + C_{11}K_{22}a_{21})/(C_{00} + D_{00}b_{20} + D_{00}K_3),$$

$$E_{14} = (C_{08}b_{26} + C_{09}b_{25} + C_{10}b_{24} + C_{11}b_{23} + C_{12}b_{22} + C_{13}b_{21} + C_{14}b_{20} + C_{14}K_3 + C_{13}K_{21} + C_{13}K_{22} + C_{08}K_3a_{26} + C_{09}K_3a_{25} + C_{10}K_3a_{24} + C_{11}K_3a_{23} + C_{12}K_3a_{22} + C_{13}K_3a_{21} + C_{07}K_{21}a_{26} + C_{08}K_{21}a_{25} + C_{09}K_{21}a_{24} + C_{10}K_{21}a_{23} + C_{11}K_{21}a_{22} + C_{12}K_{21}a_{21} + C_{07}K_{22}a_{26} + C_{08}K_{22}a_{25} + C_{09}K_{22}a_{24} + C_{10}K_{22}a_{23} + C_{11}K_{22}a_{22} + C_{12}K_{22}a_{21})/(C_{00} + D_{00}b_{20} + D_{00}K_3),$$

$$E_{15} = (C_{09}b_{26} + C_{10}b_{25} + C_{11}b_{24} + C_{12}b_{23} + C_{13}b_{22} + C_{14}b_{21} + C_{14}K_{21} + C_{14}K_{22} + C_{09}K_3a_{26} + C_{10}K_3a_{25} + C_{11}K_3a_{24} + C_{12}K_3a_{23} + C_{13}K_3a_{22} + C_{14}K_3a_{21} + C_{08}K_{21}a_{26} + C_{09}K_{21}a_{25} + C_{10}K_{21}a_{24} + C_{11}K_{21}a_{23} + C_{12}K_{21}a_{22} + C_{13}K_{21}a_{21} + C_{08}K_{22}a_{26} + C_{09}K_{22}a_{25} + C_{10}K_{22}a_{24} + C_{11}K_{22}a_{23} + C_{12}K_{22}a_{22} + C_{13}K_{22}a_{21})/(C_{00} + D_{00}b_{20} + D_{00}K_3),$$

$$E_{16} = (C_{10}b_{26} + C_{11}b_{25} + C_{12}b_{24} + C_{13}b_{23} + C_{14}b_{22} + C_{10}K_3a_{26} + C_{11}K_3a_{25} + C_{12}K_3a_{24} + C_{13}K_3a_{23} + C_{14}K_3a_{22} + C_{09}K_{21}a_{26} + C_{10}K_{21}a_{25} + C_{11}K_{21}a_{24} + C_{12}K_{21}a_{23} + C_{13}K_{21}a_{22} + C_{14}K_{21}a_{21} + C_{09}K_{22}a_{26} + C_{10}K_{22}a_{25} + C_{11}K_{22}a_{24} + C_{12}K_{22}a_{23} + C_{13}K_{22}a_{22} + C_{14}K_{22}a_{21})/(C_{00} + D_{00}b_{20} + D_{00}K_3),$$

$$E_{17} = (C_{11}b_{26} + C_{12}b_{25} + C_{13}b_{24} + C_{14}b_{23} + C_{11}K_3a_{26} + C_{12}K_3a_{25} + C_{13}K_3a_{24} + C_{14}K_3a_{23} + C_{10}K_{21}a_{26} + C_{11}K_{21}a_{25} + C_{12}K_{21}a_{24} + C_{11}K_{21}a_{23} + C_{14}K_{21}a_{22} + C_{10}K_{22}a_{26} + C_{11}K_{22}a_{25} + C_{12}K_{22}a_{24} + C_{13}K_{22}a_{23} + C_{14}K_{22}a_{22})/(C_{00} + D_{00}b_{20} + D_{00}K_3),$$

$$E_{18} = (C_{12}b_{26} + C_{13}b_{25} + C_{14}b_{24} + C_{12}K_3a_{26} + C_{13}K_3a_{25} + C_{14}K_3a_{24} + C_{11}K_{21}a_{26} + C_{12}K_{21}a_{25} + C_{13}K_{21}a_{24} + C_{14}K_{21}a_{23} + C_{11}K_{22}a_{26} + C_{12}K_{22}a_{25} + C_{13}K_{22}a_{24} + C_{14}K_{22}a_{23})/(C_{00} + D_{00}b_{20} + D_{00}K_3),$$

$$E_{19} = (C_{13}b_{26} + C_{14}b_{25} + C_{13}K_3a_{26} + C_{14}K_3a_{25} + C_{12}K_{21}a_{26} + C_{13}K_{21}a_{25} + C_{14}K_{21}a_{24} + C_{12}K_{22}a_{26} + C_{13}K_{22}a_{25} + C_{14}K_{22}a_{24})/(C_{00} + D_{00}b_{20} + D_{00}K_3),$$

$$E_{20} = (C_{14}b_{26} + C_{14}K_3a_{26} + C_{13}K_{21}a_{26} + C_{14}K_{21}a_{25} + C_{13}K_{22}a_{26} + C_{14}K_{22}a_{25})/(C_{00} +$$

$D_{00}b_{20} + D_{00}K_3)$,
$E_{21} = (C_{14}K_{21}a_{26} + C_{14}K_{22}a_{26})/(C_{00} + D_{00}b_{20} + D_{00}K_3)$,

$A_{00} = 1$,

$A_{01} = (C_{01}+C_{00}a_{21}+D_{00}b_{21}+D_{01}b_{20}+D_{01}K_3+D_{00}K_{21}+D_{00}K_{22}+D_{00}K_3a_{21})/(C_{00}+D_{00}b_{20} + D_{00}K_3)$,

$A_{02} = (C_{02} + C_{00}a_{22} + C_{01}a_{21} + D_{00}b_{22} + D_{01}b_{21} + D_{02}b_{20} + D_{02}K_3 + D_{01}K_{21} + D_{01}K_{22} + D_{00}K_3a_{22} + D_{01}K_3a_{21} + D_{00}K_{21}a_{21} + D_{00}K_{22}a_{21})/(C_{00} + D_{00}b_{20} + D_{00}K_3)$,

$A_{03} = (C_{03} + C_{00}a_{23} + C_{01}a_{22} + C_{02}a_{21} + D_{00}b_{23} + D_{01}b_{22} + D_{02}b_{21} + D_{03}b_{20} + D_{03}K_3 + D_{02}K_{21} + D_{02}K_{22} + D_{00}K_3a_{23} + D_{01}K_3a_{22} + D_{02}K_3a_{21} + D_{00}K_{21}a_{22} + D_{01}K_{21}a_{21} + D_{00}K_{22}a_{22} + D_{01}K_{22}a_{21})/(C_{00} + D_{00}b_{20} + D_{00}K_3)$,

$A_{04} = (C_{04}+C_{00}a_{24}+C_{01}a_{23}+C_{02}a_{22}+C_{03}a_{21}+D_{00}b_{24}+D_{01}b_{23}+D_{02}b_{22}+D_{03}b_{21}+D_{04}b_{20}+D_{04}K_3+D_{03}K_{21}+D_{03}K_{22}+D_{00}K_3a_{24}+D_{01}K_3a_{23}+D_{02}K_3a_{22}+D_{03}K_3a_{21}+D_{00}K_{21}a_{23}+D_{01}K_{21}a_{22}+D_{02}K_{21}a_{21}+D_{00}K_{22}a_{23}+D_{01}K_{22}a_{22}+D_{02}K_{22}a_{21})/(C_{00}+D_{00}b_{20}+D_{00}K_3)$,

$A_{05} = (C_{05}+C_{00}a_{25}+C_{01}a_{24}+C_{02}a_{23}+C_{03}a_{22}+C_{04}a_{21}+D_{00}b_{25}+D_{01}b_{24}+D_{02}b_{23}+D_{03}b_{22} + D_{04}b_{21} + D_{05}b_{20} + D_{05}K_3 + D_{04}K_{21} + D_{04}K_{22} + D_{00}K_3a_{25} + D_{01}K_3a_{24} + D_{02}K_3a_{23}+D_{03}K_3a_{22}+D_{04}K_3a_{21}+D_{00}K_{21}a_{24}+D_{01}K_{21}a_{23}+D_{02}K_{21}a_{22}+D_{03}K_{21}a_{21}+D_{00}K_{22}a_{24} + D_{01}K_{22}a_{23} + D_{02}K_{22}a_{22} + D_{03}K_{22}a_{21})/(C_{00} + D_{00}b_{20} + D_{00}K_3)$,

$A_{06} = (C_{06}+C_{00}a_{26}+C_{01}a_{25}+C_{02}a_{24}+C_{03}a_{23}+C_{04}a_{22}+C_{05}a_{21}+D_{00}b_{26}+D_{01}b_{25}+D_{02}b_{24}+D_{03}b_{23}+D_{04}b_{22}+D_{05}b_{21}+D_{06}b_{20}+D_{06}K_3+D_{05}K_{21}+D_{05}K_{22}+D_{00}K_3a_{26}+D_{01}K_3a_{25}+D_{02}K_3a_{24}+D_{03}K_3a_{23}+D_{04}K_3a_{22}+D_{05}K_3a_{21}+D_{00}K_{21}a_{25}+D_{01}K_{21}a_{24}+D_{02}K_{21}a_{23}+D_{03}K_{21}a_{22}+D_{04}K_{21}a_{21}+D_{00}K_{22}a_{25}+D_{01}K_{22}a_{24}+D_{02}K_{22}a_{23}+D_{03}K_{22}a_{22}+D_{04}K_{22}a_{21})/(C_{00} + D_{00}b_{20} + D_{00}K_3)$,

$A_{07} = (C_{07}+C_{01}a_{26}+C_{02}a_{25}+C_{03}a_{24}+C_{04}a_{23}+C_{05}a_{22}+C_{06}a_{21}+D_{01}b_{26}+D_{02}b_{25}+D_{03}b_{24}+D_{04}b_{23}+D_{05}b_{22}+D_{06}b_{21}+D_{07}b_{20}+D_{07}K_3+D_{06}K_{21}+D_{06}K_{22}+D_{01}K_3a_{26}+D_{02}K_3a_{25}+D_{03}K_3a_{24}+D_{04}K_3a_{23}+D_{05}K_3a_{22}+D_{06}K_3a_{21}+D_{00}K_{21}a_{26}+D_{01}K_{21}a_{25}+$

$D_{02}K_{21}a_{24}+D_{03}K_{21}a_{23}+D_{04}K_{21}a_{22}+D_{05}K_{21}a_{21}+D_{00}K_{22}a_{26}+D_{01}K_{22}a_{25}+D_{02}K_{22}a_{24}+$
$D_{03}K_{22}a_{23}+D_{04}K_{22}a_{22}+D_{05}K_{22}a_{21})/(C_{00}+D_{00}b_{20}+D_{00}K_3)$,

$A_{08}=(C_{08}+C_{02}a_{26}+C_{03}a_{25}+C_{04}a_{24}+C_{05}a_{23}+C_{06}a_{22}+C_{07}a_{21}+D_{02}b_{26}+D_{03}b_{25}+$
$D_{04}b_{24}+D_{05}b_{23}+D_{06}b_{22}+D_{07}b_{21}+D_{08}b_{20}+D_{08}K_3+D_{07}K_{21}+D_{07}K_{22}+D_{02}K_3a_{26}+$
$D_{03}K_3a_{25}+D_{04}K_3a_{24}+D_{05}K_3a_{23}+D_{06}K_3a_{22}+D_{07}K_3a_{21}+D_{01}K_{21}a_{26}+D_{02}K_{21}a_{25}+$
$D_{03}K_{21}a_{24}+D_{04}K_{21}a_{23}+D_{05}K_{21}a_{22}+D_{06}K_{21}a_{21}+D_{01}K_{22}a_{26}+D_{02}K_{22}a_{25}+D_{03}K_{22}a_{24}+$
$D_{04}K_{22}a_{23}+D_{05}K_{22}a_{22}+D_{06}K_{22}a_{21})/(C_{00}+D_{00}b_{20}+D_{00}K_3)$,

$A_{09}=(C_{09}+C_{03}a_{26}+C_{04}a_{25}+C_{05}a_{24}+C_{06}a_{23}+C_{07}a_{22}+C_{08}a_{21}+D_{03}b_{26}+D_{04}b_{25}+$
$D_{05}b_{24}+D_{06}b_{23}+D_{07}b_{22}+D_{08}b_{21}+D_{09}b_{20}+D_{09}K_3+D_{08}K_{21}+D_{08}K_{22}+D_{03}K_3a_{26}+$
$D_{04}K_3a_{25}+D_{05}K_3a_{24}+D_{06}K_3a_{23}+D_{07}K_3a_{22}+D_{08}K_3a_{21}+D_{02}K_{21}a_{26}+D_{03}K_{21}a_{25}+$
$D_{04}K_{21}a_{24}+D_{05}K_{21}a_{23}+D_{06}K_{21}a_{22}+D_{07}K_{21}a_{21}+D_{02}K_{22}a_{26}+D_{03}K_{22}a_{25}+D_{04}K_{22}a_{24}+$
$D_{05}K_{22}a_{23}+D_{06}K_{22}a_{22}+D_{07}K_{22}a_{21})/(C_{00}+D_{00}b_{20}+D_{00}K_3)$,

$A_{10}=(C_{10}+C_{04}a_{26}+C_{05}a_{25}+C_{06}a_{24}+C_{07}a_{23}+C_{08}a_{22}+C_{09}a_{21}+D_{04}b_{26}+D_{05}b_{25}+$
$D_{06}b_{24}+D_{07}b_{23}+D_{08}b_{22}+D_{09}b_{21}+D_{10}b_{20}+D_{10}K_3+D_{09}K_{21}+D_{09}K_{22}+D_{04}K_3a_{26}+$
$D_{05}K_3a_{25}+D_{06}K_3a_{24}+D_{07}K_3a_{23}+D_{08}K_3a_{22}+D_{09}K_3a_{21}+D_{03}K_{21}a_{26}+D_{04}K_{21}a_{25}+$
$D_{05}K_{21}a_{24}+D_{06}K_{21}a_{23}+D_{07}K_{21}a_{22}+D_{08}K_{21}a_{21}+D_{03}K_{22}a_{26}+D_{04}K_{22}a_{25}+D_{05}K_{22}a_{24}+$
$D_{06}K_{22}a_{23}+D_{07}K_{22}a_{22}+D_{08}K_{22}a_{21})/(C_{00}+D_{00}b_{20}+D_{00}K_3)$,

$A_{11}=(C_{11}+C_{05}a_{26}+C_{06}a_{25}+C_{07}a_{24}+C_{08}a_{23}+C_{09}a_{22}+C_{10}a_{21}+D_{05}b_{26}+D_{06}b_{25}+$
$D_{07}b_{24}+D_{08}b_{23}+D_{09}b_{22}+D_{10}b_{21}+D_{11}b_{20}+D_{11}K_3+D_{10}K_{21}+D_{10}K_{22}+D_{05}K_3a_{26}+$
$D_{06}K_3a_{25}+D_{07}K_3a_{24}+D_{08}K_3a_{23}+D_{09}K_3a_{22}+D_{10}K_3a_{21}+D_{04}K_{21}a_{26}+D_{05}K_{21}a_{25}+$
$D_{06}K_{21}a_{24}+D_{07}K_{21}a_{23}+D_{08}K_{21}a_{22}+D_{09}K_{21}a_{21}+D_{04}K_{22}a_{26}+D_{05}K_{22}a_{25}+D_{06}K_{22}a_{24}+$
$D_{07}K_{22}a_{23}+D_{08}K_{22}a_{22}+D_{09}K_{22}a_{21})/(C_{00}+D_{00}b_{20}+D_{00}K_3)$,

$A_{12}=(C_{12}+C_{06}a_{26}+C_{07}a_{25}+C_{08}a_{24}+C_{09}a_{23}+C_{10}a_{22}+C_{11}a_{21}+D_{06}b_{26}+D_{07}b_{25}+$
$D_{08}b_{24}+D_{09}b_{23}+D_{10}b_{22}+D_{11}b_{21}+D_{12}b_{20}+D_{12}K_3+D_{11}K_{21}+D_{11}K_{22}+D_{06}K_3a_{26}+$
$D_{07}K_3a_{25}+D_{08}K_3a_{24}+D_{09}K_3a_{23}+D_{10}K_3a_{22}+D_{11}K_3a_{21}+D_{05}K_{21}a_{26}+D_{06}K_{21}a_{25}+$
$D_{07}K_{21}a_{24}+D_{08}K_{21}a_{23}+D_{09}K_{21}a_{22}+D_{10}K_{21}a_{21}+D_{05}K_{22}a_{26}+D_{06}K_{22}a_{25}+D_{07}K_{22}a_{24}+$
$D_{08}K_{22}a_{23}+D_{09}K_{22}a_{22}+D_{10}K_{22}a_{21})/(C_{00}+D_{00}b_{20}+D_{00}K_3)$,

$A_{13}=(C_{13}+C_{07}a_{26}+C_{08}a_{25}+C_{09}a_{24}+C_{10}a_{23}+C_{11}a_{22}+C_{12}a_{21}+D_{07}b_{26}+D_{08}b_{25}+$

$D_{09}b_{24}+D_{10}b_{23}+D_{11}b_{22}+D_{12}b_{21}+D_{13}b_{20}+D_{13}K_3+D_{12}K_{21}+D_{12}K_{22}+D_{07}K_3a_{26}+D_{08}K_3a_{25}+D_{09}K_3a_{24}+D_{10}K_3a_{23}+D_{11}K_3a_{22}+D_{12}K_3a_{21}+D_{06}K_{21}a_{26}+D_{07}K_{21}a_{25}+D_{08}K_{21}a_{24}+D_{09}K_{21}a_{23}+D_{10}K_{21}a_{22}+D_{11}K_{21}a_{21}+D_{06}K_{22}a_{26}+D_{07}K_{22}a_{25}+D_{08}K_{22}a_{24}+D_{09}K_{22}a_{23}+D_{10}K_{22}a_{22}+D_{11}K_{22}a_{21})/(C_{00}+D_{00}b_{20}+D_{00}K_3)$,

$A_{14}=(C_{14}+C_{08}a_{26}+C_{09}a_{25}+C_{10}a_{24}+C_{11}a_{23}+C_{12}a_{22}+C_{13}a_{21}+D_{08}b_{26}+D_{09}b_{25}+D_{10}b_{24}+D_{11}b_{23}+D_{12}b_{22}+D_{13}b_{21}+D_{13}K_{21}+D_{13}K_{22}+D_{08}K_3a_{26}+D_{09}K_3a_{25}+D_{10}K_3a_{24}+D_{11}K_3a_{23}+D_{12}K_3a_{22}+D_{13}K_3a_{21}+D_{07}K_{21}a_{26}+D_{08}K_{21}a_{25}+D_{09}K_{21}a_{24}+D_{10}K_{21}a_{23}+D_{11}K_{21}a_{22}+D_{12}K_{21}a_{21}+D_{07}K_{22}a_{26}+D_{08}K_{22}a_{25}+D_{09}K_{22}a_{24}+D_{10}K_{22}a_{23}+D_{11}K_{22}a_{22}+D_{12}K_{22}a_{21})/(C_{00}+D_{00}b_{20}+D_{00}K_3)$,

$A_{15}=(C_{09}a_{26}+C_{10}a_{25}+C_{11}a_{24}+C_{12}a_{23}+C_{13}a_{22}+C_{14}a_{21}+D_{09}b_{26}+D_{10}b_{25}+D_{11}b_{24}+D_{12}b_{23}+D_{13}b_{22}+D_{09}K_3a_{26}+D_{10}K_3a_{25}+D_{11}K_3a_{24}+D_{12}K_3a_{23}+D_{13}K_3a_{22}+D_{08}K_{21}a_{26}+D_{09}K_{21}a_{25}+D_{10}K_{21}a_{24}+D_{11}K_{21}a_{23}+D_{12}K_{21}a_{22}+D_{13}K_{21}a_{21}+D_{08}K_{22}a_{26}+D_{09}K_{22}a_{25}+D_{10}K_{22}a_{24}+D_{11}K_{22}a_{23}+D_{12}K_{22}a_{22}+D_{13}K_{22}a_{21})/(C_{00}+D_{00}b_{20}+D_{00}K_3)$,

$A_{16}=(C_{10}a_{26}+C_{11}a_{25}+C_{12}a_{24}+C_{13}a_{23}+C_{14}a_{22}+D_{10}b_{26}+D_{11}b_{25}+D_{12}b_{24}+D_{13}b_{23}+D_{10}K_3a_{26}+D_{11}K_3a_{25}+D_{12}K_3a_{24}+D_{13}K_3a_{23}+D_{09}K_{21}a_{26}+D_{10}K_{21}a_{25}+D_{11}K_{21}a_{24}+D_{12}K_{21}a_{23}+D_{13}K_{21}a_{22}+D_{09}K_{22}a_{26}+D_{10}K_{22}a_{25}+D_{11}K_{22}a_{24}+D_{12}K_{22}a_{23}+D_{13}K_{22}a_{22})/(C_{00}+D_{00}b_{20}+D_{00}K_3)$,

$A_{17}=(C_{11}a_{26}+C_{12}a_{25}+C_{13}a_{24}+C_{14}a_{23}+D_{11}b_{26}+D_{12}b_{25}+D_{13}b_{24}+D_{11}K_3a_{26}+D_{12}K_3a_{25}+D_{13}K_3a_{24}+D_{10}K_{21}a_{26}+D_{11}K_{21}a_{25}+D_{12}K_{21}a_{24}+D_{13}K_{21}a_{23}+D_{10}K_{22}a_{26}+D_{11}K_{22}a_{25}+D_{12}K_{22}a_{24}+D_{13}K_{22}a_{23})/(C_{00}+D_{00}b_{20}+D_{00}K_3)$,

$A_{18}=(C_{12}a_{26}+C_{13}a_{25}+C_{14}a_{24}+D_{12}b_{26}+D_{13}b_{25}+D_{12}K_3a_{26}+D_{13}K_3a_{25}+D_{11}K_{21}a_{26}+D_{12}K_{21}a_{25}+D_{13}K_{21}a_{24}+D_{11}K_{22}a_{26}+D_{12}K_{22}a_{25}+D_{13}K_{22}a_{24})/(C_{00}+D_{00}b_{20}+D_{00}K_3)$,

$A_{19}=(C_{13}a_{26}+C_{14}a_{25}+D_{13}b_{26}+D_{13}K_3a_{26}+D_{12}K_{21}a_{26}+D_{13}K_{21}a_{25}+D_{12}K_{22}a_{26}+D_{13}K_{22}a_{25})/(C_{00}+D_{00}b_{20}+D_{00}K_3)$,
$A_{20}=(C_{14}a_{26}+D_{13}K_{21}a_{26}+D_{13}K_{22}a_{26})/(C_{00}+D_{00}b_{20}+D_{00}K_3)$,
$A_{21}=0$.

$$M_{k,0} = E_{00}/(K_i + b_{k0}),$$
$$M_{k,1} = (E_{01} + E_{00}a_{k1})/(K_i + b_{k0}),$$
$$M_{k,2} = (E_{02} + E_{00}a_{k2} + E_{01}a_{k1})/(K_i + b_{k0}),$$
$$M_{k,3} = (E_{03} + E_{00}a_{k3} + E_{01}a_{k2} + E_{02}a_{k1})/(K_i + b_{k0}),$$
$$M_{k,4} = (E_{04} + E_{00}a_{k4} + E_{01}a_{k3} + E_{02}a_{k2} + E_{03}a_{k1})/(K_i + b_{k0}),$$
$$M_{k,5} = (E_{05} + E_{00}a_{k5} + E_{01}a_{k4} + E_{02}a_{k3} + E_{03}a_{k2} + E_{04}a_{k1})/(K_i + b_{k0}),$$
$$M_{k,6} = (E_{06} + E_{00}a_{k6} + E_{01}a_{k5} + E_{02}a_{k4} + E_{03}a_{k3} + E_{04}a_{k2} + E_{05}a_{k1})/(K_i + b_{k0}),$$
$$M_{k,7} = (E_{07} + E_{01}a_{k6} + E_{02}a_{k5} + E_{03}a_{k4} + E_{04}a_{k3} + E_{05}a_{k2} + E_{06}a_{k1})/(K_i + b_{k0}),$$
$$M_{k,8} = (E_{08} + E_{02}a_{k6} + E_{03}a_{k5} + E_{04}a_{k4} + E_{05}a_{k3} + E_{06}a_{k2} + E_{07}a_{k1})/(K_i + b_{k0}),$$
$$M_{k,9} = (E_{09} + E_{03}a_{k6} + E_{04}a_{k5} + E_{05}a_{k4} + E_{06}a_{k3} + E_{07}a_{k2} + E_{08}a_{k1})/(K_i + b_{k0}),$$
$$M_{k,10} = (E_{10} + E_{04}a_{k6} + E_{05}a_{k5} + E_{06}a_{k4} + E_{07}a_{k3} + E_{08}a_{k2} + E_{09}a_{k1})/(K_i + b_{k0}),$$
$$M_{k,11} = (E_{11} + E_{05}a_{k6} + E_{06}a_{k5} + E_{07}a_{k4} + E_{08}a_{k3} + E_{09}a_{k2} + E_{10}a_{k1})/(K_i + b_{k0}),$$
$$M_{k,12} = (E_{12} + E_{06}a_{k6} + E_{07}a_{k5} + E_{08}a_{k4} + E_{09}a_{k3} + E_{10}a_{k2} + E_{11}a_{k1})/(K_i + b_{k0}),$$
$$M_{k,13} = (E_{13} + E_{07}a_{k6} + E_{08}a_{k5} + E_{09}a_{k4} + E_{10}a_{k3} + E_{11}a_{k2} + E_{12}a_{k1})/(K_i + b_{k0}),$$
$$M_{k,14} = (E_{14} + E_{08}a_{k6} + E_{09}a_{k5} + E_{10}a_{k4} + E_{11}a_{k3} + E_{12}a_{k2} + E_{13}a_{k1})/(K_i + b_{k0}),$$
$$M_{k,15} = (E_{15} + E_{09}a_{k6} + E_{10}a_{k5} + E_{11}a_{k4} + E_{12}a_{k3} + E_{13}a_{k2} + E_{14}a_{k1})/(K_i + b_{k0}),$$
$$M_{k,16} = (E_{16} + E_{10}a_{k6} + E_{11}a_{k5} + E_{12}a_{k4} + E_{13}a_{k3} + E_{14}a_{k2} + E_{15}a_{k1})/(K_i + b_{k0}),$$
$$M_{k,17} = (E_{17} + E_{11}a_{k6} + E_{12}a_{k5} + E_{13}a_{k4} + E_{14}a_{k3} + E_{15}a_{k2} + E_{16}a_{k1})/(K_i + b_{k0}),$$
$$M_{k,18} = (E_{18} + E_{12}a_{k6} + E_{13}a_{k5} + E_{14}a_{k4} + E_{15}a_{k3} + E_{16}a_{k2} + E_{17}a_{k1})/(K_i + b_{k0}),$$
$$M_{k,19} = (E_{19} + E_{13}a_{k6} + E_{14}a_{k5} + E_{15}a_{k4} + E_{16}a_{k3} + E_{17}a_{k2} + E_{18}a_{k1})/(K_i + b_{k0}),$$
$$M_{k,20} = (E_{20} + E_{14}a_{k6} + E_{15}a_{k5} + E_{16}a_{k4} + E_{17}a_{k3} + E_{18}a_{k2} + E_{19}a_{k1})/(K_i + b_{k0}),$$
$$M_{k,21} = (E_{21} + E_{15}a_{k6} + E_{16}a_{k5} + E_{17}a_{k4} + E_{18}a_{k3} + E_{19}a_{k2} + E_{20}a_{k1})/(K_i + b_{k0}),$$
$$M_{k,22} = (E_{16}a_{k6} + E_{17}a_{k5} + E_{18}a_{k4} + E_{19}a_{k3} + E_{20}a_{k2} + E_{21}a_{k1})/(K_i + b_{k0}),$$
$$M_{k,23} = (E_{17}a_{k6} + E_{18}a_{k5} + E_{19}a_{k4} + E_{20}a_{k3} + E_{21}a_{k2})/(K_i + b_{k0}),$$
$$M_{k,24} = (E_{18}a_{k6} + E_{19}a_{k5} + E_{20}a_{k4} + E_{21}a_{k3})/(K_i + b_{k0}),$$
$$M_{k,25} = (E_{19}a_{k6} + E_{20}a_{k5} + E_{21}a_{k4})/(K_i + b_{k0}),$$
$$M_{k,26} = (E_{20}a_{k6} + E_{21}a_{k5})/(K_i + b_{k0}),$$
$$M_{k,27} = (E_{21}a_{k6})/(K_i + b_{k0}).$$
$$N_{k,0} = 1,$$
$$N_{k,1} = (K_{k1} + K_{02} + b_{01} + A_{01}b_{00} + K_1a_{01} + A_{01}K_1)/(K_1 + b_{00}),$$
$$N_{k,2} = (b_{k2} + A_{k1}b_{k1} + A_{02}b_{k0} + K_ia_{k2} + K_{k1}a_{k1} + K_{k2}a_{k1} + A_{k2}K_i + A_{01}K_{k1} + A_{k1}K_{k2} + A_{01}K_ia_{k1})/(K_i + b_{k0}),$$
$$N_{k,3} = (b_{k3} + A_{01}b_{k2} + A_{02}b_{k1} + A_{03}b_{k0} + K_ia_{k3} + K_{k1}a_{k2} + K_{k2}a_{k2} + A_{03}K_i + A_{02}K_{k1} + A_{02}K_{k2} + A_{01}K_ia_{k2} + A_{02}K_ia_{k1} + A_{01}K_{k1}a_{k1} + A_{01}K_{k2}a_{k1})/(K_i + b_{k0}),$$

$$N_{k,4} = (b_{k4} + A_{01}b_{k3} + A_{02}b_{k2} + A_{03}b_{k1} + A_{04}b_{k0} + K_i a_{k4} + K_{k1}a_{k3} + K_{k2}a_{k3} + A_{04}K_i + A_{03}K_{k1} + A_{03}K_{k2} + A_{01}K_i a_{k3} + A_{02}K_i a_{k2} + A_{03}K_i a_{k1} + A_{01}K_{k1}a_{k2} + A_{02}K_{k1}a_{k1} + A_{01}K_{k2}a_{k2} + A_{02}K_{k2}a_{k1})/(K_i + b_{k0}),$$

$$N_{k,5} = (b_{k5}+A_{01}b_{k4}+A_{02}b_{k3}+A_{03}b_{k2}+A_{04}b_{k1}+A_{05}b_{k0}+K_i a_{k5}+K_{k1}a_{k4}+K_{k2}a_{k4}+A_{05}K_i+A_{04}K_{k1}+A_{04}K_{k2}+A_{01}K_i a_{k4}+A_{02}K_i a_{k3}+A_{03}K_i a_{k2}+A_{04}K_i a_{k1}+A_{01}K_{k1}a_{k3}+A_{02}K_{k1}a_{k2} + A_{03}K_{k1}a_{k1} + A_{01}K_{k2}a_{k3} + A_{k2}K_{k2}a_{k2} + A_{03}K_{k2}a_{k1})/(K_i + b_{k0}),$$

$$N_{k,6} = (b_{k6} + A_{01}b_{k5} + A_{02}b_{k4} + A_{03}b_{k3} + A_{04}b_{k2} + A_{k5}b_{k1} + A_{06}b_{k0} + K_i a_{k6} + K_{k1}a_{k5} + K_{k2}a_{k5} + A_{06}K_i + A_{05}K_{k1} + A_{05}K_{k2} + A_{01}K_i a_{k5} + A_{02}K_i a_{k4} + A_{03}K_i a_{k3} + A_{04}K_i a_{k2}+A_{05}K_i a_{k1}+A_{01}K_{k1}a_{k4}+A_{02}K_{k1}a_{k3}+A_{03}K_{k1}a_{k2}+A_{04}K_{k1}a_{k1}+A_{01}K_{k2}a_{k4}+A_{02}K_{k2}a_{k3} + A_{03}K_{k2}a_{k2} + A_{04}K_{k2}a_{k1})/(K_i + b_{k0}),$$

$$N_{k,7} = (A_{01}b_{k6} + A_{02}b_{k5} + A_{03}b_{k4} + A_{04}b_{k3} + A_{05}b_{k2} + A_{06}b_{k1} + A_{07}b_{k0} + K_{k1}a_{k6} + K_{k2}a_{k6} + A_{07}K_i + A_{06}K_{k1} + A_{06}K_{k2} + A_{01}K_i a_{k6} + A_{02}K_i a_{k5} + A_{03}K_i a_{k4} + A_{04}K_i a_{k3} + A_{05}K_i a_{k2}+A_{06}K_i a_{k1}+A_{01}K_{k1}a_{k5}+A_{02}K_{k1}a_{k4}+A_{03}K_{k1}a_{k3}+A_{04}K_{k1}a_{k2}+A_{05}K_{k1}a_{k1}+A_{01}K_{k2}a_{k5} + A_{02}K_{k2}a_{k4} + A_{03}K_{k2}a_{k3} + A_{04}K_{k2}a_{k2} + A_{05}K_{k2}a_{k1})/(K_i + b_{k0}),$$

$$N_{k,8} = (A_{02}b_{k6} + A_{03}b_{k5} + A_{04}b_{k4} + A_{05}b_{k3} + A_{06}b_{k2} + A_{07}b_{k1} + A_{08}b_{k0} + A_{08}K_i + A_{07}K_{k1} + A_{07}K_{k2} + A_{02}K_i a_{k6} + A_{03}K_i a_{k5} + A_{04}K_i a_{k4} + A_{05}K_i a_{k3} + A_{06}K_i a_{k2} + A_{07}K_i a_{k1}+A_{01}K_{k1}a_{k6}+A_{02}K_{k1}a_{k5}+A_{03}K_{k1}a_{k4}+A_{04}K_{k1}a_{k3}+A_{05}K_{k1}a_{k2}+A_{06}K_{k1}a_{k1}+A_{01}K_{k2}a_{k6} + A_{02}K_{k2}a_{k5} + A_{03}K_{k2}a_{k4} + A_{04}K_{k2}a_{k3} + A_{05}K_{k2}a_{k2} + A_{06}K_{k2}a_{k1})/(K_i + b_{k0}),$$

$$N_{k,9} = (A_{03}b_{06} + A_{04}b_{k5} + A_{05}b_{04} + A_{06}b_{k3} + A_{07}b_{k2} + A_{08}b_{k1} + A_{09}b_{k0} + A_{09}K_i + A_{08}K_{k1} + A_{08}K_{k2} + A_{03}K_i a_{k6} + A_{04}K_i a_{k5} + A_{05}K_i a_{k4} + A_{06}K_i a_{k3} + A_{07}K_i a_{k2} + A_{08}K_i a_{k1}+A_{02}K_{k1}a_{k6}+A_{03}K_{k1}a_{k5}+A_{04}K_{k1}a_{k4}+A_{05}K_{k1}a_{k3}+A_{06}K_{k1}a_{k2}+A_{07}K_{k1}a_{k1}+A_{02}K_{k2}a_{k6} + A_{03}K_{k2}a_{k5} + A_{04}K_{k2}a_{k4} + A_{05}K_{k2}a_{k3} + A_{06}K_{k2}a_{k2} + A_{07}K_{k2}a_{k1})/(K_i + b_{k0}),$$

$$N_{k,10} = (A_{04}b_{k6} + A_{05}b_{k5} + A_{06}b_{k4} + A_{07}b_{k3} + A_{08}b_{k2} + A_{09}b_{k1} + A_{10}b_{k0} + A_{10}K_i + A_{09}K_{k1} + A_{09}K_{k2} + A_{04}K_i a_{k6} + A_{05}K_i a_{k5} + A_{06}K_i a_{k4} + A_{07}K_i a_{k3} + A_{08}K_i a_{k2} + A_{09}K_i a_{k1}+A_{03}K_{k1}a_{k6}+A_{04}K_{k1}a_{k5}+A_{05}K_{k1}a_{k4}+A_{06}K_{k1}a_{k3}+A_{07}K_{k1}a_{k2}+A_{08}K_{k1}a_{k1}+A_{03}K_{k2}a_{k6} + A_{04}K_{k2}a_{k5} + A_{05}K_{k2}a_{k4} + A_{06}K_{k2}a_{k3} + A_{07}K_{k2}a_{k2} + A_{08}K_{k2}a_{k1})/(K_i +$$

b_{k0}),

$N_{k,11} = (A_{05}b_{k6} + A_{06}b_{k5} + A_{07}b_{k4} + A_{08}b_{k3} + A_{09}b_{k2} + A_{10}b_{k1} + A_{11}b_{k0} + A_{11}K_i + A_{10}K_{k1} + A_{10}K_{k2} + A_{05}K_i a_{k6} + A_{06}K_i a_{k5} + A_{07}K_i a_{k4} + A_{08}K_i a_{k3} + A_{09}K_i a_{k2} + A_{10}K_i a_{k1} + A_{04}K_{k1}a_{k6} + A_{05}K_{k1}a_{k5} + A_{06}K_{k1}a_{k4} + A_{07}K_{k1}a_{k3} + A_{08}K_{k1}a_{k2} + A_{09}K_{k1}a_{k1} + A_{04}K_{k2}a_{k6} + A_{05}K_{k2}a_{k5} + A_{06}K_{k2}a_{k4} + A_{07}K_{k2}a_{k3} + A_{08}K_{k2}a_{k2} + A_{09}K_{k2}a_{k1})/(K_i + b_{k0})$,

$N_{k,12} = (A_{06}b_{k6} + A_{07}b_{k5} + A_{08}b_{k4} + A_{09}b_{k3} + A_{10}b_{k2} + A_{11}b_{k1} + A_{12}b_{k0} + A_{12}K_i + A_{11}K_{k1} + A_{11}K_{k2} + A_{06}K_i a_{k6} + A_{07}K_i a_{k5} + A_{08}K_i a_{k4} + A_{09}K_i a_{k3} + A_{10}K_i a_{k2} + A_{11}K_i a_{k1} + A_{05}K_{k1}a_{k6} + A_{06}K_{k1}a_{k5} + A_{07}K_{k1}a_{k4} + A_{08}K_{k1}a_{k3} + A_{09}K_{k1}a_{k2} + A_{10}K_{k1}a_{k1} + A_{05}K_{k2}a_{k6} + A_{06}K_{k2}a_{k5} + A_{07}K_{k2}a_{k4} + A_{08}K_{k2}a_{k3} + A_{09}K_{k2}a_{k2} + A_{10}K_{k2}a_{k1})/(K_i + b_{k0})$,

$N_{k,13} = (A_{07}b_{k6} + A_{08}b_{k5} + A_{09}b_{k4} + A_{10}b_{k3} + A_{11}b_{k2} + A_{12}b_{k1} + A_{13}b_{k0} + A_{13}K_i + A_{12}K_{k1} + A_{12}K_{k2} + A_{07}K_i a_{k6} + A_{08}K_i a_{k5} + A_{09}K_i a_{k4} + A_{10}K_i a_{k3} + A_{11}K_i a_{k2} + A_{12}K_i a_{k1} + A_{06}K_{01}a_{k6} + A_{07}K_{01}a_{k5} + A_{08}K_{k1}a_{k4} + A_{09}K_{k1}a_{k3} + A_{10}K_{01}a_{02} + A_{11}K_{k1}a_{k1} + A_{06}K_{k2}a_{k6} + A_{07}K_{k2}a_{k5} + A_{08}K_{k2}a_{k4} + A_{09}K_{k2}a_{k3} + A_{10}K_{k2}a_{k2} + A_{11}K_{k2}a_{k1})/(K_i + b_{k0})$,

$N_{k,14} = (A_{08}b_{k6} + A_{09}b_{k5} + A_{10}b_{k4} + A_{11}b_{k3} + A_{12}b_{k2} + A_{13}b_{k1} + A_{14}b_{k0} + A_{14}K_i + A_{13}K_{k1} + A_{13}K_{k2} + A_0 K_i a_{k6} + A_{09}K_i a_{k5} + A_{10}K_i a_{k4} + A_{11}K_i a_{k3} + A_{12}K_i a_{k2} + A_{13}K_i a_{k1} + A_{07}K_{k1}a_{k6} + A_{08}K_{k1}a_{k5} + A_{09}K_{k1}a_{k4} + A_{10}K_{k1}a_{k3} + A_{11}K_{k1}a_{k2} + A_{12}K_{k1}a_{k1} + A_{07}K_{k2}a_{k6} + A_{08}K_{k2}a_{k5} + A_{09}K_{k2}a_{k4} + A_{k1}K_{k2}a_{k3} + A_{11}K_{k2}a_{k2} + A_{12}K_{k2}a_{k1})/(K_i + b_{k0})$,

$N_{k,15} = (A_{09}b_{k6} + A_{10}b_{k5} + A_{11}b_{k4} + A_{12}b_{k3} + A_{13}b_{k2} + A_{14}b_{k1} + A_{15}b_{k0} + A_{15}K_i + A_{14}K_{k1} + A_{14}K_{k2} + A_{09}K_i a_{k6} + A_{10}K_i a_{k5} + A_{11}K_i a_{k4} + A_{12}K_i a_{k3} + A_{13}K_i a_{k2} + A_{14}K_i a_{k1} + A_{08}K_{k1}a_{k6} + A_{09}K_{k1}a_{k5} + A_{10}K_{k1}a_{k4} + A_{11}K_{k1}a_{k3} + A_{12}K_{k1}a_{k2} + A_{13}K_{k1}a_{k1} + A_{08}K_{k2}a_{k6} + A_{09}K_{k2}a_{k5} + A_{10}K_{k2}a_{k4} + A_{11}K_{k2}a_{k3} + A_{12}K_{k2}a_{k2} + A_{13}K_{k2}a_{k1})/(K_i + b_{k0})$,

$N_{k,16} = (A_{10}b_{k6} + A_{11}b_{k5} + A_{12}b_{k4} + A_{13}b_{k3} + A_{14}b_{k2} + A_{15}b_{k1} + A_{16}b_{k0} + A_{16}K_i + A_{15}K_{k1} + A_{15}K_{k2} + A_{10}K_i a_{k6} + A_{11}K_i a_{k5} + A_{12}K_i a_{k4} + A_{13}K_i a_{k3} + A_{14}K_i a_{k2} +$

$A_{15}K_ia_{k1}+A_{09}K_{k1}a_{k6}+A_{10}K_{k1}a_{05}+A_{11}K_{k1}a_{k4}+A_{12}K_{k1}a_{k3}+A_{13}K_{k1}a_{k2}+A_{14}K_{k1}a_{k1}+$
$A_{09}K_{k2}a_{k6}+A_{10}K_{k2}a_{k5}+A_{11}K_{k2}a_{k4}+A_{12}K_{k2}a_{k3}+A_{13}K_{k2}a_{k2}+A_{14}K_{k2}a_{k1})/(K_i+$
$b_{k0}),$

$N_{k,17}=(A_{11}b_{k6}+A_{12}b_{k5}+A_{13}b_{k4}+A_{14}b_{k3}+A_{15}b_{k2}+A_{16}b_{k1}+A_{17}b_{k0}+A_{17}K_i+$
$A_{16}K_{k1}+A_{16}K_{k2}+A_{11}K_ia_{k6}+A_{12}K_ia_{k5}+A_{13}K_ia_{k4}+A_{14}K_ia_{k3}+A_{15}K_ia_{k2}+$
$A_{16}K_ia_{k1}+A_{10}K_{k1}a_{k6}+A_{11}K_{k1}a_{k5}+A_{12}K_{k1}a_{k4}+A_{13}K_{k1}a_{k3}+A_{14}K_{k1}a_{k2}+A_{15}K_{k1}a_{k1}+$
$A_{10}K_{k2}a_{k6}+A_{11}K_{k2}a_{k5}+A_{12}K_{k2}a_{k4}+A_{13}K_{k2}a_{k3}+A_{14}K_{k2}a_{k2}+A_{15}K_{k2}a_{k1})/(K_i+$
$b_{k0}),$

$N_{k,18}=(A_{12}b_{k6}+A_{13}b_{k5}+A_{14}b_{k4}+A_{15}b_{k3}+A_{16}b_{k2}+A_{17}b_{k1}+A_{18}b_{k0}+A_{18}K_i+$
$A_{17}K_{k1}+A_{17}K_{k2}+A_{12}K_ia_{k6}+A_{13}K_ia_{k5}+A_{14}K_ia_{k4}+A_{15}K_ia_{k3}+A_{16}K_ia_{k2}+$
$A_{17}K_ia_{k1}+A_{11}K_{k1}a_{k6}+A_{12}K_{k1}a_{k5}+A_{13}K_{k1}a_{k4}+A_{14}K_{k1}a_{k3}+A_{15}K_{k1}a_{k2}+A_{16}K_{k1}a_{k1}+$
$A_{11}K_{k2}a_{k6}+A_{12}K_{k2}a_{k5}+A_{13}K_{k2}a_{k4}+A_{14}K_{k2}a_{k3}+A_{15}K_{k2}a_{k2}+A_{16}K_{k2}a_{k1})/(K_i+$
$b_{k0}),$

$N_{k,19}=(A_{13}b_{k6}+A_{14}b_{k5}+A_{15}b_{k4}+A_{16}b_{k3}+A_{17}b_{k2}+A_{18}b_{k1}+A_{19}b_{k0}+A_{19}K_i+$
$A_{18}K_{k1}+A_{18}K_{k2}+A_{13}K_ia_{k6}+A_{14}K_ia_{k5}+A_{15}K_ia_{k4}+A_{16}K_ia_k+A_{17}K_ia_{k2}+$
$A_{18}K_ia_{k1}+A_{12}K_{k1}a_{k6}+A_{13}K_{k1}a_{k5}+A_{14}K_{k1}a_{k4}+A_{15}K_{k1}a_{k3}+A_{16}K_{k1}a_{k2}+A_{17}K_{k1}a_{k1}+$
$A_{12}K_{k2}a_{k6}+A_{13}K_{k2}a_{k5}+A_{14}K_{k2}a_{k4}+A_{15}K_{k2}a_{k3}+A_{16}K_{k2}a_{k2}+A_{17}K_{k2}a_{k1})/(K_i+$
$b_{k0}),$

$N_{k,20}=(A_{14}b_{k6}+A_{15}b_{k5}+A_{16}b_{k4}+A_{17}b_{k3}+A_{18}b_{k2}+A_{19}b_{k1}+A_{20}b_{k0}+A_{20}K_i+$
$A_{19}K_{k1}+A_{19}K_{k2}+A_{14}K_ia_{k6}+A_{15}K_ia_{k5}+A_{16}K_ia_{k4}+A_{17}K_ia_{k3}+A_{18}K_ia_{k2}+$
$A_{19}K_ia_{k1}+A_{13}K_ka_{k6}+A_{14}K_{k1}a_{k5}+A_{15}K_{k1}a_{k4}+A_{16}K_{k1}a_{k3}+A_{17}K_{k1}a_{k2}+A_{18}K_{k1}a_{k1}+$
$A_{13}K_{k2}a_{k6}+A_{14}K_{k2}a_{k5}+A_{15}K_{k2}a_{k4}+A_{16}K_{k2}a_{k3}+A_{17}K_{k2}a_{k2}+A_{18}K_{k2}a_{k1})/(K_i+$
$b_{k0}),$

$N_{k,21}=(A_{15}b_{k6}+A_{16}b_{k5}+A_{17}b_{k4}+A_{18}b_{k3}+A_{19}b_{k2}+A_{20}b_{k1}+A_{20}K_{k1}+A_{20}K_{k2}+$
$A_{15}K_ia_{k6}+A_{16}K_ia_{k5}+A_{17}K_ia_{k4}+A_{18}K_ia_{k3}+A_{19}K_ia_{k2}+A_{20}K_ia_{k1}+A_{14}K_{k1}a_{k6}+$
$A_{15}K_{k1}a_{k5}+A_{16}K_{k1}a_{k4}+A_{17}K_{k1}a_{k3}+A_{18}K_{k1}a_{k2}+A_{19}K_{k1}a_{k1}+A_{14}K_{k2}a_{k6}+A_{15}K_{k2}a_{k5}+$
$A_{16}K_{k2}a_{k4}+A_{17}K_{k2}a_{k3}+A_{18}K_{k2}a_{k2}+A_{19}K_{k2}a_{k1})/(K_i+b_{k0}),$

$N_{k,22}=(A_{16}b_{k6}+A_{17}b_{k5}+A_{18}b_{k4}+A_{19}b_{k3}+A_{20}b_{k2}+A_{16}K_ia_{k6}+A_{17}K_ia_{k5}+$

$A_{18}K_ia_{k4}+A_{19}K_ia_{k3}+A_{20}K_ia_{k2}+A_{15}K_{k1}a_{k6}+A_{16}K_{k1}a_{k5}+A_{17}K_{k1}a_{k4}+A_{18}K_{k1}a_{k3}+A_{19}K_{k1}a_{k2}+A_{20}K_{k1}a_{k1}+A_{15}K_{k2}a_{k6}+A_{16}K_{k2}a_{k5}+A_{17}K_{k2}a_{k4}+A_{18}K_{k2}a_{k3}+A_{19}K_{k2}a_{k2}+A_{20}K_{k2}a_{k1})/(K_i+b_{k0})$,

$N_{k,23}=(A_{17}b_{k6}+A_{18}b_{k5}+A_{19}b_{k4}+A_{20}b_{k3}+A_{17}K_ia_{k6}+A_{18}K_ia_{k5}+A_{19}K_ia_{k4}+A_{20}K_ia_{k3}+A_{16}K_{k1}a_{k6}+A_{17}K_{k1}a_{k5}+A_{18}K_{k1}a_{k4}+A_{19}K_{k1}a_{k3}+A_{20}K_{k1}a_{k2}+A_{16}K_{k2}a_{k6}+A_{17}K_{k2}a_{k5}+A_{18}K_{k2}a_{k4}+A_{19}K_{k2}a_{k3}+A_{20}K_{k2}a_{k2})/(K_i+b_{k0})$,

$N_{k,24}=(A_{18}b_{k6}+A_{19}b_{k5}+A_{20}b_{k4}+A_{18}K_ia_{k6}+A_{19}K_ia_{k5}+A_{20}K_ia_{k4}+A_{17}K_{k1}a_{k6}+A_{18}K_{k1}a_{k5}+A_{19}K_{k1}a_{k4}+A_{20}K_{k1}a_{k3}+A_{17}K_{k2}a_{k6}+A_{18}K_{k2}a_{k5}+A_{19}K_{k2}a_{k4}+A_{20}K_{k2}a_{k3})/(K_i+b_{k0})$,

$N_{k,25}=(A_{19}b_{k6}+A_{20}b_{k5}+A_{19}K_{k1}a_{k6}+A_{20}K_ia_{k5}+A_{18}K_{k1}a_{k6}+A_{19}K_{k1}a_{k5}+A_{20}K_{k1}a_{k4}+A_{18}K_{k2}a_{k6}+A_{19}K_{k2}a_{k5}+A_{20}K_{k2}a_{k4})/(K_i+b_{k0})$,

$N_{k,26}=(A_{20}b_{k6}+A_{20}K_ia_{k6}+A_{19}K_{k1}a_{k6}+A_{20}K_{k1}a_{k5}+A_{19}K_{k2}a_{k6}+A_{20}K_{k2}a_{k5})/(K_i+b_{k0})$,

$N_{i,27}=(A_{20}K_{k1}a_{k6}+A_{20}K_{k2}a_{k6})/(K_i+b_{k0})$.

Bibliography

[1] Pollet, B. G., I. Staffell, and J. L. Shang (2012) "Current Status of Hybrid, Battery and Fuel Cell Vehicles: From Electrochemistry to Market Prospects," *Electrochemica Acta*, **84**, pp. 235–249.

[2] Office of the Press Secretary (2013), "The White House Press Release, Washington DC," On the WWW, URL `http://www.whitehouse.gov/the-press-office`.

[3] Leistikow, D. (2012), "An Update on Advanced Battery Manufacturing, Washington DC," On the WWW, URL http://www.energy.gov/articles/update-advanced-battery-manufacturing.

[4] Thomas, C. E. S. (2009) "Transportation Options in a Carbon-Constrained World: Hybrids, Plug-in Hybrids, Biofuels, Fuel Cell Electric Vehicles, and Battery Electric Vehicles," *Int. J. Hydrogen Energy*, **34**(23), pp. 9279–9296.

[5] Rahn, C. D. and C. Y. Wang (2013) *Battery Systems Engineering*, John Wiley and Sons Inc, State College, PA.

[6] USCAR (2013), "Energy Storage System Goals," On the WWW, URL `http://uscar.org/guest/article_view.php?articles_id=85`.

[7] Plett, G. L. (2004) "Extended Kalman Filtering for Battery Management Systems of LiPB-Based HEV Battery Packs Part 1. Background," *J. Power Sources*, **134**(2), pp. 252–261.

[8] ——— (2004) "Extended Kalman Filtering for Battery Management Systems of LiPB-Based HEV Battery Packs Part 2. Modeling and Identification," *J. Power Sources*, **134**(2), pp. 262–276.

[9] ——— (2004) "Extended Kalman Filtering for Battery Management Systems of LiPB-Based HEV Battery Packs Part 3. State and Parameter Estimation," *J. Power Sources*, **134**, pp. 277–292.

[10] Verbrugge, M. W. and R. S. Conell (2002) "Electrochemical and Thermal Characterization of Battery Modules Commensurate with Electric Vehicle Integration," *J. Electrochem. Soc.*, **149**(1), pp. A45–A53.

[11] Verbrugge, M. and P. Liu (2007) "Electrochemical Characterization of High-Power Lithium Ion Batteries Using Triangular Voltage and Current Excitation Sources," *J. Power Sources*, **174**(1), pp. 2–8.

[12] Schweighofer, B., K. M. Raab, and G. Brasseur (2003) "Modeling of High Power Automotive Batteries by The Use of an Automated Test System," *IEEE Trans. Instrum. Meas.*, **52**(4), pp. 1087–1091.

[13] Moss, P. L., G. Au, E. J. Plichta, and J. P. Zheng (2008) "An Electrical Circuit for Modeling the Dynamic Response of Li-Ion Polymer Batteries," *J. Electrochem. Soc.*, **155**(12), pp. A986–A994.

[14] Smith, K. A., C. D. Rahn, and C. Y. Wang (2007) "Control Oriented 1D Electrochemical Model of Lithium Ion Battery," *Energy Convers. and Manage.*, **48**(9), pp. 2565–2578.

[15] ——— (2008) "Model Order Reduction of 1D Diffusion Systems Via Residue Grouping," *ASME J Dyn. Syst. Meas. Control*, **130**(5), p. 011012.

[16] Kim, I. (2006) "The Novel State of Charge Estimation Method for Lithium Ion Battery using Sliding Mode Observer," *J. Power Sources*, **163**(1), pp. 584–590.

[17] Cho, S., H. Jeong, C. Han, S. Jin, J. H. Lim, and J. Oh (2012) "State of Charge Estimation for Lithium-ion Batteries Under Various Operating Conditions Using an Equivalent Circuit Model," *Computers and Chem. Engg.*, **220**, pp. 430–448.

[18] He, H., X. Zhang, R. Xiong, Y. Xu, and H. Guo (2012) "Online Model-Based Estimation of State of Charge and Open Circuit Voltage of Lithium-ion Batteries in Electric Vehicles," *Energy*, **39**(1), pp. 310–318.

[19] Xu, J., C. C. Mi, B. Cao, and J. Cao (2013) "A New Method to Estimate the State of Charge of Lithium-ion Batteries Based on the Battery Impedance Model," *J. Power Sources*, **223**, pp. 227–284.

[20] Lee, J., O. Nam, and B. H. Cho (2007) "Li-ion Battery SOC Estimation Method Based on the Reduced Order Extended Kalman Filtering," *J. Power Sources*, **174**(1), pp. 9–15.

[21] Hu, X., F. Sun, and Y. Zou (2010) "Estimation of State of Charge of a Lithium-Ion Battery Pack for Electric Vehicles Using an Adaptive Luenberger Observer," *Energies*, **3**(9), pp. 1586–1603.

[22] Smith, K. A., C. D. Rahn, and C. Y. Wang (2010) "Model-Based Electrochemical Estimation and Constraint Management for Pulse Operation of Lithium Ion Batteries," *IEEE Trans. Control Syst. Technol.*, **18**(3), pp. 654–663.

[23] Lee, J. L., A. Chemistruck, and G. L. Plett (2012) "One Dimensional Physics-Based Reduced-Order Model of Lithium-ion Dynamics," *J. Power Sources*, **220**, pp. 430–448.

[24] Klein, R., N. A. Chaturvedi, J. Christensen, J. Ahmed, R. Findeisen, and A. Kojic (2010) "State Estimation of A Reduced Electrochemical Model of A lithium-Ion Battery," in *American Control Conference*, Baltimore, MD, USA.

[25] ——— (2013) "Electrochemical Model Based Observer Design for a Lithium-Ion Battery," *IEEE Trans. Control Syst. Technol.*, **21**(2), pp. 289–301.

[26] Santhanagopalan, S., Q. Guo, P. Ramadass, and R. E. White (2006) "Review of Models for Predicting the Cycling Performance of Lithium Ion Batteries," *J. Power Sources*, **156**(2), pp. 620–628.

[27] Domenico, D. D., A. Stefanopoulou, and G. Fiengo (2010) "Lithium-ion Battery State of Charge and Critical Surface Change Estimation Using an Electrochemical Model-Based Extended Kalman Filter," *ASME J Dyn. Syst. Meas. Control*, **132**(6), pp. 061302–1–061302–11.

[28] Moura, S. J., N. Chaturvedi, and M. Krstić (2012) "PDE Estimation Techniques for Advanced Battery Management Systems - Part I: SOC Estimation," in *American Control Conference*, Montreal, QC, Canada, pp. 559–565.

[29] Prasad, G. K. and C. D. Rahn (2012) "Development of a First Principles Equivalent Circuit Model for a Lithium Ion Battery," in *ASME Dyn. Syst. and Control Conference*, Florida, USA.

[30] Rayman, S., R. E. White, M. Z. B. H. C. Yu, and K. Thornton (2013) "Extension of Physics-Based Single Particle Model for Higher Charge-Discharge Rates," *J Power Sources*, **224**, pp. 180–194.

[31] Marcicki, J., M. Canova, A. T. Conlisk, and G. Rizzoni (2013) "Design and Parameter Analysis of a Reduced-Order Electrochemical Model of Graphite/ $LiFePO_4$ Cells for SOC/SOH Estimation," *J. Power Sources*, **237**, pp. 310–324.

[32] Padhi, A. K., K. S. Nanjundaswamy, C. Masquelier, and J. B. Goodenough (1997) "Effect of Structure on the $Fe3^+/Fe2^+$ Redox Couple in Iron Phosphates." *J. Electrochem. Soc.*, **144**(5), pp. 1609–1613.

[33] Yamada, A., M. Hosoya, S. Chung, Y. Kudo, K. Hinokuma, K. Liu, and Y. Nishi (2003) "Olivine-type Cathodes: Achievements and Problems." *J. Power Sources*, **119-121**, pp. 232–238.

[34] Striebel, K., A. Guerfi, J. Shim, M. Armand, M. Gauthier, and K. Zaghib (2003) "$LiFePO_4$/Gel/Natural Graphite Cells for the BATT Program," *J. Power Sources*, **119-121**, pp. 951–954.

[35] Liu, P., J. Wang, J. Hicks-Garner, E. Sherman, S. Soukiazian, M. Verbrugge, H. Tataria, J. Musser, and P. Finamore (2010) "Aging Mechanisms of $LiFePO_4$ Batteries Deduced by Electrochemical and Structural Analyses," *J. Electrochem. Soc.*, **157**(3), pp. A499–A509.

[36] Dubarry, M. and B. Y. Liaw (2009) "Identify Capacity Fading Mechanism in a Commercial $LiFePO_4$ Cell," *J. Power Sources*, **194**(1), pp. 541–549.

[37] Srinivasan, V. and J. Newman (2004) "Discharge Model for the Lithium Iron-Phosphate Electrode," *J. Electrochem. Soc.*, **151**, pp. A1517–A1529.

[38] Laffont, L., C. Delacourt, P. Gibot, M. Y.Wu, P. Kooyman, C. Masquelier, and J. M. Tarascon (2006) "Study of the $LiFePO_4/FePO_4$ Two-Phase System by High-Resolution Electron Energy Loss Spectroscopy," *Chem. Mater.*, **18**, pp. 5520–5529.

[39] Tang, M., H. Y. Huang, N. Meethong, Y. H. Kao, W. C. Carter, and Y. M. Chiang (2009) "Model for the Partic Size, Overpotential, and Strain Dependence of Phase Transition Pathways in Storage Electrodes: Application to Nanoscale Olivines," *Chem. Mater.*, **21**(8), pp. 1557–1571.

[40] Wang, C., U. S. Kasavajjula, and P. E. Arce (2007) "A Discharge Model for Phase Transformation Electrodes: Formulation, Experimental Validaiton, and Analysis." *Physical Chemistry*, **111**, pp. 16656–16663.

[41] Kasavajjula, U. S., C. Wang, and P. E. Arce (2008) "Discharge Model for $LiFePO_4$ Accounting for the Solid Solution Range," *J. Electrochem. Soc.*, **155**(11), pp. A866–A874.

[42] Dargaville, S. and T. W. Farrell (2010) "Predicting Active Material Utilization in $LiFePO_4$ Electrodes Using a Multiscale Mathematical Model," *J. Electrochem. Soc.*, **157**(7), pp. A830–A840.

[43] Thorat, I., T. Joshi, K. Zaghib, J. Harb, and D. Wheeler (2011) "Understanding Rate-Limiting Mechanisms in $LiFePO_4$ Cathodes for Li-ion Batteries," *J. Electrochem. Soc.*, **158**(11), pp. A1185–A1193.

[44] Singh, G. K., M. Z. Bazant, and G. Ceder (2007) *Condensed Matter-Material Science*, **arXiv:0707.1858v1**.

[45] Bai, P., D. A. Cogswell, and M. Z. Bazant (2011) "Suppression of Phase Separation in $LiFePO_4$ Nanoparticles During Battery Discharge," *Nano Lett.*, **11**(11), pp. 4890–4896.

[46] Cogswell, D. A. and M. Z. Bazant (2012) "Coherency Strain and the Kinetics of Phase Separation in $LiFePO_4$ Nanoparticles," *ACS Nano*, **6**(3), pp. 2215–2225.

[47] Orvananos, B., T. R. Ferguson, H. C. Yu, M. Z. Bazant, and K. Thornton (2013) "Particle-Level Modeling of the Charge-Discharge Behavior of Nanoparticulate Phase-Separating Li-Ion Battery Electrodes," **arxiv.org/abs/1309.6495**.

[48] Thomas-Alyea, K. E. (2008) "Modeling Resistive-Reactant and Phase-Change Materials in Battery Electrodes," *ECS Trans.*, **16**(13), pp. 155–165.

[49] Safari, M. and C. Delacourt (2011) "Mathematical Modeling of Lithium Iron Phosphate Electrode: Galvanostatic Charge/Discharge and Path Dependence," *J. Electrochem. Soc.*, **158**(2), pp. A63–A73.

[50] Christensen, J. and J. Newman (2004) "A Mathematical Model for the Lithium-Ion Negative Electrode Solid Electrolyte Interphase," *J. Electrochem. Soc.*, **151**(11), pp. A1977–A1988.

[51] Ploehn, H. J., P. Ramadass, and R. E. White (2004) "Solvent Diffusion Model for Aging of Lithium-Ion Cells," *J. Electrochem. Soc.*, **151**(3), pp. A456–A462.

[52] Safari, M., M. Morcrette, A. Teyssot, and C. Delacourt (2009) "Multimodal Physics Based Aging Model for Life Prediction of Li-Ion Batteries," *J. Electrochem. Soc.*, **156**(3), pp. A145–A153.

[53] Ramadass, P., B. Haran, P. M. Gomadam, R. White, and B. N. Popov (2004) "Development of First Principle Capacity Fade Model for Li-Ion Cells," *J. Electrochem. Soc.*, **151**(2), pp. A196–A203.

[54] Randall, A., R. D. Perkins, X. Zhang, and G. Plett (2012) "Control Oriented Reduced Order Modeling of Solid-Electrolyte Interphase Layer Growth," *J. Power Sources*, **209**, pp. 282–288.

[55] USABC (1996), "Electric Vehicle Battery Test Procedures Manual," On the WWW, URL `http://avt.inl.gov/battery/pdf/usabc_manual_rev2.pdf`.

[56] K.J., K., M. Mihalic, and M. Zolot (2002) "Battery Usage and Thermal Performance of the Toyota Prius and Honda Insight During Chassis Dynamometer Testing," in *The 17th Annual Battery Conference on Application and Advances*, IEEE, Long Beach, California, pp. 247–252.

[57] Doyle, M. and J. Newman (1996) "Comparison of Modeling Predictions with Experimental Data From Plastic Lithium Ion Cells," *J. Electrochem. Soc.*, **143**(6), pp. 1890–1903.

[58] Doyle, M. and Y. Fuentes (2003) "Computer Simulations of a Lithium-Ion Polymer Battery and Implications for Higher Capacity Next-Generation Battery Designs," *J. Electrochem. Soc.*, **150**(6), pp. A706–A713.

[59] Gu, W. B. and C. Y. Wang (2000) "Thermal-Electrochemical Modeling of Battery Systems," *J. Electrochem. Soc.*, **147**(8), pp. 2910–2922.

[60] Jacobsen, T. and K. West (1995) "Diffusion Impedance In Planar, Cylindrical and Spherical Geometry," *Electrochem. Acta*, **40**(2), pp. 255–262.

[61] Forman, J. C., S. Bashash, J. L. Stein, and H. K. Fathy (2011) "Reduction of an Electrochemistry-Based Li-ion Battery Model Via Quasi-Linearization and Padé Approximation," *J. Electrochem. Soc.*, **158**(2), pp. A93–A101.

[62] Shi, Y., G. K. Prasad, Z. Shen, and C. D. Rahn (2011) "Discretization Methods for Battery Systems Modeling," in *American Control Conference*, California, USA.

[63] Gebhart, B. (1993) *Heat Conduction and Mass Diffusion*, McGraw-Hill, New York, NY.

[64] Subramanian, V. R., J. A. Ritter, and R. E. White (2001) "Approximate Solutions for Galvanostatic Discharge of Spherical Particles," *J. Electrochem. Soc.*, **148**(11), pp. E444–E449.

[65] Subramanian, V. R., D. Tapriyal, and R. E. White (2004) "A Boundary Condition for Porous Electrodes," *Electrochem. Solid State Letters*, **7**(9), pp. A259–A263.

[66] Frankline, G. F., J. D. Powell, and A. E. Naeini (2011) *Feedback Control of Dynamic Systems*, Pearson, New Delhi, India.

[67] Valøen, L. O. and J. N. Reimers (2005) "Transport Properties of $LiPF_6$-Based Li-Ion Battery Electrolytes," *J. Electrochem. Soc.*, **152**(5), pp. A882–A891.

[68] EC Power (2013), "Software Products," On the WWW, URL `http://ecpowergroup.com/products-2/software-licensing`.

[69] Safari, M. and C. Delacourt (2011) "Modeling of a Commercial Graphite/ $LiFePO_4$ Cell," *J. Electrochem. Soc.*, **158**(5), pp. A562–A571.

[70] Chaturvedi, N. A., R. Klein, J. Christensen, J. Ahmed, and A. Kojic (2010) "Algorithms for Advanced Battery-Management Systems," *IEEE Control Syst. Magazine*, pp. 40–68.

[71] Sarasketa-Zabala, E., I. Gandiaga, L. Rodriguez-Martinez, and I. Villarreal (2014) "Calendar Aging Analysis of a $LiFePO_4$/Graphite Cell with Dynamic Model Validations: Towards Realistic Lifetime Predictions," *J. of Power Sources*, **272**, pp. 45–57.

[72] Prada, E., D. D. Domenico, Y. Creff, J. Bernard, V. Sauvant-Moynot, and F. Huet (2013) "A Simplified Electrochemical and Thermal Aging Model of $LiFePO_4$- Graphite Li-ion Batteries: Power and Capacity Fade Simulations," *J. Electrochem. Soc.*, **160**(4), pp. A616–A628.

[73] Safari, M. and C. Delacourt (2011) "Aging of a Commercial Graphite/ $LiFePO_4$ Cell," *J. Electrochem. Soc.*, **158**(10), pp. A1123–A1135.

[74] Broussely, M., S. Herreyre, P. Biensan, P. Kasztejna, K. Nechev, and R. Staniewicz (2001) "Aging Mechanism in Li-ion Cell and Calendar Life Predictions," *J. Power Sources*, **97-98**, pp. 13–21.

[75] Ramadass, P., B. Haran, R. White, and B. N. Popov (2002) "Capacity Fade of Sony 18650 Cells Cycled at Elevated Temperatures Part I. Cycling Performance," *J. Power Sources*, **112**, p. 606.

[76] Monem, M., K. Trad, N. Omar, O. Hegazy, B. Mantels, G. Mulder, P. V. Bossche, and J. V. Mierlo (2015) "Lithium-ion Batteries: Evaluation Study of Different Charging Methodologies Based on Aging Process," *Applied Energy*, **152**, p. 143âĂŞ155.

[77] Eddahech, A., O. Briat, and J. Vinassa (2015) "Performance Comparison of Four Lithium-ion Battery Technologies Under Calendar Aging," *Energy*, **84**, pp. 542–550.

[78] Safari, M. and C. Delacourt (2011) "Simulation- Based Analysis of Aging Phenomena in a Commercial Graphite/ $LiFePO_4$ Cell," *J. Electrochem. Soc.*, **158**(12), pp. A1436–A1447.

[79] Zhang, Y. and C. Y. Wang (2009) "Cycle-life Characterization of Automotive Lithium-ion Batteries with $LiNiO_2$ Cathode," *J. Electrochem. Soc.*, **156**(7), pp. A527–A535.

[80] Narayanrao, R., , M. M. Joglekar, and S. Inguva (2013) "A Phenomenological Degradation Model for Cyclic Aging of Lithium Ion Cell Materials," *J. Electrochem. Soc.*, **1**(160), pp. A125–A137.

[81] Deshpande, R., M. Verbrugge, Y.-T. Cheng, J. Wang, and P. Liu (2012) "Battery Cycle Life Prediction with Coupled Chemical Degradation and Fatigue Mechanics," *J. Electrochem. Soc.*, **159**(10), pp. A1730–A1738.

Vita

Tanvir R. Tanim

Education:
Pennsylvania State University, Ph.D. Mechanical Engineering, 2015.
Ohio University, M.S. Mechanical Engineering, 2011.
Bangladesh University of Engineering and Technology, B.S. Mechanical Engineering, 2007.

Work Experience:
Summer Research Co-op: **The Raymond Corporation**, May 2015-August 2015.
Research Assistant, **Penn State**, June 2012-October 2015.
Graduate Teaching Assistant, **Penn State**, Fall 2011 and Spring 2012.
Graduate Research Assistant, **Ohio University**, July 2010-August 2011.
Graduate Teaching Assistant, **Ohio University**, August 2009-June 2010.
Lecturer, Dept. of Mechanical Engineering, **Bangladesh University of Engineering and Technology**, June 2007-August 2009.

Publications

1. T. R. Tanim, C. D. Rahn, and Niklas Legnedahl, Elevated temperatures can extend the life of lithium iron phosphate cells in hybrid electric vehicles, ASME Dynamic Systems and Control Conference, 2015, Columbus, Ohio.

2. T. R. Tanim, and C. D. Rahn, Aging formula for lithium ion batteries with solid electrolyte interphase layer growth, *J. Power Sources*, 294 (2015) 239-247.

3. T. R. Tanim, C. D. Rahn, and C. Y. Wang, State of charge estimation of a lithium ion cell using a temperature dependent, electrolyte enhanced single particle model, *Energy*, 80 (2015) 731-739.

4. T. R. Tanim, C. D. Rahn, and C. Y. Wang, A temperature dependent, single particle, lithium ion cell model including electrolyte diffusion, *J. Dynamic Systems, Measurement, and Control*, 137 (1)(2014) 011005.

5. T. R. Tanim, C. D. Rahn, and C. Y. Wang, A reduced order electrolyte enhanced single particle lithium ion cell model for hybrid vehicle applications, *American Control Conf.*, June 2014, Portland, OR, 141-146.

6. T. R. Tanim, D. J. Bayless, and J. Trembly, Modeling of a 5 kWe tubular solid oxide fuel cell based system operating on desulfurized JP-8 fuel for auxiliary and mobile power applications, *J. Power Sources*, 221 (2013) 387-396.

Professional Affiliations: American Society of Mechanical Engineers.